INSTITUTO POLITÉCNICO DE BRAGANÇA
Escola Superior de Tecnologia e de Gestão

Design and finite element analysis of formula student braking system

Emad Mazen Sweed

Dissertation presented to Escola Superior de Tecnologia e Gestão of Instituto Politécnico de Bragança to obtain the Master's Degree in Industrial Engineering

Supervised by:

Professor Doutor João Eduardo Pinto Castro Ribeiro

Bragança

November 2021

Design and finite element analysis of formula student braking system

Emad Mazen Sweed

Dissertation presented to Escola Superior de Tecnologia e Gestão of Instituto Politécnico de Bragança to obtain the Master's Degree in Industrial Engineering

Supervised by:

Professor Doutor João Eduardo Pinto Castro Ribeiro

Bragança

November 2021

Acknowledgement

First of all, I would like to thank God for giving me the strength and patience to accomplish this humble work.

I would like to express my sincere gratitude to my supervisor, Prof. Dr João Eduardo Pinto Castro Ribeiro, for all his efforts, continual support, and faith in me on a daily basis. Working with you has been a true pleasure.

The Study was funded by a grant from the Global Platform for Syrian students founded in November 2013 by Dr Jorge Sampaio, former President of Portugal. They exemplify outstanding morality to assist me in pursuing my education and progressing to this level. I'm pretty appreciative.

I want to express my appreciation to Cesar Hernandez and Bruno Ribeiro, members of the IPB Motor Sport, for their generosity in providing me with critical diameters of the vehicle, their interest in reviewing and enriching this document with their suggestions.

My parents, unlimited support since my first breath in this world. Years of studying this accomplishment wouldn't have been possible without them, all the love.

Abstract

The present project focuses on the research and design of a braking system for sports vehicles. The braking system will be included in a vehicle being developed by the IPB Motorsport Team in order to participate in an annual worldwide collegiate design competition called Formula Student. The competition evaluates a Formula style car's engineering, performance, and cost.

Since it was the first vehicle of this style to be designed at IPB, the values were analysed and estimated for the under-design vehicle. A methodology has been developed using the theory of vehicle dynamics to design a braking system capable of meeting the technical requirements of the competition.

Another part of this research included analysing the behaviour of brake rotors made of various materials (Gray Cast Iron, Aluminium Alloy) and Geometry (Drilled, Solid) using Finite Element Analysis (FEA) more precisely the ANSYS software version 21. Static and thermal simulations were conducted for the design.

As a result, a brake system assembly capable of achieving a four-wheel lock is demonstrated. Gray cast iron has superior thermal and static capabilities than aluminium, and the rotor geometry has an effect on the stress distribution.

The simulations proved to be very useful in determining the most suitable brake rotor material and cooling shape for the brake rotors.

Keywords: Braking System - Finite element analysis - Formula Student - Vehicle dynamics - Transient thermal analysis - Static structural analysis.

Resumo

O presente projeto centra-se na investigação e concepção de um sistema de travagem para veículos desportivos. O sistema de frenagem será incluído em um veículo que está sendo desenvolvido pela IPB Motorsport Team para participar de uma competição universitária anual de design chamada Formula Student. A competição avalia a engenharia, o desempenho e o custo de um carro estilo Fórmula.

Por ter sido o primeiro veículo desse estilo a ser projetado no IPB, os valores foram analisados e estimados para o veículo em projeto. Foi desenvolvida uma metodologia a partir da teoria da dinâmica veicular para projetar um sistema de frenagem capaz de atender aos requisitos técnicos da competição.

Outra parte desta pesquisa incluiu a análise do comportamento dos rotores dos freios feitos de diversos materiais (Ferro Fundido Cinza, Liga de Alumínio) e da Geometria (Perfurada, Sólida) utilizando a Análise de Elementos Finitos (FEA), mais precisamente o software ANSYS versão 21. Estático e térmico simulações foram realizadas para o projeto.

Como resultado, é demonstrado um conjunto de sistema de freio capaz de obter um travamento nas quatro rodas. O ferro fundido cinzento tem capacidades térmicas e estáticas superiores do que o alumínio, e a geometria do rotor tem um efeito na distribuição de tensões.

As simulações provaram ser muito úteis para determinar o material do rotor do freio e a forma de refrigeração mais adequados para os rotores do freio.

Palavras-chave: Sistema de travagem - Análise de elementos finitos - Formula Student - Dinâmica do veículo - Análise térmica transitória - Análise estrutural estática.

Table of Contents

List of Figures

List of Tables

List of Abbreviations and Symbols

Abbreviations

BEM	Boundary Element Method.
CAD	Computer-Aided Design.
CAM	Computer-Aided Manufacturing.
CG	Center of Gravity.
CV	Combustion Engine Vehicle.
DOFs	Degrees of Freedom.
EV	Electric Vehicle.
FDM	Finite Difference Method.
FEA	Finite Element Analysis.
FEM	Finite Element Method.
FSAE	Formula SAE Competition.
FVM	Finite Volume Method.
IMA	Mechanical Advantage.
NSL	Newton's Second Law.
PDEs	Partial Differential Equations.
R&D	Research and Development.
SAE	Society of Automotive Engineers.

Symbols

$\boldsymbol{A_{Calliper}}$	m^2	Area of the Calliper.
$\boldsymbol{A_{mc}}$	m^2	Area of The Master Cylinder.
$\boldsymbol{A}$	m^2	Area.
$\boldsymbol{a_x}$	m/s^2	Acceleration in The x-direction.
$[\boldsymbol{D}]$		Nodal Displacement.
$\boldsymbol{D}$	m	Distance.
$\boldsymbol{D_A}$	N	Aerodynamic Load.
$\boldsymbol{D_{Braking}}$	m	Braking Distance.
$\boldsymbol{D_b}$	m	Bore Diameter.
$\boldsymbol{D_{cp}}$	m	Diameter of Callipers Piston.
$\boldsymbol{D_r}$	m	Outer Radius of The Rotor.
$\boldsymbol{d}$	m/s^2	Deacceleration of Vehicle.
$\boldsymbol{d_f}$	m/s^2	Deacceleration of The Vehicle on The Front Axle.
$\boldsymbol{d_r}$	m/s^2	Deacceleration of the Vehicle on The Front Axle.
$\boldsymbol{d_r}$	m	Inner Radius of The Rotor.
$\boldsymbol{F}$	N	Force.
$\boldsymbol{F_{Clamping}}$	N	Clamping force of The Calliper.
$\boldsymbol{F_{Friction}}$	N	Friction Force of the Pads.
$\boldsymbol{F_b}$	N	Total Braking Force.
$\boldsymbol{F_{bf}}$	N	Front Braking Force.
$\boldsymbol{F_{br}}$	N	Rear Braking Force.

$\boldsymbol{F_{mc}}$	N	Force on Master Cylinder.
$\boldsymbol{F_{mc}}$	N	Force on The Master Cylinder.
$\boldsymbol{F_p}$	N	Force on The Pedal.
$\boldsymbol{F_{pedal}}$	N	Force on Pedal.
$\boldsymbol{F_x}$	N	Longitudinal Force.
$\boldsymbol{F_{xf}}$	N	Traction Force at The Front.
$\boldsymbol{F_{xr}}$	N	Traction Force at The Rear.
$\boldsymbol{F_y}$	N	Lateral Force.
$\boldsymbol{F_z}$	N	Normal Force.
$\boldsymbol{g}$	m/s^2	Gravity.
$\boldsymbol{h}$	$W/(m^2 * k)$	Coefficient of Convective Heat Transfer.
$\boldsymbol{h}$	m	Height of Gravity Centre.
$\boldsymbol{I_{xx}}$	$kg\ m^2$	Moment of Inertia about The x-axis.
$[\boldsymbol{K}]$		Global Stiffness Matrix.
$\boldsymbol{KE}$	J	Kinetic Energy.
$\boldsymbol{K_{bf}}$		Front Dynamic Weight Transfer.
$\boldsymbol{K_{br}}$		Rear Dynamic Weight Transfer.
$\boldsymbol{K_f}$	$W/(m^2 * k)$	Thermal Conductivity of air.
$\boldsymbol{L}$	m	Length.
$\boldsymbol{l1}$	m	Length from The Front Axle to CG.
$\boldsymbol{l2}$	m	Length from The Rear Axle to CG.
$\boldsymbol{m}$	kg	Mass.
$\boldsymbol{N_u}$		Nusselt Number
$\boldsymbol{n_{avg}}$		Average Nusselt Number.
$\boldsymbol{P_{Rotor}}$	Pa	Pressure on The Rotor.
$\boldsymbol{P_{mc}}$	Pa	Pressure on The Master Cylinder.
$\boldsymbol{P_r}$		Prandtl Number.
$\boldsymbol{P}$	Pa	Pressure.
$\boldsymbol{p}$		Roll Velocity about the x-axis.
$\boldsymbol{Q_H}$	mW/m^2	Heat Flow.
$\boldsymbol{Q_{conv}}$	$W/(m^2 * K)$	Rate of Convective Heat Transfer.
$\boldsymbol{Re}$		Reynolds Number.
$\boldsymbol{R_{hr}}$	N	Longitudinal Load Under Towing Condition.
$\boldsymbol{R_{hz}}$	N	Vertical Load Under Towing Condition.
$\boldsymbol{R_w}$	m	Wheel Radius.
$\boldsymbol{R_{xf}}$	N	Rolling Resistance at The Front.
$\boldsymbol{R_{xr}}$	N	Rolling Resistance at The Rear.
$\boldsymbol{r}$		Yaw Velocity about the z-axis.
$\boldsymbol{T_\infty}$	℃	Bulk Temperature of The Surrounding Fluid.
$\boldsymbol{T_{Df}}$	Nm	Produced Torque by The Front Rotor.
$\boldsymbol{T_{Dr}}$	Nm	Produced Torque by The Rear Rotor.
$\boldsymbol{T_{Film}}$	℃	Film temperature.
$\boldsymbol{T_f}$	℃	Film Temperature.
$\boldsymbol{T_f}$	m/s^2	Torque on Front Wheels.

$\boldsymbol{T_r}$	m/s^2	Torque on Rear Wheels.
$\boldsymbol{T_s}$	℃	Surface Temperature.
$\boldsymbol{T_x}$	Nm	Torques About The x-axis.
$\boldsymbol{t}$	S	Time.
$\boldsymbol{v}$	m/s	Velocity.
$\boldsymbol{\nu}$	m^2s^{-1}	Kinematic Viscosity.
$\boldsymbol{W_f}$	N	Dynamic Load on The Front Axle.
$\boldsymbol{W_r}$	N	Dynamic Load on The Rear Axle.
$\boldsymbol{w_f}$	N	Weight at The Front Wheel.
$\boldsymbol{w_r}$	N	Weight at The Rear Wheel.
$\boldsymbol{w}$	N	Weight at The CG.
$\boldsymbol{q}$		Pitch Velocity about the y axis.
$\boldsymbol{\mu}$		Coefficient of Friction.
$\boldsymbol{\mu_{Pad}}$		Pads Coefficient of Friction.
$\boldsymbol{\beta}$		Sideslip Angle.
$\boldsymbol{\psi}$		Heading Angle.

1. Introduction

Automobiles are composed of many technical systems that operate in harmony to accomplish different tasks within the vehicle. The braking system is one of the most critical systems for the driver's safety as well as the overall performance of the vehicle.

While braking mechanisms have existed since the creation of automobiles, the mechanical drum brake is generally regarded as the foundation of today's braking system. While Louis Renault of France invented the mechanical drum brake in 1902, it was really envisioned a year earlier by Gottlieb Daimler [1].

Vehicles have evolved significantly throughout the years, both in terms of driver demand and competitiveness in the motor vehicle business. Globally, the development of the braking system has increased safety and reduced car accidents.

Automobile competition is fundamental to the most significant improvements in the way vehicles are used today. As a result, an unprecedented quantity of research into improving competitive vehicles are witnessed.

Different braking systems evolved throughout the years of development for a range of vehicles and purposes, and in order to select the suitable system, there is many characteristics and calculations concerning the system, and the vehicle behaviour needs to be taken into consideration, especially when it’s a sport vehicle.

Winning races is an essential thing in motorsport. Entertainment of this kind is regarded as a Research and Development (R&D) activity. It is incredibly complex and intense as it deals with the vehicle's dynamic behaviour.

Numerical simulation can be a very effective method to simulate and optimize the design, thanks to its flexibility of use with different out puts, geometry, materials and boundary conditions.

1.1. Framework

This thesis project can be a part of future opportunities for the Polytechnic Institute of Bragança to compete in the Formula Student competition.

Adding several students in a working group, formed a team with diverse skills and committed with the primary objective of winning the project test (class 2) of the Formula Student competition (Edition 2021).

1.2. The Formula Student Competition

Formula Student is a competition for engineering students that is held annually in England. Student teams worldwide participate in designing, building, testing, and racing Formula miniature racing cars. Cars are evaluated through several tests divided into two main parts: Evaluation in stillness and evaluation in motion. The competition is organized by the Society of Mechanical Engineers, using the same rules as the Formula SAE Competition (FSAE), with additional modifications [2].

The Formula Student Championship was created out of the spirit of competition, utmost delivery, and flair for this car method. This test, intended for engineering students, resulted from a program started in 1981 in the USA by SAE (Society of Automotive Engineers). Nearly two decades after its inception, the FSAE program arrived in Europe, changing its name to Formula Student in England. This competition aims to create a prototype that must above all be high performance in terms of acceleration, braking and driving characteristics, but also must be low cost, easy to maintain, reliable and safe.

The competition consists of four entry classes that teams can participate in: Class 1, for fully built and operational cars as defined in the racing rules; Class 1A is similar to Class 1, with the difference that the vehicle must have an innovative propulsion technology, such as electric propulsion; Class 2 refers to the project category for teams wishing to enter into Class 1 who do not have the fully built and operational vehicle, with the teams being able to take the parts so far produced. It is a category that mainly targets colleges that are participating in the competition for the first time. Finally, Class 2A is also a project class for teams who want to enter Class 1A but do not have a built and operational vehicle. It is a similar class to Class 2, emphasising sustainability, like cars with alternative propulsion systems.

The joint and specialist work of the IPB Motorsport Team will be assessed through two events: static and dynamic. The static event includes the following tests: cost presentation and vehicle modelling to the jury, technical checks, 45 ° and 60 ° tilt testing, braking and

noise testing. In turn, a dynamic event completes the tests: Skid Pad Test, autocross, acceleration, endurance, and fuel economy.

After completing all stages, the results are presented to the teams after a detailed analysis by the jury.

1.3. Motivation and Objectives

The main objective of this work is to design a braking system for the IPB vehicle to enable it to participate in the Formula Student competition while respecting the requirements imposed by the organization controlling this car competition. The car will go through many tests during the competition period, with the brake system being an essential aspect of that car's success.

The following steps were taken to complete this project:

- ✓ Bibliographic search and reading of vehicle dynamics.
- ✓ In-depth research of Formula Student Competition rules and regulations defining design limitations and requirements.
- ✓ Calculating the needed formulas to obtain the values and dimensions for the vehicle.
- ✓ Modelling the components of the brake system on SolidWorks.
- ✓ Performing a thermo-mechanical analysis of the disc rotor using the Finite element method on Ansys software.

1.4. Structure of the Work

This report is divided into six chapters, starting with the introduction of the work and its main aspects in **chapter 1,**

Chapter 2 provides a bibliographic review of the dynamic development of vehicles, the functions of the vehicle's braking system, and the general components of the braking system. It will present the terms and definitions associated with the braking system, clarify the tests that the car will undergo during the Formula Student Contest, and outline the rules for the same competition and the requirements for the braking system,

Chapter 3 consist of explaining the numerical simulation, its methods and implementation,

Chapter 4 approaches the methodology used in the project to choose the components of the system and will explain the simulations and tests performed to verify the system response and obtain the results,

Chapter 5 provides a presentation of the obtained design, discussion of the results obtained, and the adjustments made to the design in response to the results,

Chapter 6 is the conclusion of the work, with some proposals for future work.

2. Theoretical concepts

2.1. Braking concept and its development

The early braking systems to be used in vehicles with steel-rimmed wheels consisted of nothing more than a block of wood and a lever system. The brakes slow the car down or stop it completely, according to the desire of the driver. It is the most critical control element in the event of sudden dangers on the road.

In 1902, a significant test of braking systems was held in New York City. Ransom E. Olds had prepared for the test with an innovative braking system consisting of a single flexible stainless-steel band wrapped around the rear axle drum. The band contracted to grab the drum when the brake pedal was pushed.

The Oldsmobile ended up winning two of the race's nine blue ribbons, and the car's braking mechanism made such an influence on other manufacturers that by 1903, the majority of manufacturers had implemented it. By 1904, almost all automobile manufacturers were producing automobiles with an external brake on each rear wheel.

However, the external brake revealed many severe problems. For instance, on gradients, the brake loosened and eventually gave way, causing the car to roll backwards. Furthermore, its bands and drums rapidly became worn due to the lack of protection from dirt. Getting a new set of brakes every 200 to 300 miles was the standard.

The external brake's issues were solved by the internal brake. There was no need to worry about the automobile moving backwards on gradients as long as the brake shoes remained in contact with the rotors. Drivers could travel more than 1,000 miles between brake renovations since the components were housed in drums and shielded from dirt.

Disc brakes were more or less common on European automobiles in the 1950s, and the most significant issue was noise. Herbert Frood came with the idea of lining pads with asbestos as a solution in 1907, and then many carmakers quickly embraced the concept.

Manufacturers realised the need for more braking power as roads improved and automobiles started to be driven at higher speeds. The key to producing great stopping force was simple to put a brake on each front and back wheel[3].

Modern vehicles use a hydraulic brake system; that is, the brakes work by means of brake fluid under pressure, and by the car's driver, this fluid is pushed through tubes and cylinders, leading to the operation of the brakes.

The kinetic energy must be disposed of to stop a car, but the energy is neither perishable nor created from scratch. Therefore, kinetic energy must be converted into another form of energy, so we use wheel friction to reduce kinetic energy.

2.1.1. Types of Braking Systems

There are mainly two kinds of braking systems used on modern vehicles: disc brakes and drum brakes. Although drum brakes are less expensive, they typically wear out faster and need more maintenance. As a result, they have a worse economic and overall efficiency. On the other hand, Disc brakes have become associated with extraordinary braking force, owing to their greater effectiveness and higher cost than drum brakes. Modern braking systems are essentially defined by the technologies utilised to operate disc or drum brakes, which mainly include the following:

Air Braking System:

Air brakes operate by compressing ambient air and storing it in a storage tank. However, before entering the compressor, air goes through an air filter and drier. This causes a piston-cylinder arrangement brake drum to travel outward and exert force on the brake shoes, producing a friction force between the brake shoes and brake drum[4].

Mechanical Braking System:

It is the type of braking system in which a certain force is applied to the pedal and is transmitted to the final brake drum or disc rotor by mechanical components such as wires, shafts, and camshafts used to transmit motion force to slow the vehicle, as shown in Figure (1). Brake speed or amplitude deceleration depends on surface friction as well as the operating force applied to it.

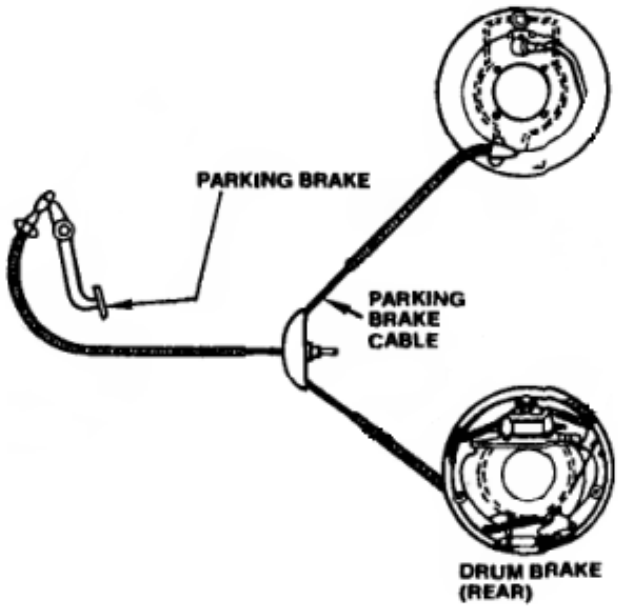

Figure 1 Mechanical Braking System[5]

Mechanical brakes were used in a large number of old vehicles; however, their effectiveness is now outdated [6].

Electrical Braking System:

In an electric braking system, electronic control units and electrical wiring replace hydraulic lines and equipment, while electromechanical actuators replace hydraulic pistons.

A computer transmits information to a control box when the pilot presses the brake pedal. The control box then transforms the electrical impulses into an electromechanical order, which is executed by the actuators on the brake ring, which operate in place of the hydraulic pistons[7].

Hydraulic Braking System:

As the name indicates, fluid pressure is what defines this system, as brake fluid is used to transfer force, where the brake pedal relays the driver foot effort high pressure within the master cylinder that pushes the fluid across the lines to the calliper cylinder piston that causes movement from the pads since it is attached to the piston resulting in a vertical connection between the pads and the disc rotor of the wheel[8]. The schematic diagram of the hydraulic braking system is displayed in Figure (2).

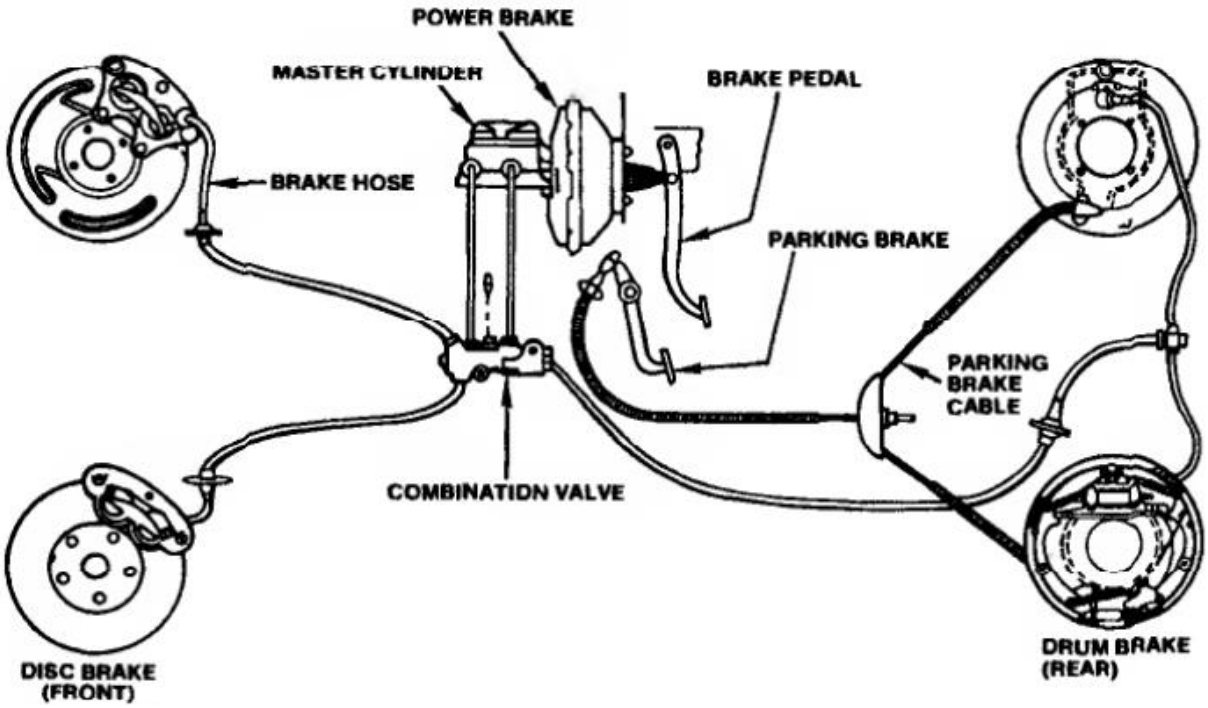

Figure 2 Hydraulic Braking System[5]

2.1.2. Components of a hydraulic Braking System

Brake Pedal:

The driver initiates the braking process by pushing the brake pedal. It is mechanically attached to the master cylinder through the connecting rod. When the driver applies force to the brake pedal, the force is transferred to the master cylinder's piston and delivers force to the master cylinder's piston. The pedal acts to increase this force. The pedal is secured to a holder placed under the car's dashboard or to a holder set at the pedal box's base.

Master Cylinder:

A critical component of any hydraulic braking system, when a driver hits the brake pedal in a race vehicle, he applies force to two hydraulic cylinders referred to as master cylinders. It transmits the mechanical force applied to the pedal. Still, because the force is insufficient to achieve actual braking, the master cylinder converts the mechanical force to high hydraulic pressure and transfers it to the brake calliper [9].

Types of master cylinder:

- Single circuit master cylinder
- Dual circuit master cylinder

The master cylinder and its components are shown in Figure (3).

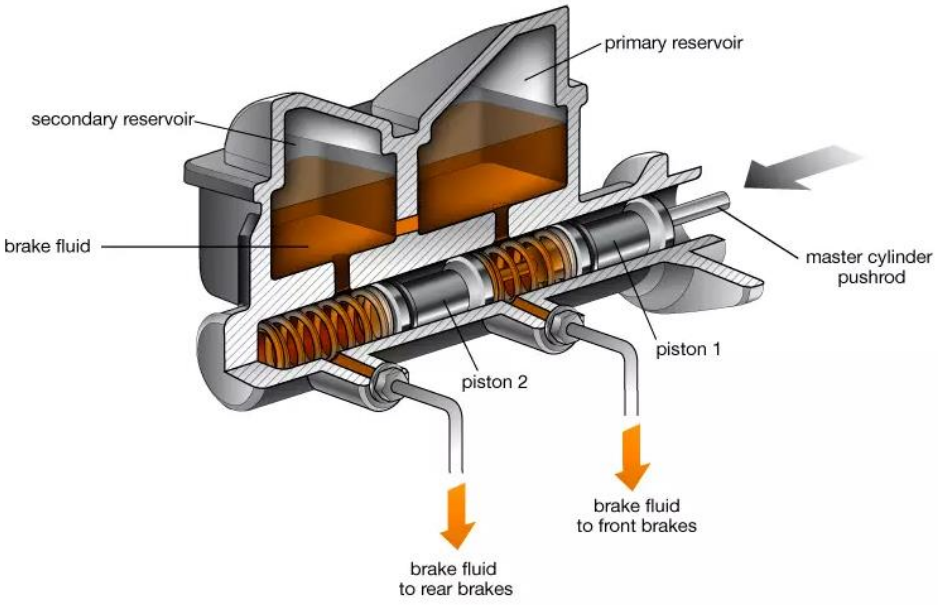

Figure 3 Master Cylinder [10].

- **Reservoir**

It is the container used to store brake fluid; it is typically constructed of plastic. The reservoir for the master cylinder must be situated in such a way that "g" forces cannot expose the feed holes to prevent air from entering the master cylinder. The reservoir volume must be sufficient to fill all calliper pistons with "worn-out" pads (bottomed).

- **Cylinder**

It is the airtight container inside which the piston travels when the brake pedal is pressed. Typically, cylinders are composed of cast iron or aluminium.

- **Piston**

The piston compresses the braking fluid inside the cylinder, resulting in high hydraulic pressure. If binding occurs in the dual master cylinder system equipped with a balance bar, the brake balance may be affected.

- **Returning Spring**

It is a basic coil spring that is employed inside the cylinder to assist the piston and brake pedal in returning to their original positions once the brake pedal is relaxed. For the piston to fully return when the pedal is released, the master cylinder pushrod must be adjusted.

- **Valve**

It is the output valve in a single circuit master cylinder that connects the brake line. The pressurised brake fluid is then transmitted to the calliper through this valve. Due to the dual circuit nature of the tandem master cylinder, two inlet and two exit valves are needed.

Brake fluid:

Brake fluids are critical to the brake system and the safety of cars. As such, they must reflect characteristics and follow quality requirements for the braking system to function effectively [11].

Continuously repeated braking causes an increase in the temperature of the brake fluid. It may result in brake fade, premature wear, brake fluid vaporisation, bearing failure and thermal cracks, affecting braking performance.

Evaporation is a concern because steam is highly compressible compared to liquid, thus affecting the transmission of hydraulic braking force. To ensure that the hydraulic braking system operates well, the temperature of the brake fluid must be maintained below the boiling point. The boiling point of the braking fluid is strongly impacted by the fluid's water content [12].

DOT 3 brake fluid is commonly used for cars in the USA, and its boiling point as a function of water content can be seen in Figure (4).

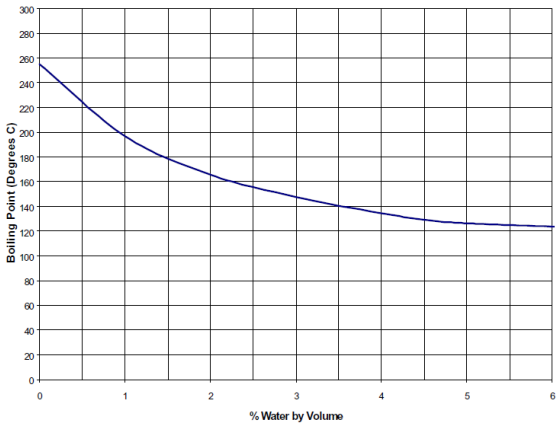

Figure 4 DOT 3 brake fluid boiling point VS water content [12].

Increased water content not only reduces the boiling point of brake fluid but also leads to corrosion in the brake system components affecting overall braking efficiency by increasing the danger of vapour lock [11][12].

Callipers:

Callipers are responsible for securing the brake pistons in place while the brakes are not engaged and for channelling brake fluid into the rear of the brake pistons when the brakes are applied. The calliper is made of multiple components that are critical to the braking system's successful performance, including the following parts: Calliper body, Piston, Retraction seal, Scraper seal, Friction pads, Bleed port, and Fluid inlet port. Floating callipers and Fixed callipers are two significant categories of callipers [13].

A floating calliper has a single piston on the inboard side and is positioned on a guiding pin that acts as cylindrical support for the calliper, allowing it to move in and out laterally, as seen in Figure (5).

When braking pressure is applied to the piston through the braking fluid, the piston pushes out from one side, forcing the calliper to move back on the calliper pins until the brake pad on the non-piston side applies sufficient return pressure to the rotor to stop it.

Fixed callipers are mounted rigidly to the rotor. When the brake pedal is pushed, brake fluid pressurises both pistons simultaneously, forcing them outward to press the brake pads against the rotors [14]. The mechanism of the fixed calliper is described in Figure (6).

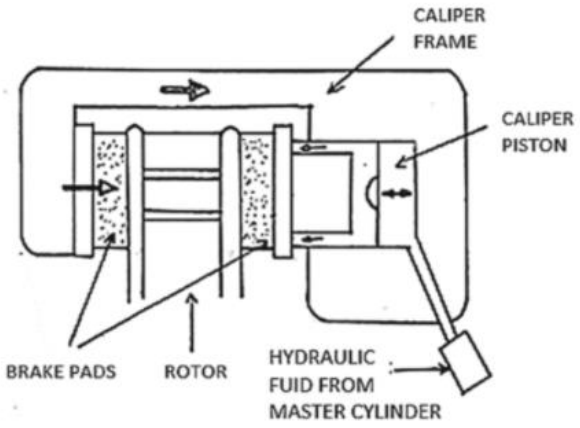

Figure 5 Floating calliper [15].

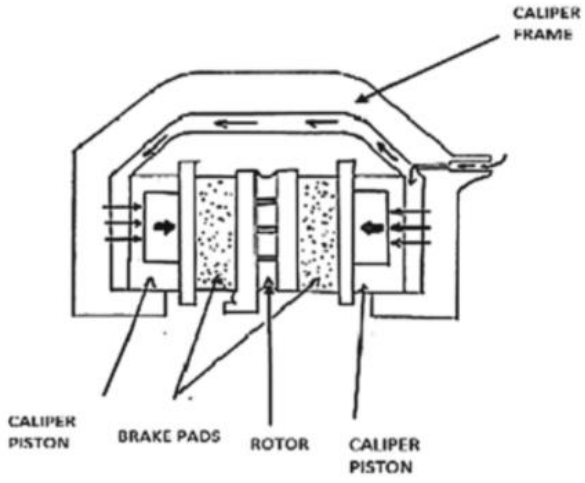

Figure 6 Fixed calliper [15].

A calliper's key characteristics are its lightweight and good stiffness. To generate effective braking force, adequate stiffness and uniformly distributed pressure on the pads are required. That's why automobile companies started converting from ductile iron to such material as an aluminium alloy (A354, 356 and 357). Aluminium alloys help in the weight reduction up to 40% since it has a lower density than ductile iron [16].

Rotors:

The biggest and heaviest component of the disc brake system is the rotor. It is a circular metal plate with two machined friction surfaces on each side that the Pads rub against. The vehicle's kinetic energy is converted into heat energy by friction; therefore, it must quickly absorb and disperse the produced heat [17].

Types:

The disc is made solid or vented regarding the cooling criteria, and they may come drilled or slotted as shown in Figure (7):

A solid disc has no gap between its two sides and is cooled by air flowing over them. In the case of the vented disc, cooling blades are sandwiched between the disc's two sides, and the blades are intended to drive air from the disc's centre to its edge, aimed towards lowering operational temperatures and reducing fading.

Figure 7 Disc rotor types [18].

Brake rotors may be drilled to improve in the evacuation of water and gazes caused by the pads rubbing on the rotor or maybe slotted, which serve the same purpose but also help with shaving the uneven surface of the pads and improve the braking efficiency.

Materials:

The disc is typically made of cast iron due to its adequate material properties such as (hardness, wear resistance, stiffness, and thermal expansion). Aluminium alloy is another material that can be tested as a possible material to be used in rotors due to its lightweight, but it comes with a sacrifice in the previous properties, so a test and proper analysis of the rotor should be performed before it is used. Additional material choices with excellent properties, such as carbon and ceramic materials, come at a high cost[19].

2.2. Definitions and Terminology

Different factors impact the performance of a racing automobile at the level of the braking system. Because no braking system is optimal for every condition that a vehicle may encounter, it is essential to consider each of these aspects and adjust them to the race and track.

2.2.1. Vehicle Dynamics and Brake Distribution

The term "vehicle dynamics" refers to the movement of vehicles on a road surface, including cars, buses, and special-purpose vehicles. Acceleration and braking, riding, and turning are all crucial motions. The dynamic behaviour of a vehicle is dictated by the forces applied to it by the tyres, gravity, and aerodynamics. The vehicle and its elements are analysed to identify the forces generated by each of these sources during a specific manoeuvre and the vehicle's response to these forces. To perform these analyses, an axis system was created to which accelerations and velocities, as well as the forces/torques responsible for them, may be referenced.

Earth-Fixed Axis System

This system is set to the ground. The letters X - Y - Z indicate the three primary directions; X and Y are horizontal and perpendicular to one another, whereas Z is vertical downward, as shown in Figure (8). The vehicle's height and trajectory during a manoeuvre are determined in relation to the Earth's axis.

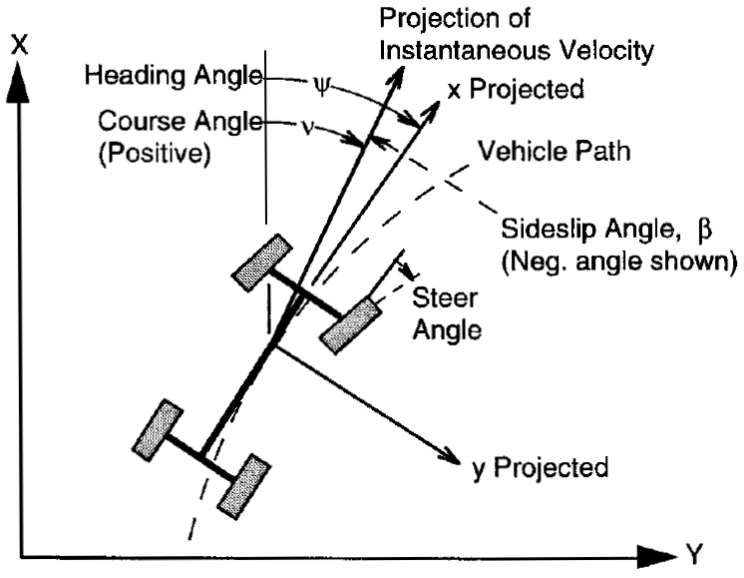

Figure 8 Vehicle in an Earth Fixed Coordinate System [20].

X Forward travel.
Y Travel to the right.
Z Vertical travel (+ downward).

ψ Heading angle.
ν Course angle.
β Sideslip angle.

Vehicle Axis System

The vehicle's movements are specified on-board in a right-hand orthogonal coordinate system that begins at the vehicle's center of gravity (CG) and moves along with it, as explained in Figure (9). Because it is permanently attached to the vehicle, its inertia properties are assumed to be constant [20].

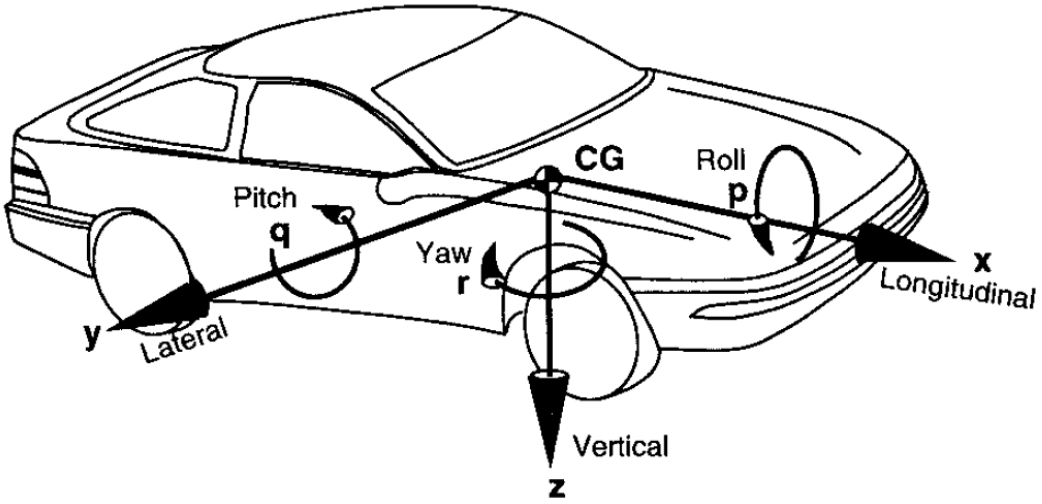

Figure 9 Vehicle axis System [20].

The coordinates are as follows:

x: Forward and on the longitudinal plane of symmetry,
y: Lateral out the right side of the vehicle,
z: Downward with respect to the vehicle,
p: Roll velocity about the x-axis,
q: Pitch velocity about the y axis,
r: Yaw velocity about the z-axis.

Euler angles:

Euler angles describe the connection between the vehicle's fixed coordinate system and the earth's fixed coordinate system. Euler angles are obtained using a three-step angular rotation process.

Beginning with the earth fixed system, the component of the moment vector that tends to turn the vehicle around the z-axis in a positive clockwise direction when seen from the positive z-axis direction, it referred to as Yawing Moment (Yaw).

Then it tends to turn the vehicle around the y-axis in a positive clockwise direction when seen in the positive direction of the y-axis. This component is known as the Pitching Moment (Pitch).

Finally, it rotates the vehicle about the x-axis (roll), positive clockwise to line up with the vehicle fixed coordinate system.

To get the resulting altitude, the rotation arrangement must be followed appropriately.

Forces:

External forces occurring on the car may be summarised as a single force vector consisting of the following components presented in Figure (10).

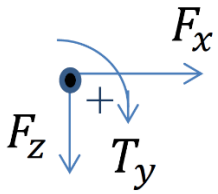

Figure 10 Force's components

Longitudinal Force (***Fx***): is the component of the force vector along the x-axis,

Lateral Force(***Fy***): is the component of the force vector in the y-direction,

Normal Force(***Fz***): is the component of the force vector in the z-direction.

The force associated with the load on a tire acts upward and is hence negative in magnitude (in the negative z-direction). Due to the inconvenient nature of this norm, the SAEJ670e, "Vehicle Dynamics Terminology," defines Normal Force as downward force and Vertical Force as the inverse of Normal Force.

Newton's Second Law

The primary law upon which most vehicle dynamics analysis is based is Newton's Second Law (**NSL**). The principle takes place for translational as well as rotational systems.

Translational system:

The product of a body's mass and its acceleration in a given direction equals the total of the external forces operating on it in that direction (assuming the mass is fixed).

$$\boldsymbol{F_x = m * a_x} \quad (1)$$

Where:

$\boldsymbol{F_x}$: Forces in the x-direction,

$\boldsymbol{m}$: Mass of the body,

$\boldsymbol{a_x}$**:** Acceleration in the x-direction.

Rotational System:

The product of the rotating moment of inertia and the rotational acceleration of a body along a particular axis equals the torques operating on it at that axis.

$$\boldsymbol{T_x = I_{xx} * a_x} \quad (2)$$

Where:

$\boldsymbol{T_x}$: Torques about the x-axis,

$\boldsymbol{I_{xx}}$: Moment of inertia about the x-axis,

$\boldsymbol{a_x}$: Acceleration about the x-axis.

By establishing a boundary around the object of interest, NSL can be applied. At each point of interaction with the outside environment, the necessary forces and/or moments are replaced, together with any gravitational forces. This results in the formation of a free-body diagram.

Dynamic axle load

The weights determine proper brake balance on the wheels, which are in turn determined by the rate of deceleration. The car will not reach its maximum brake deceleration until all four tires are simultaneously pushed to their friction peak. Improper brake balance causes one end to lock up first, reducing the braking power on an axle and resulting in some loss of vehicle control. The objective is to bring both axles up to the lockup point simultaneously.

Balancing the braking outputs on the front and rear axles are accomplished by "proportioning" the vehicle's foundation brakes pressure. Proportioning modifies the braking torque output at the front and rear wheels to match the maximum traction forces attainable. The instantaneous load and the peak coefficient of friction are the first-order determinants of peak traction force on an axle. When the rear axle is braking, a dynamic load transfer happens from the rear to the front axle, resulting in the static load on an axle plus the dynamic load transfer contributions.

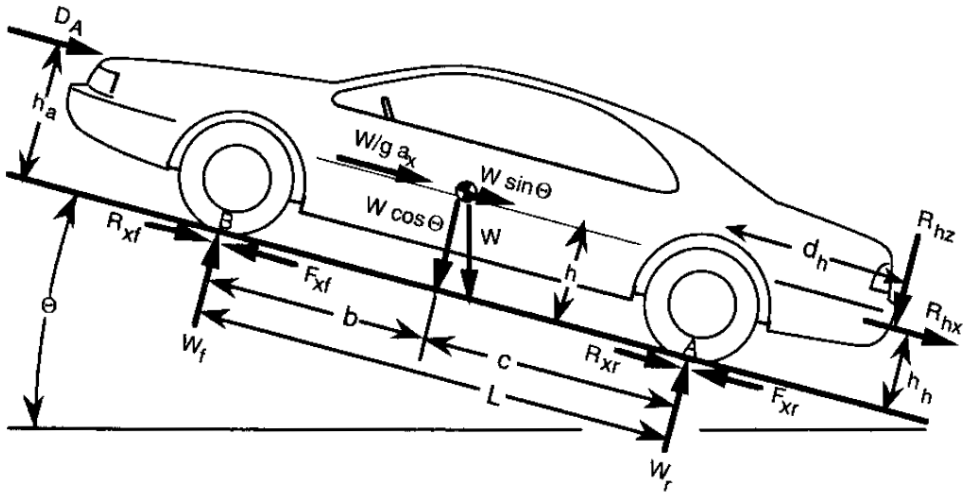

Figure 11 Vehicle under Arbitrary forces[20].

$\boldsymbol{w}$: mg =weight at the CG,

$\boldsymbol{w_f}$: Weight at the front wheel,

$\boldsymbol{w_r}$: Weight at the rear wheel,

$\boldsymbol{F_{xf}}$: Traction force at the front,

$\boldsymbol{F_{xr}}$: Traction force at the rear,

$\boldsymbol{R_{xf}}$: Rolling resistance at the front,

$\boldsymbol{R_{xr}}$: Rolling resistance at the rear,

$\boldsymbol{R_{hr}}$: Longitudinal load under towing condition,

$\boldsymbol{R_{hz}}$: Vertical load under towing condition,

$\boldsymbol{D_A}$: Aerodynamic load acting on the body at ha.

As seen in Figure (11), each axle will carry a static load in addition to load transmitted from rear to front (or vice versa) as a result of other forces operating on the vehicle. The front axle load may be determined by adding torques around point A underneath the rear tires. If the vehicle is not pitching, the total of the torques at point A must equal zero.

$$W_f\ L + D_A\ h_a + \frac{W}{g}\ a_x\ h + R_{hx}\ h_h + R_{hz}\ d_h + Whsin\theta - W\ c\ cos\theta = 0 \quad (3)$$

We can solve for W_f using Eq. (1.2), and for W_r using a similar equation at point B. The axle load equations become as follows:

$$W_f = \frac{(\ W\ c\ cos\theta + R_{hx}\ h_h + R_{hz}\ d_h + \frac{W}{g}\ a_x\ h + \ D_A\ h_a + W\ h\ sin\theta)}{L} \quad (4)$$

$$W_r = \frac{(\ W\ b\ cos\theta - R_{hx}\ h_h - R_{hz}\ d_h - \frac{W}{g}\ a_x\ h - \ D_A\ h_a - W\ h\ sin\theta)}{L} \quad (5)$$

Static load

When the vehicle is static on level ground, the load calculations become much more straightforward.

$\theta = 0$, and the variables R_{hx}, R_{hz}, a_x, and D_A equal zero. Thus:

$$W_{fs} = W\frac{c}{L} \quad (6)$$

$$W_{fr} = W\frac{b}{L} \quad (7)$$

Dynamic load

$$W_f = W\frac{c}{L} + \frac{h}{L}\frac{W}{g}D_x = W_{fs} + W_d \quad (8)$$

$$W_r = W\frac{c}{L} - \frac{h}{L}\frac{W}{g}D_x = W_{fs} - W_d \quad (9)$$

2.2.2. Mechanical Advantage

A pedal magnification doubles the force exerted on the driver's foot. The mechanical pedal advantage is also known as the pedal ratio. For the braking system, Without servo-brakes, it is within (5:1), whereas servo brakes are within (3:1).

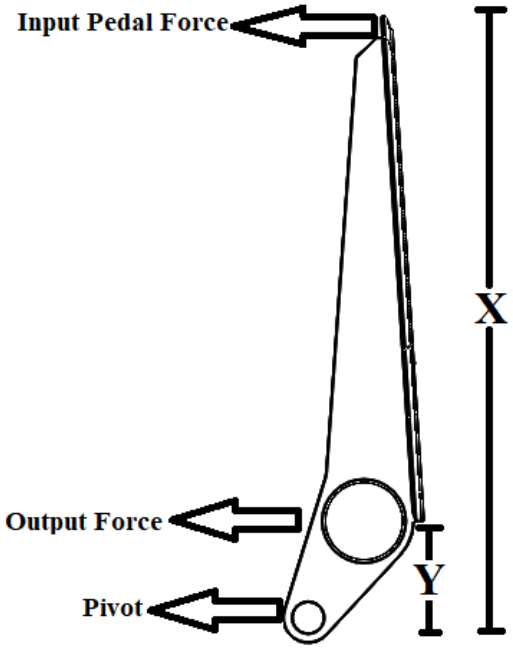

Figure 12 Pedal ratio

The mechanical advantage is defined as the ratio of the distance between the input pedal force and the pivot (X) to the pedal output force point distance from the pedal pivot(Y)[21], as shown in Figure (12).

As a result, the output pedal force can be calculated from Equation (10):

$$F_{mc} = F_{pedal} \times Pedal\ Ratio \quad (10)$$

2.2.3. Pascal's law

Non-compressible fluids, such as oil or water, are used in hydraulic systems to transfer force within a fluid from one place to another. Pascal's law asserts that as the pressure of

a contained fluid increases at any location, it increases equally at all other points in the container [22].

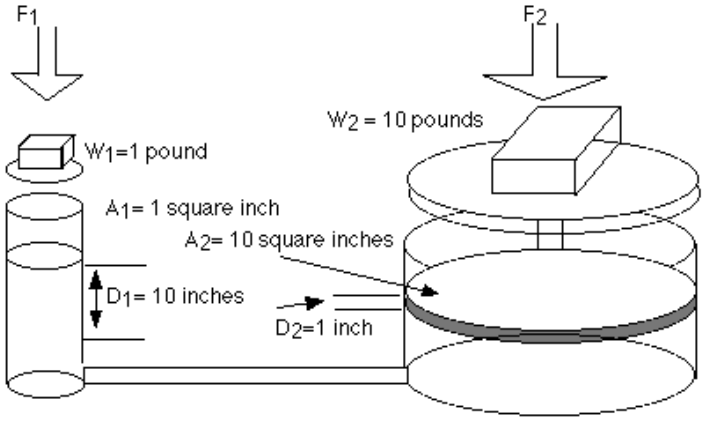

Figure 13 Hydraulic Car Lift [22].

As shown in Figure (13) a hydraulic car lift, Pascal's law allows forces to be multiplied. The cylinder on the left shows a cross-section area of 1 square cm, while the cylinder on the right shows a cross-section area of 10 square cm. The cylinder on the left has a weight (force) of 1 kg acting downward on the piston, which lowers the fluid 10 cm. As a result of this force, the piston on the right lifts a 10 kg weight a distance of 1 cm. Below are the formulas pertaining to this:

Since the pressures stay constant throughout then,

$$P1=P2 \tag{11}$$

And given the fact that pressure is equal to force per unit area, this follows,

$$F1/A1=F2/A2 \tag{12}$$

By substituting, it can be proved that the above values are accurate,

$$1kg/1cm=10kg/10cm$$

Also, the following formula is correct because the amount of fluid displaced on the left side is equal to the amount of fluid raised on the right side,

$$V1=V2 \tag{13}$$

Think of it as a basic mechanism (lever) that uses force. To calculate the mechanical advantage (IMA), first rearrange the Equation into this form:

$$IMA = D1/D2 = A2/A1 \tag{14}$$

For the sample problem above, the IMA would be 10:1.

2.2.4. Forced Convection Heat Transfer

Convection is the heat transfer process that occurs when a fluid is in motion due to bulk fluid motion. Newton's Law of Cooling is the fundamental Equation governing convection heat transfer rate [23].

$$Q_{conv} = hA(T_\infty - T_s) \quad (15)$$

Where:

$\boldsymbol{Q_{conv}}$: The rate of convective heat transfer,

$\boldsymbol{h}$: The coefficient of convective heat transfer,

$\boldsymbol{A}$: The surface area of the item being cooled or heated,

$\boldsymbol{T_\infty}$: The bulk temperature of the surrounding fluid,

$\boldsymbol{T_s}$: The object's surface temperature.

The convective heat transfer coefficient, h, is highly dependent on the fluid characteristics and roughness of the solid surface and the type of fluid flow, laminar or turbulent.

Natural convection and forced convection are two types of convection, depending on how the fluid motion is started. Any fluid motion in natural convection is produced by natural forces such as the buoyancy effect, which causes warmer fluid to rise and colder fluid to descend. In comparison, forced convection occurs when fluid is pushed to flow across a surface or through a tube via the use of an external force such as a pump or fan. Engineers rely heavily on forced convection as a method of heat transmission since it is capable of effectively transporting vast quantities of thermal energy. Forced convection is utilised in a variety of technologies, including air conditioning systems, electronics cooling, and many others.

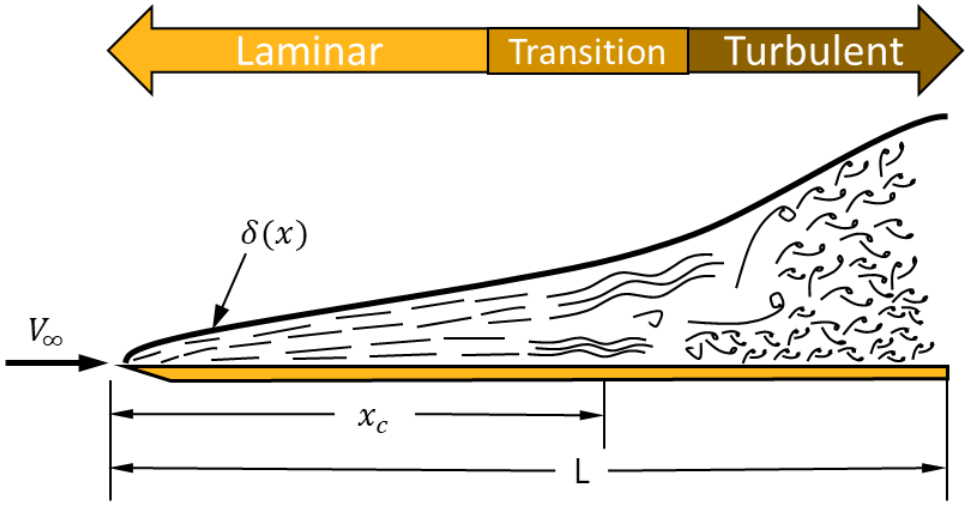

Figure 14 Flow over a flat plate [24].

Flow across a heated flat plate, as demonstrated in Figure (14), is viewed as a major area of interest in the science of heat transfer. A flat plate's friction and heat transfer coefficients may be calculated by solving mass, momentum, and energy conservation equations (either approximately or numerically) [25].

Additionally, they may be quantified empirically. The Nusselt number is determined to be:

$$N_u = \frac{hL}{k} = C\ Re_L^m Pr^n \tag{16}$$

Where *C*, *m*, and *n* are constants and *L* is the flat plate's length. Typically, the fluid's characteristics are tested at the film temperature, defined as:

$$T_f = \frac{T_{s+}T_\infty}{2} \tag{17}$$

Prandtl number ($\boldsymbol{P_r}$): is a measure of the relative thickness of the velocity and thermal boundary layer.

Laminar Flow

For laminar flow across a flat plate, the local Nusselt number are:

$$Nu = \frac{hx}{k} = 0.332\ Re_x^{\frac{1}{2}} Pr^{\frac{1}{3}} \tag{18}$$

$$Pr \geq 0.6$$

where x is the distance from the leading edge of the plate and

$$Re_x = \frac{V_\infty x}{\mu} \tag{19}$$

For the laminar regime, the averaged Nusselt number are as follows:

$$Nu = \frac{hL}{k} = 0.664\, Re_L^{\frac{1}{2}} Pr^{\frac{1}{3}} \tag{20}$$

$$Pr \geq 0.6$$

With a critical Reynolds number of 5×10^5, the length of the laminar plate x_{cr} may be calculated from:

$$Re_{cr} = 5 \times 10^5 = \frac{V_\infty x_{cr}}{v} \tag{21}$$

Turbulent Flow

For turbulent flow across a flat isothermal plate, the local friction coefficient and Nusselt number are as follows:

$$Nu = \frac{hx}{k} = 0.0296\, Re_x^{\frac{4}{5}} Pr^{\frac{1}{3}} \tag{22}$$

$$0.6 \leq Pr \leq 60$$

$$5 \times 10^5 \leq Re_x \leq 10^7$$

Over the isothermal plate in turbulent area, the averaged friction coefficient and Nusselt number are as follows:

$$Nu = \frac{hL}{k} = 0.037\, Re_x^{\frac{4}{5}} Pr^{\frac{1}{3}} \tag{23}$$

$$0.6 \leq Pr \leq 60$$

$$5 \times 10^5 \leq Re_L \leq 10^7$$

2.3. Formula Student Overview and Requirements.

This chapter will detail the testing that the car will take throughout the Formula Student competition and some of the competition rules that are directly relevant to the braking system's design. Additionally, the specifications that a braking system must meet when it is built for the competition will be discussed.

2.3.1. Overview

The competition aims to check university teams ability to conceptualise, design, optimize, manufacture, and race compact, formula-style racing vehicles.

Classifications for the competition include the following:

Internal Combustion Engine Vehicle (CV), Electric Vehicle (EV).

All vehicles must comply with the prescribed guidelines.

The competition begins with a series of technical checks intended to ensure the vehicle's safety and compliance with the regulations.

The competition is organised into several static and dynamic events.

The most points that may be earned from the two classes are described in Table (1).

The team with the highest total points will win their class competition [26].

Table 1 Maximum earned points [26].

CV & EV	
Static	
Business Plan Presentation	75 Points
Cost & Manufacturing	100 Points
Engineering Design	150 Points
Dynamic	
Skid Pad	50 Points
DV Skid Pad	75 Points
Acceleration	50 Points
DV Acceleration	75 Points
Autocross	100 Points
Endurance	250 Points
Efficiency	75 Points
Overall	1000 Points

2.3.2. Technical Requirements for Braking System

All four wheels of the vehicle should have a hydraulic braking system handled by a single control. Two separate hydraulic circuits are required to ensure that efficient braking power is maintained on at least two wheels in the event of a brake system leak or failure. Each hydraulic circuit must have its own reservoir, either separate or dammed.

It is legal to have a single brake acting on a limited-slip differential.

In manual mode, "brake-by-wire" systems are forbidden.

Plastic brake lines that are not armoured are forbidden.

The braking system must be shielded against powertrain failure, contact with any moveable component, and accidental collision.

Any piece of the braking system positioned on the sprung section of the vehicle shall not extend beyond the chassis' lower surface inside view.

The brake pedal and its installation must be capable of withstanding a force of 2 kN without causing any damage to the braking system or pedal box. This may be verified by pushing the pedal with the highest force that any official can exert while sitting correctly.

Steel or aluminium must be used to fabric the brake pedal or machined from steel, aluminium, or titanium [26].

Brake Over-Travel Switch

As part of the shutdown circuit, a brake pedal over-travel switch must be placed on the vehicle. This switch must be set in such a way that when at least one of the braking circuits fails, the brake pedal over-travel opens the shutdown circuit. This must operate in all imaginable brake pedal and brake balance settings without causing damage to any vehicle component.

Brake Light

The vehicle must be equipped with a single brake light that illuminates only when the hydraulic brake system is actuated.

2.3.3. Technical Inspections

The competition begins with a series of technical inspections designed to ensure the vehicle's safety and adherence to the regulations. The dynamic area is where technical inspections and other dynamic activities take place. Vehicles must have passed all technical checks in order to utilise the practise track.

2.3.4. Brake Test Procedure

All four wheels must be locked, and the vehicle must come to a complete stop in a straight path at the end of an acceleration run defined by the examiners without stopping the engine. The brake light and TSAL illumination will be inspected, and inspectors will evaluate if the lighting is sufficient for external observation [26].

2.3.5. Formula Student tests

The car must take a series of tests during the Formula Student competition to verify that it fits the rules' standards and evaluate its overall performance, as follows:

Static

- ✓ Design, Cost and Sustainability, and Business Presentation Judging,
- ✓ Technical and Safety Scrutineering,
- ✓ Tilt Test,
- ✓ Brake and Noise Test.

Dynamic

- ✓ Skid Pad,
- ✓ Sprint,
- ✓ Acceleration,
- ✓ Endurance,
- ✓ Fuel Economy.

2.3.6. Wheels

Any wheel mounting technique that employs a single retaining nut must have a mechanism that prevents the nut and the wheel from being unfastened. Lug bolts and studs used in standard wheels must be manufactured of steel and are classified as engineering fasteners. Teams who use modified lug bolts, studs, or bespoke designs will

be expected to demonstrate that they used sound engineering procedures in their design. The lug bolts and studs on the wheels cannot be hollow.

2.3.7. Tires

Vehicles must be equipped with two distinct tire types:

Dry tires: The tires on the vehicle at the time of technical examination are referred to as the vehicle's "dry tires".

Wet tires: Wet tires may be any size or kind of treaded or grooved tyre as long as the following conditions are met:

- The tread pattern or grooves were moulded in or cut by the tyre manufacturer or their designated representative.
- A minimum tread depth of 2.4 mm is required.

Tires mounted on the same axle must be identical in terms of brand, size, and compound

.

3. Numerical simulation

The product development process consists of many stages, from conceptual design to manufacturing. Simulation is a critical early stage in the process. Engineers use simulation to determine how their product design will function in the actual world. Simulations may be carried out experimentally or numerically, as shown in Figure (15), utilizing techniques such as Finite Element Analysis (FEA). FEA has become widespread in recent years and has grown to become the foundation of a multibillion-dollar business. Numerical solutions to even the most complex stress issues can now be found regularly using FEA.

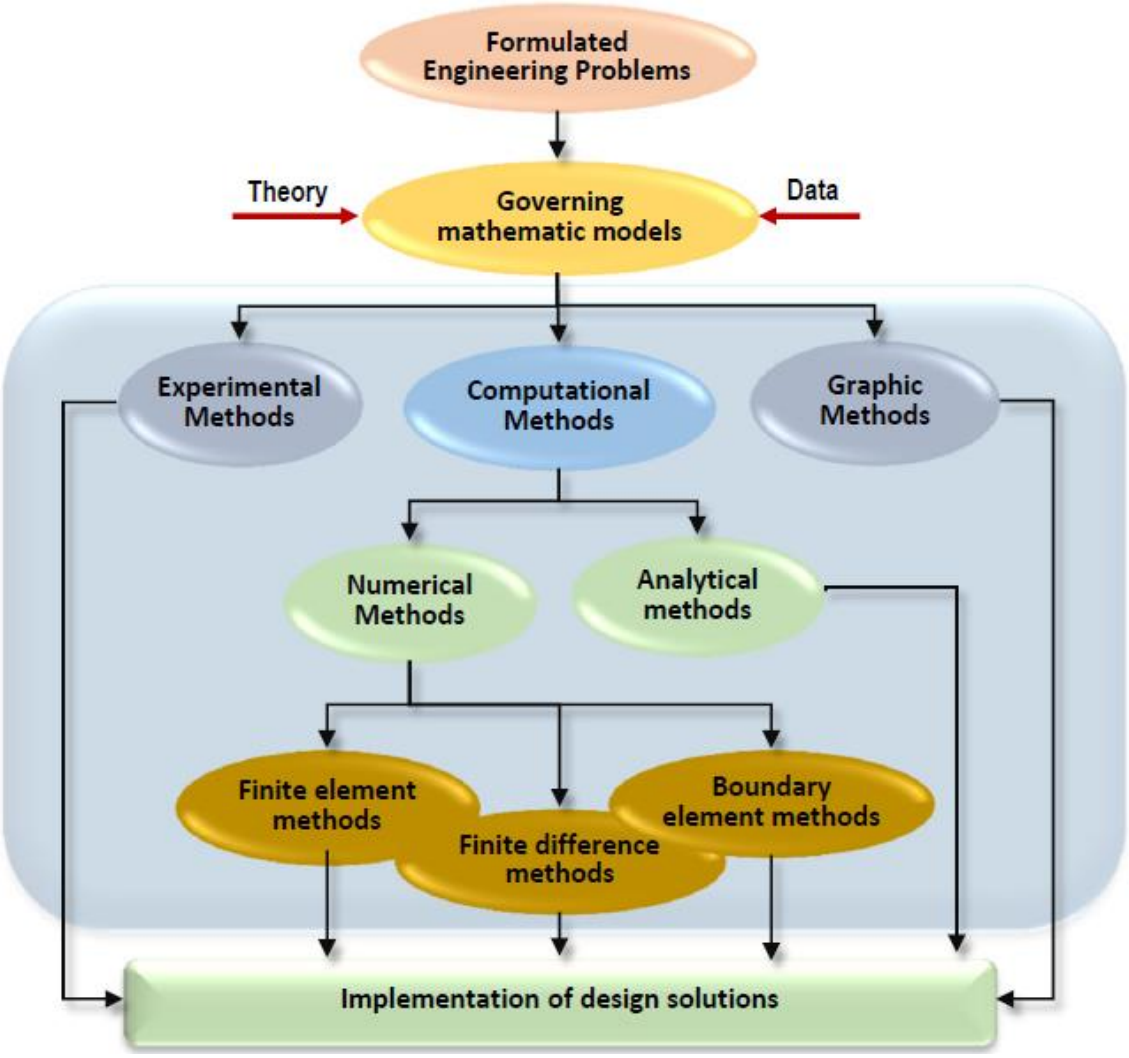

Figure 15 Methods to solve an engineering problem[27].

3.1. Numerical Methods

Numerical methods are often employed to solve Partial Differential Equations (PDEs) numerically, and the solution of PDEs should be consistent, stable, and convergent. The most frequently used numerical methods are as follows [28]:

- Finite Element Method (FEM)
- Boundary Element Method (BEM)
- Finite Volume Method (FVM)
- Finite Difference Method (FDM)

3.2. Finite Element Method

FEM is the most used numerical method, and it is a numerical method for determining the approximate solution to a system of PDEs over a specified domain. The main difficulty in solving the PDEs is constructing a function base that approximates the answer. There are several approaches for creating the approximation base, and The formulation used determines how this is done. The Finite Element Method performs very well for solving PDEs across complicated domains that change over time. Linear, nonlinear, buckling, thermal, dynamic, and fatigue analysis are possible applications[29] [30].

3.3. Discretization of problem

All things in real life are continuous. This implies that no physical space exists between two successive particles. According to material science, all objects are composed of tiny particles, molecules, and atoms, which are held together by the force of attraction.

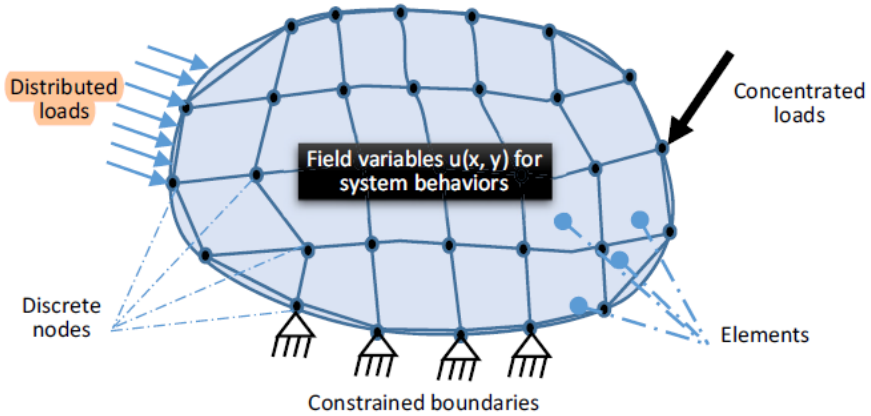

Figure 16 Discretization of Problem [30]

It is challenging to solve a real-world issue using the continuous material method. All numerical methods begin with the goal of simplifying the issue via discretization. In other words, nodes function similarly to atoms, and the space between them is filled by an object known as an element. Calculations are performed at the nodes, and the elements' values are interpolated. Figure (16) describes the Discretization method [31].

3.4. Degree of freedom

The minimum of elements (motion, coordinates, temperature, etc.) needed to fully describe the location and state of an entity in space are indicated in Degrees of Freedom (DOFs).

DOFs is a critical topic. It is used in FEA to represent individual computation points. The total number of DOFs in a particular mesh model equals the number of nodes multiplied by the number of degrees of freedom per node. Not all elements have six DOFs per node.

The number of DOFs varies according to the element type (1D, 2D, or 3D), the element family (thin shell, plane stress, plane strain, membrane, etc.), and the kind of analysis. For instance, a light shell element used in a structural analysis has six degrees of freedom per node (unknown displacement, three translations, and three rotations). In contrast, the identical element used in the thermal analysis has a single degree of freedom per node [31].

3.5. Nodes and elements

After discretizing a continuous system, it is represented by elements and nodes. Elements are continuous subdomains, while nodes are a collection of corners that represent elements. State or field variables are used to characterise the actions of a particular entity. Generally, increasing the number of lines and calculation points lowers the error margin, as shown in Figure (17), thus improving accuracy.

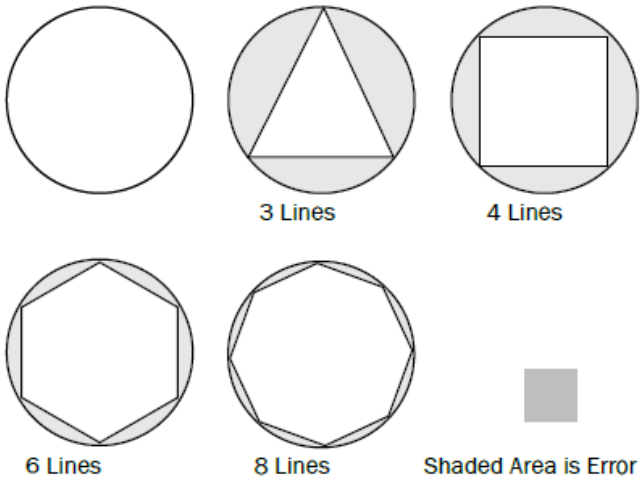

Figure 17 Nodes and Elements[31].

However, constructing a highly fine mesh with the most significant number of nodes and elements feasible is not necessarily the optimal method since the solution time is directly related to the number of nodes and elements (DOFs) [31].

3.6. Meshing

Any continuous system has an infinite degree of freedom. Thus, solving the problem in this manner is unachievable. The FEM employs meshing to accomplish two primary goals:

Firstly, it discretizes a continuous domain into a set of elements and nodes, reducing the number of unknowns in the problem to a manageable number. Secondly, it approximates the system solution by assembling a group of simple sub-models for elements, as shown in Figure (18).

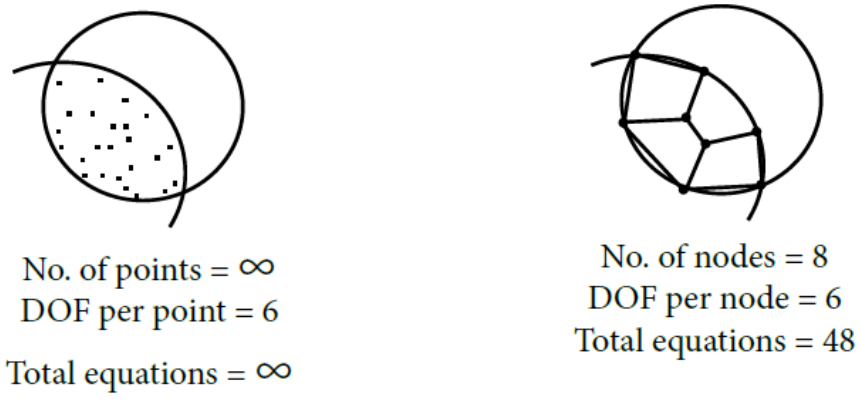

Figure 18 Meshing Process[31]

Even though the computer does the meshing procedure automatically, but to create a decent mesh, manual involvement is required.

3.7. Advantages of FEA

- Visualization,
- Design cycle time,
- No. of prototypes,
- Testing,
- Optimum design.

3.8. Stiffness matrix

The primary characteristics of a finite element are embodied in the element stiffness matrix, which contains information about the geometric and material behaviour of the element and defines how much displacement each node in the element will experience when a set of forces and moments are applied to it. This matrix is critical for solving displacements at each node of a mesh. The linear static analysis equation is as follows:

$$[\boldsymbol{F}] = [\mathbf{K}][\mathbf{D}] \tag{24}$$

Typically, the force is known, the displacement is unknown, and the element's stiffness is a typical feature.

This implies that if we construct the stiffness matrix for a particular shape, such as a line, quadrilateral, or tetrahedron, we can mesh it and then solve the nodal displacements to compute the strain and eventually the stresses.

The term stiffness matrix is also used for finite elements utilized in the analysis, such as fluid flow and heat transfer, since the matrix reflects the element's resistance to change when exposed to external forces.

Various techniques exist for calculating these stiffness matrices, which are essentially founded on the basic concept of equilibrium.

- Direct method,
- Variational method
- Weighted residual method.

A typical finite element mesh can easily have a hundred thousand degrees of freedom, making it impossible to solve by hand. Therefore, applying the finite element method to anything more complicated than a straightforward model requires the use of appropriate software, which performs many of the necessary tasks such as calculating the stiffness matrices, assembling the global stiffness matrix, and solving the model. Nevertheless, the engineer is responsible for correctly defining the situation, selecting an appropriate mesh, understanding, and verifying the outcomes.

3.9. FEA Procedures

There are three general stages in using any commercial software:

Pre-processing

- **CAD Data:** A FEM simulation process starts with the import of the CAD geometry (STEP, IGES and solidThinking) into the pre-processor.
- **Meshing:** To convert an infinite DOF to a finite one, use discretization.
- **Material Information:** Material properties (e.g. Young's Modulus) is given to the elements once meshing is performed.
- **Boundary condition:** Several loads and restrictions are included in the model to reflect the loading circumstances under which the part operate.

Processing

Little can be done during the solution phase of a basic linear static analysis or an eigenfrequency investigation. The default settings of the Finite Element application perform an adequate job of handling these groups of issues. Practice teaches you that if the solution process is interrupted due to an "error," it is most often due to model construction errors.

Post-processing

Following the conclusion of the solution, the simulation results are post-processed. The stresses and deformations of the component are plotted and analysed to see how it reacted to the different loading conditions. Adjustments can be made to the design in response to the results, and a new analysis can be performed to determine the effect of the modifications.

3.10. ANSYS Workbench Software

Analyses are created in ANSYS Workbench as systems that may be merged into a project. The project is guided by a schematic process that handles the systems' relationships. Interaction is possible with ANSYS Workbench's native programmes directly from the schematic (workspaces). Native workspaces include those for planning a project, engineering data management, and design exploration.

Analysis types

Workbench allows users to begin an analysis by selecting an analysis system from the toolbox. Then a project schematic will emerge with all the essential components for that analysis type. Some of these analysis systems are as follows:

- Electric
- Fluid Flow
- Linear Buckling
- Static Structural
- Transient Structural
- Transient Thermal
- Steady-State Thermal
- Shape Optimization
- Thermal Electric

Transient Thermal Analysis

Temperatures and other thermal parameters that fluctuate over time are determined using transient thermal studies. The variance of temperature distribution over time is essential in various applications, such as with the cooling of electronic packages or a quenching analysis for heat treatment. Attention also raises that the temperature dispersion produces thermal stresses that might result in failure. In these instances, the temperatures obtained from a transient thermal analysis are utilised as inputs to structural analysis for the purpose of thermal stress evaluation. The ANSYS solver can be used to do transient thermal analysis.

Numerous heat transfer applications, including heat treatment, electronic package design, nozzles, engine blocks, pressure vessels, and fluid-structure interaction, requires transient thermal analysis [32].

Static Structural Analysis

Static structural analysis is performed on structures or components to calculate the deformation, stress, strain, and force levels induced by loads with negligible inertia and damping effects. Steady loading and response conditions are assumed; that is, the loads and the structure's response are assumed to vary slowly with respect to time.

The ANSYS solver can be used to compute a static structural load. The following forms of loading can be used in a static analysis:

- Externally applied forces and pressures,
- Steady-state inertial forces (such as gravity or rotational velocity),
- Imposed (nonzero) displacements,
- Temperatures (for thermal strain).

Linear and nonlinear static structure analyses are also possible. Deformation, plasticity, stress stiffening, contact (gap) elements, hyper elasticity, and anything else are possible, but available nonlinearities can differ from one solver to another [32].

Displacement

A three-dimensional body consists of a volume and a surface. The coordinates of any point on this body are x, y, and z. A portion of this body's territory may be limited by boundary conditions that specify displacements. The presence of forces per unit of area or concentrated forces causes deformations in the body, which result in changes in the structure's geometry. Internal forces generated at each place create a condition of stress.

Equivalent Stress (von Mises):

The equivalent von mises stress is a frequently used result of finite element stress analysis. Contour plots are generally used to depict the distribution of the von mises equivalent stress inside a component since they enable the identification of places at risk of yielding. Equivalent stress is often used to describe the state of a ductile material. In engineering, this basic scalar number is used to indicate if a material has yielded or failed[33].

4. Methodology

4.1. Introduction

This chapter will discuss the procedure used to design or select each braking system component after calculating the required braking force, which was determined by considering the vehicle's weight, the centre of gravity, wheelbase, and other critical factors. It will then discuss the various stages followed to perform a transient and static simulation on the brake rotor using the finite element analysis.

4.2. Vehicle calculation:

It is worth noting that all the relations assume maximum system efficiency. All dimensions in the following Table (2) are in standard international units.

Table 2 Data required for calculation

Data Required for Calculation			
No.	Parameters	Values	Units
1	Pedal Ratio	1/5	N/A
2	Master Cylinder Bore Size	19.1	mm
3	Calliper Piston Diameter	25.4	mm
4	Front Brake Rotor	205	mm
	Rear Brake Rotor	180	mm
5	Vehicle Mass	260	kg
6	Wheelbase (L)	1,6	m
7	CG (h)	0,25	m
8	L2 (Rear axle to CG)	0,72	m
9	L1 (Front axle to CG)	0,88	m
10	Tire Rad	266,7	mm

4.2.1. Dynamic load on axels

In order to verify and confirm the selected components, we had to do a dynamic load calculation to obtain the needed torque on each axle:

Dynamic load of the front axel

$$W_f = w\frac{l2}{L} + w * \mu * \frac{h}{L} \quad (26)$$

Where:

W_f: Dynamic load on the front axle,

w: Weight of the vehicle,

L**:** Wheelbase,

$l2$: length from the rear axle to CG,

μ: Coefficient of friction,

h: Centre of gravity.

$$W_f = 2548\frac{0.720}{1.6} + 2548 * 0.7 * \frac{0.25}{1.6}$$

$$\underline{W_f = 1425.29\ N}$$

Rear axel

$$W_r = w\frac{l1}{L} - w * \mu * \frac{h}{L} \quad (27)$$

Where:

W_r: Dynamic load on the rear axle,

$l1$: length from the front axle to CG.

$$W_r = 2548\frac{0,88}{1.6} - 2548 * 0.7 * \frac{0.25}{1.6}$$

$$\underline{W_r = 1122.71N}$$

4.2.2. Weight distribution percentage

Front

$$K_{bf} = \frac{W_f}{W} \quad (28)$$

Where:

$\boldsymbol{K_{bf}}$: Front dynamic weight transfer.

$$\boldsymbol{K_{bf} = \frac{1425.29}{2548}}$$

$$\underline{\boldsymbol{K_{bf} = 0.56 = 56\%}}$$

Rear

$$\boldsymbol{K_{br} = \frac{W_r}{W}} \quad (29)$$

Where:

$\boldsymbol{K_{br}}$: Rear dynamic weight transfer.

$$\boldsymbol{K_{br} = \frac{1122.71}{2548}}$$

$$\underline{\boldsymbol{K_{br} = 0.44 = 44\%}}$$

4.2.3. Braking Force

Since we consider that the vehicle mass is 260 kg and the typical coefficient of friction between asphalt and rubber for the dry road is 0.7, according to Jones and Childers [34], the total braking force can be calculated using Equation (30) :

$$\boldsymbol{F_b = \mu * W} \quad (30)$$

Where:

$\boldsymbol{F_b}$: Total braking force.

$$\boldsymbol{F_b = 0.7 * 2548}$$

$$\underline{\boldsymbol{F_b = 1783.6\ N}}$$

Front braking force:

$$\boldsymbol{F_{bf} = K_{bf} * F_b} \quad (31)$$

Where:

F_{bf}: Front braking force.

$$F_{bf} = 0.559 * 1783.6$$

$$\underline{F_{bf} = 997.032\ N}$$

Rear braking force:

$$F_{br} = K_{br} * F_b \quad (32)$$

Where:

F_{br}: Rear braking force.

$$F_{br} = 0.440 * 1783.6$$

$$\underline{F_{br} = 784.784\ N}$$

4.2.4. Deacceleration of Vehicle

The total deacceleration of the vehicle can be calculated according to the following Equation:

$$d = \frac{\mu * (W_f + W_r)}{\left(\frac{W}{g}\right)} = \frac{Fb}{M} \quad (33)$$

Where:

d: Deacceleration of vehicle,

g: Gravity,

M: Mass.

$$d = \frac{1783.6}{260}$$

$$\underline{d = 6.9\ g}$$

Through Equation (34), it is possible to calculate the Front deacceleration of the vehicle:

$$d_f = \frac{\mu * (W_f + W_r)}{\left(\frac{W}{g}\right)} = \frac{F_{bf}}{M} \quad (34)$$

Where:

$\boldsymbol{d_f}$: Deacceleration of the vehicle on the front axle.

$$\boldsymbol{d_f = \frac{997.032}{260}}$$

$$\underline{\boldsymbol{d_f = 3.8g}}$$

Similarly, Equation (35) will be used to compute the vehicle's rear deceleration:

$$\boldsymbol{d_r = \frac{\mu * (W_f + W_r)}{\left(\frac{W}{g}\right)} = \frac{F_{br}}{M}} \quad (35)$$

Where:

$\boldsymbol{d_r}$: Deacceleration of the vehicle on the front axle.

$$\boldsymbol{d_r = \frac{784.784}{260}}$$

$$\underline{\boldsymbol{d_r = 3.0g}}$$

4.2.5. Torque on wheels

Torque on the front wheels is given as Equation (36):

$$\boldsymbol{T_{ff} = R_w * F_{bf}} \quad (36)$$

Where:

$\boldsymbol{T_f}$: Torque on front wheels,

$\boldsymbol{R_w}$: Wheel radius.

$$\boldsymbol{T_f = 0.2667 * 997}$$

$$\underline{\boldsymbol{T_f = 265.9\ Nm}}$$

$$\underline{\boldsymbol{Each\ wheel = 133.0Nm}}$$

Torque on the rear wheels is given by Equation (37):

$$\boldsymbol{T_{fr} = R_w * F_{br}} \quad (37)$$

Where:

T_r: Torque on rear wheels.

$$T_r = 0.2667 * 784.784$$

$$\underline{T_r = 209.3\ Nm}$$

$$\underline{Each\ wheel = 104.7Nm}$$

4.3. Braking system calculation and characteristics of selected components

This section will go through the characteristics of the various parts of the braking system, beginning with the pedal and working our way up to the tyre.

4.3.1. Pedal

Although it is often neglected, selecting the pedal ratio is critical. The pedal will be very sensitive if the proper pedal ratio is not attained.

Because the formula student competition does not permit the use of booster brakes, the human power has been increased by the pedal leverage ratio and applied to the master cylinder.

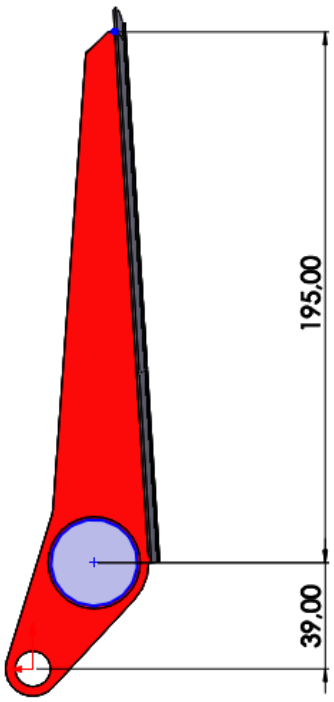

Figure 19 Pedal dimensions.

The pedal ratio that best suited the design and computation was determined to be 5:1, as shown in Figure (19), which is one of the recommended ratios for manual systems.

4.3.2. Balance bar

Due to the dual master cylinder configuration, a balancing bar is required to convert the force to the master cylinders; one master cylinder feeds the front brakes, while the other provides the rear brakes.

The AP RACING CP5500 was employed in the system, as seen in Figure (20).

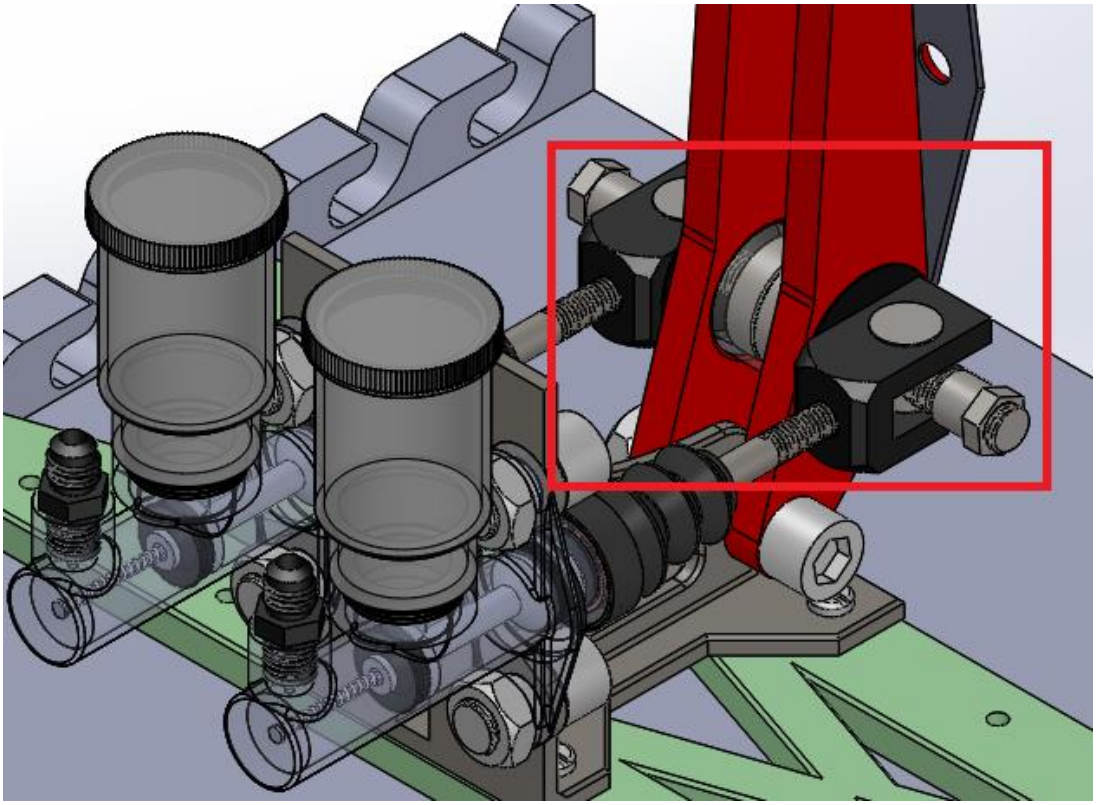

Figure 20 Balance bar.

4.3.3. Master Cylinder

As seen in Figure (21), the master cylinder chosen is the CP2623 Type from AP RACING, which meets the specifications listed in Table (3):

Table 3 CP2623 Master cylinder specs.

Material	**Aluminium Alloy**
Weight	0.31kg
Bore size	19.1mm
Full Stroke	25.4 mm

Figure 21 Master cylinder [35].

Equation (38) was used to determine the force transmitted from the pedal to the master cylinder.

$$\boldsymbol{F_{mc} = F_p * Pedal\ Ratio} \tag{38}$$

Where:

$\boldsymbol{F_{mc}}$: Force on the master cylinder,

$\boldsymbol{F_p}$: Force on the pedal.

$$\boldsymbol{F_{mc} = 300 * 5}$$

$$\boldsymbol{\underline{F_{mc} = 1500\ N}}$$

Next, the hydraulic pressure was determined in Equation (39) by dividing the force on the master cylinder by its area.

- **Pressure on the master cylinder**

$$\boldsymbol{P_{mc} = \frac{F_{mc}}{A_{mc}}} \tag{39}$$

Where:

$\boldsymbol{P_{mc}}$: Pressure on the master cylinder,

$\boldsymbol{A_{mc}}$: Area on the master cylinder.

Therefore, the area of the master cylinder must be determined first using Equation (40).

$$\boldsymbol{A_{mc} = \frac{\pi * D^2}{4}} \tag{40}$$

Where:

$\boldsymbol{D_b}$: Bore diameter.

$$\boldsymbol{A_{mc} = \frac{\pi * (19.1)^2}{4}}$$

$$\boldsymbol{A_{mc} = 286.521 * 10^{-6} m^2}$$

Using the computed values

$$\boldsymbol{P_{mc} = \frac{1500}{286.521 * 10^6}}$$

$$\boldsymbol{\underline{P_{mc} = 5.2 * 10^6 \frac{N}{mm^2}}}$$

4.3.4. Reservoir

A 75cc AP racing brake fluid reservoir, as shown in Figure (22), was selected because it is compatible with the master cylinders and meets the required conditions for having a suitable volume and not reacting with the fluid.

Figure 22 Reservoir of brake fluid [36].

Reservoirs were chosen to be compatible with the brake bleeding equipment, ensuring that brakes could be bled effectively. It may be attached directly to the master cylinder or mounted higher near the pedal box to avoid air leakage into the system, affecting the brake feel and efficiency.

4.3.5. Callipers

Selecting the calliper depends on many different factors such as the number of pistons, piston size, mounting style and weight CP4226 calliper.

As seen in Figure (23), the CP4226 calliper is lug mount style and has two pieces of an aluminium body. Its pistons are made of aluminium, and other specifications are included in Table (4).

Table 4 CP4226 calliper specs.

Piston Diameter	25.4 mm
Number of pistons	2
Disc Thickness	4 mm
Weight	0.24 kg

Figure 23 AP Racing CP4226 calliper [37].

Fixed calliper brakes are preferred for racing since they have a limited volume capacity and may be made very light. Moreover, owing to the excellent stiffness of fixed callipers, they show very consistent brake pad wear.

Two piston callipers are adequate for the formula student cars' braking force level. The same callipers were used for the front and rear.

Force on calliper and clamping force

Given the fact that clippers convert hydraulic line pressure to clamping force translated to the pad, the clamping force was determined starting by Equation (41) which calculate the force in the calliper depending on the calliper piston area

$$\boldsymbol{F_{Calliper} = P_{mc} * A_{Calliper}} \quad (41)$$

Where:

$\boldsymbol{F_{Calliper}}$: Force on the calliper,

$\boldsymbol{A_{Calliper}}$: Area of the calliper.

Equation (42) was used to get the piston area based on the piston diameter.

$$\boldsymbol{A_{Calliper} = \frac{\pi * D_{cp}^2}{4}} \quad (42)$$

Where:

$\boldsymbol{D_{cp}}$: Diameter of callipers piston.

$$\boldsymbol{A_{Calliper} = \frac{\pi * (25.4)^2}{4} = 506.707 * 10^{-6}\ m^2}$$

$$\boldsymbol{F_{calliper} = 5.23522 * 10^6 * 506.707 * 10^{-6}}$$

$$\underline{\boldsymbol{F_{calliper} = 2652.72}}$$

Next, the force produced in a calliper is multiplied by the number of pistons in Equation (43) to get the clamping force.

$$\boldsymbol{F_{Clamping} = F_{Calliper} * Number\ of\ pistons} \quad (43)$$

Where:

$\boldsymbol{F_{Clamping}}$: The clamping force of the calliper.

$$\boldsymbol{F_{Clamping} = 2652.72 * 2}$$

$$\underline{\boldsymbol{F_{Clamping} = 5305.45\ N}}$$

4.3.6. Pads

The primary purpose of the braking system is to convert the clamping force to friction force delivered to the rotor using pads. As a result of CP4226 calliper selection, APRACING-selected pads are the CP4226D27 kind.

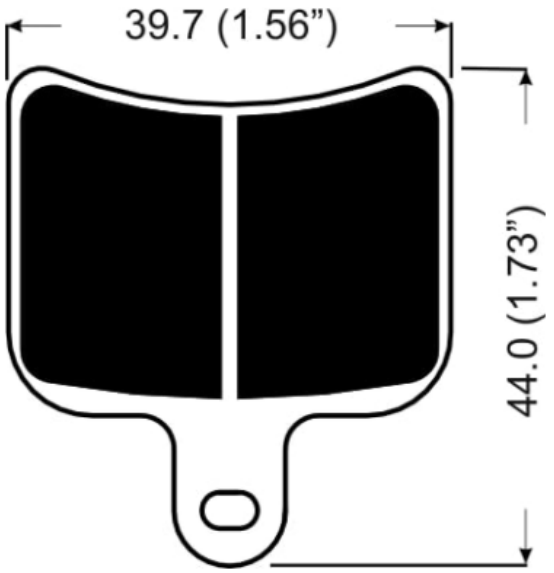

Figure 24 CP4226D27 Pad dimensions [38].

The pads are shown in Figure (24) are available with APH420 material. This SBS (hard rubber) based substance is made of soft organic compounds and is used on both stainless steel and cast-iron discs. And It has an average friction coefficient of 0.39.

The friction force mentioned in Equation (44) is calculated by multiplying the pad's coefficient of friction by the clamping force.

$$\boldsymbol{F_{Friction} = \mu_{pad} * F_{Callmping}} \quad (44)$$

Where:

$\boldsymbol{F_{Friction}}$: Friction force of the pads,

$\boldsymbol{\mu_{pad}}$: Pads coefficient of friction.

$$\boldsymbol{F_{Friction} = 0.39 * 5305.45}$$

$$\underline{\boldsymbol{F_{Friction} = 2069.12N}}$$

$$\underline{\boldsymbol{Each\ pad = 1034.5N}}$$

4.3.7. Rotors

Due to the rotor's fixed connection to the wheel's movement is employed to convert friction force into braking torque, which is proportional to the rotor's effective radius. The rotor's capacity for absorbing braking torque should be sufficient. The rotor material should be very thermally conductive and capable of effectively dissipating heat. Later the material will be selected depending on the simulation results which will be performed on the front and rear rotors with two different materials.

Front rotor torque

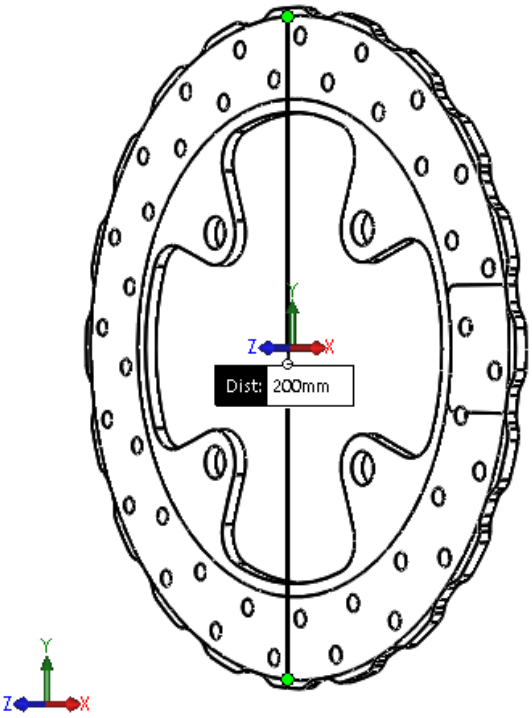

Figure 25 Front Rotor with section lines illustrating the region of contact with the pad.

Increasing the rotor radius reduces the amount of effort needed by the driver. The brake calliper and rotor must fit inside the rim's usable inner diameter of about 300 mm. Given the dimensions of the AP RACING CP4226-2S0 calliper, the maximum rotor diameter is 220 mm. In light of the previous data, the front rotor is shown in Figure (25) was designed using SOLIDWORKS® with the following specifications, as detailed in Table (5):

Table 5 Front rotor parameters

Overall diameter	**205 *mm***
Outer diameter	200 *mm*

Inner diameter	150 mm
Thickness	4 mm

The calculation to obtain the produced torque by the front rotor was done using equation number (44):

$$\boldsymbol{T_{Df} = \text{Effective radius} * F_{Friction}} \quad (44)$$

Where:

$\boldsymbol{T_{Df}}$: Produced torque by the front rotor.

To determine the effective radius, Equation (45) took the inner and outer diameters into account.

$$\textbf{Effective radius} = \frac{\mathbf{1}}{\mathbf{3}}\left(\frac{\boldsymbol{D_r^3 - d_r^3}}{\boldsymbol{D_r^2 - d_r^2}}\right) \quad (45)$$

Where:

$\boldsymbol{D_r}$: Outer radius of the rotor,

$\boldsymbol{d_r}$: Inner radius of the rotor.

$$\textbf{Effective radius} = \frac{\mathbf{1}}{\mathbf{3}}\left(\frac{\mathbf{200^3 - 150^3}}{\mathbf{200^2 - 150^2}}\right) = \mathbf{83.1\ mm = 0,083\ m}$$

$$\boldsymbol{T_{Df} = 0,083\ * 2069.1}$$

$$\underline{\boldsymbol{T_{Df} = 171,7Nm}}$$

Rear rotor torque

Due to the previous calculation, the required braking power in the front is more than in the back. The rear rotor is shown in Figure (26), was designed to be a smaller diameter as specified in Table (6), therefore generating less torque.

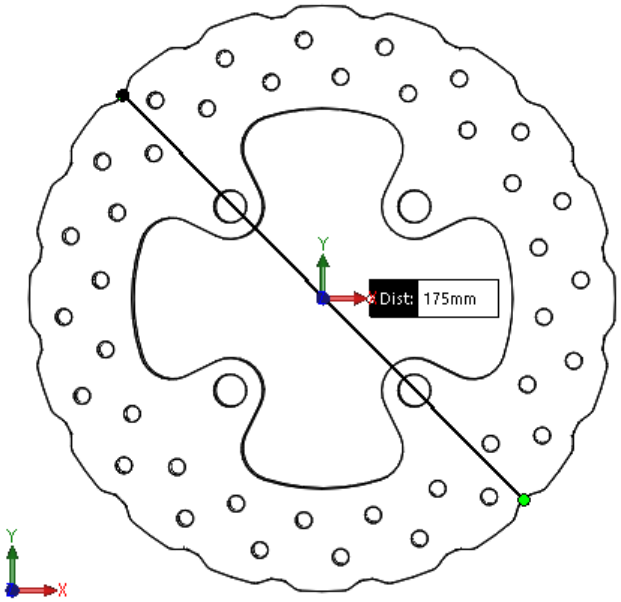

Figure 26 Front view of Rear Rotor without section lines.

Table 6 Rear rotor parameters

Overall diameter	**180 mm**
Outer diameter	175 mm
Inner diameter	125 mm
Thickness	4 mm

The rear rotor torque was calculated using Equation (46):

$$\boldsymbol{T_{Dr} = \text{Effective radius} * F_{Friction}} \quad (46)$$

Where:

$\boldsymbol{T_{Dr}}$: Produced torque by the rear rotor.

Again, Equation (45) used the inner and outer diameters to calculate the effective radius.

$$\textbf{Effective radius} = \frac{1}{3}\left(\frac{D_r^3 - d_r^3}{D_r^2 - d_r^2}\right)$$

$$\textbf{Effective radius} = \frac{1}{3}\left(\frac{175^3 - 125^3}{175^2 - 125^2}\right)$$

$$\textbf{Effective radius} = 75.7 \text{ mm} = 0.0757 \text{ m}$$

$$\underline{T_{Dr} = 0.0757 * 2016.07 = 152.6\ Nm}$$

4.3.8. Rim and tire

The rim and tire diameter were selected previously by the IPB motorsport team to use in the calculation of the CG and other characteristics of the car. The assembly is shown in Figure (27).

Figure 27 Rim and Tire Assembly.

Rim

The Mg Cast 7*13 Wheel from O.Z company was selected, the 4h style were chosen instead of the CL since it's more suitable to implement design criteria.

Indicative weight: 2.450 Kg.

Bolt pattern: 100x4 and centre hole diameter 50 mm for wheels to be fixed by bolts [39].

Tire

The 178/54 R13 tire from Hoosier was chosen, and its dimensions are shown in the following Table (7).

Table 7 Tire specification

Size	Overall Diameter	Thread width	Section width	Approx. Weight
178/54 R13	533.4 mm	177.8 mm	203.2 mm	4.9 kg

4.4. Finite element analysis

A vehicle is considered to have kinetic energy while it is in motion. A vehicle's brakes are intended to stop it by absorbing the vehicle's kinetic energy and dispersing it as heat. As this energy transfer occurs in the rotor, it is critical to guarantee that the rotor can endure the thermal and static stresses.

Since we know that the vehicle mass is 260 kg, and the vehicle is travelling at 33.33 m/s a vehicle's kinetic energy is calculated by Equation (48):

$$\boldsymbol{KE = \frac{mv^2}{2}} \tag{48}$$

Where:

$\boldsymbol{KE}$: kinetic energy,

$\boldsymbol{m}$: Mass,

$\boldsymbol{v}$: Velocity.

$$\boldsymbol{KE = \frac{260 * (33.33)^2}{2} = 144416\,J}$$

The simulation will proceed in three Stages, as shown in Figure (28), beginning with the import of the geometry to be analysed and applying an appropriate mesh. After that, a transient thermal analysis will be carried by applying the boundary condition and obtaining the thermal results. Following that, a static structural analysis will be performed using the transient analysis's thermal loading and the associated boundary condition.

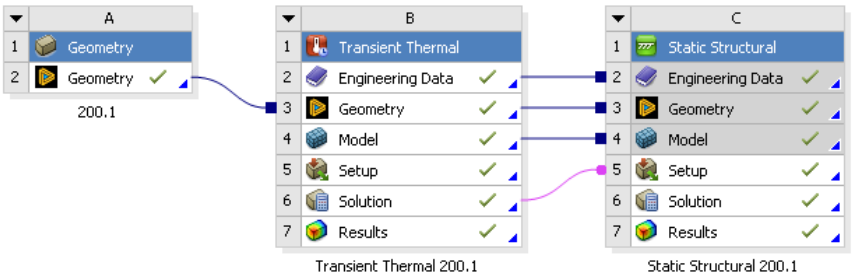

Figure 28 Simulation stages.

The ANSYS Workbench 2021 R2 software will be used to analyse two proposed materials by performing transient thermal and static analysis. A final choice will be made by picking the material that performs best.

4.5. Geometry Importing and Meshing

4.5.1. Import geometry

To begin, the previously created cad geometry in SOLIDWORKS must be imported into ANSYS to apply the boundary condition.as shown in Figure (29).

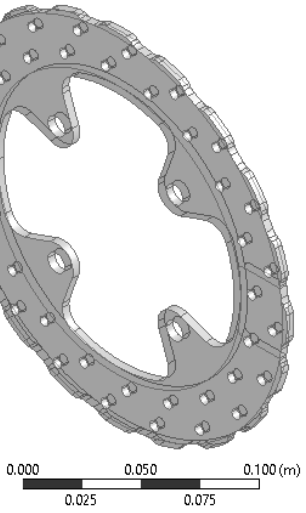

Figure 29 Geometry importing.

4.5.2. Applied materials

The following materials with the characteristics listed in Table (8) will be applied to the geometry in order to implement the numerical simulation.

Table 8 Mechanical properties and chemical composition of applied materials..

Materials	***Gray Cast Iron***		***Aluminium Alloy***	
Density (kg/m3)	7200		2770	
Thermal Conductivity (W/mc)	52		144	
Young´s Modulus (GPa)	180		88.5	
Poisson Ratio	0,29		0,33	
Yield Strength (MPa)	420		280	
Ultimate Strength (MPa)	700		310	
Chemical Composition	Carbon	2.6- 4.0%	Silicon- Iron	0.1%
	Silicon	1,0 -3.0%	Manganese	0.05%
	Manganese	0.6 –0.9 %	Copper	0.05%
	Sulfur	0 –0.15%	Zinc	0.1%
	Phosphorous	0 – 0.10%	Titanium	0.05%
	Iron	Rest of them	Aluminium	Rest of them

Figure (30) illustrates the materials library in Ansys that was used to identify the material for the rotors.

Outline of Schematic B2, C2: Engineering Data

	A	B	C	D	E
1	Contents of Engineering Data			Source	Description
2	Material				
3	Aluminum Alloy				General aluminum alloy. Fatigue properties come from MIL-HDBK-5H, page 3-277.
4	Gray Cast Iron				
*	Click here to add a new material				

Properties of Outline Row 3: Aluminum Alloy

	A	B	C	D	E
1	Property	Value	Unit		
2	Material Field Variables	Table			
3	Density	2770	kg m^-3		
4	Isotropic Secant Coefficient of Thermal Expansion				
6	Isotropic Elasticity				
12	S-N Curve	Tabular			
16	Tensile Yield Strength	2.8E+08	Pa		
17	Compressive Yield Strength	2.8E+08	Pa		
18	Tensile Ultimate Strength	3.1E+08	Pa		
19	Compressive Ultimate Strength	0	Pa		
20	Isotropic Thermal Conductivity	Tabular			
23	Specific Heat Constant Pressure, C_p	875	J kg^-1 C^-1		

Figure 30 Materials library in Ansys.

4.5.3. Mesh generated

The SOLID187 element was used to generate the mesh. The SOLID187 element is a three-dimensional, ten-node element of higher-order, as shown in Figure (31).

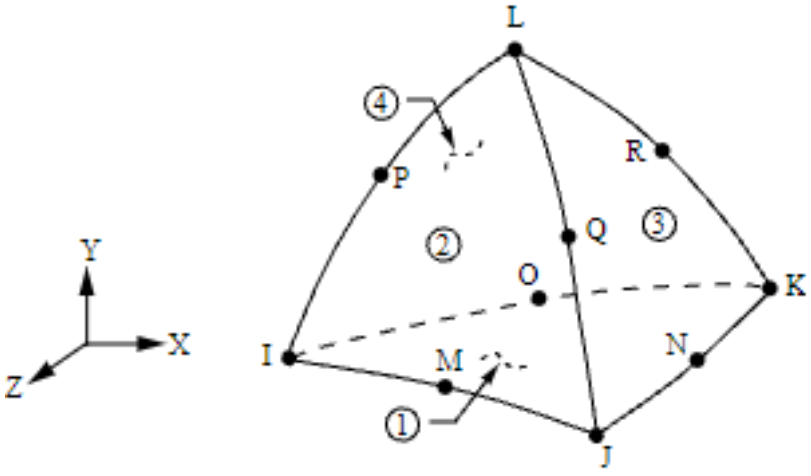

Figure 31 SOLID187 Geometry [40]

SOLID187 has quadratic displacement behaviour, making it ideal for modelling irregular meshes (such as those generated by different CAD/CAM systems) [40].

The element size was set to 2 mm, resulting in a total of 43533 nodes and 22932 elements. The mesh quality scale in Figure (32) ranges from 0 to 1, with the majority of elements falling between good and excellent.

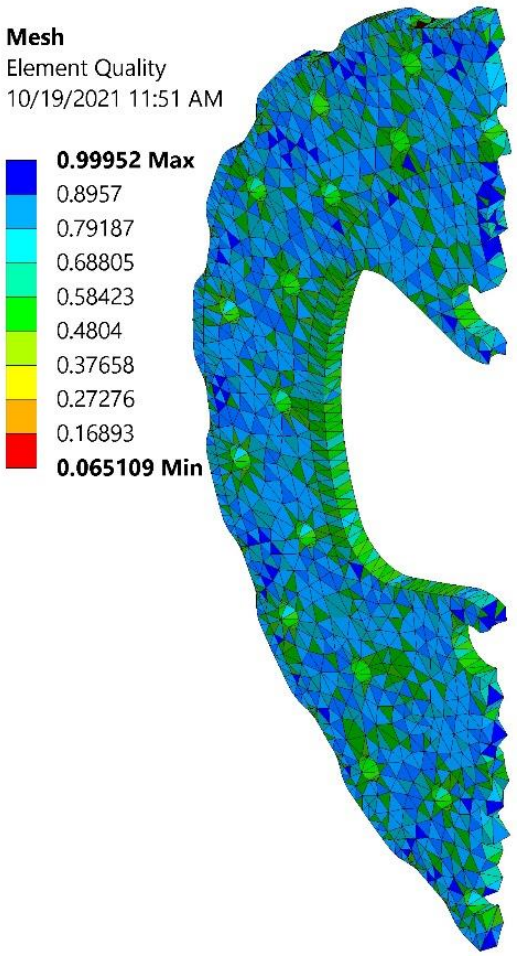

Figure 32 Mesh Quality.

4.6. Transient thermal analysis

Transient analysis is used to investigate heat distribution while braking from 33.33m/s to a complete stop. Stopping time may be figured by first determining the force required to stop the vehicle.

The distance needed to stop the vehicle is calculated using Equation (49):

$$\boldsymbol{D_{Braking} = \frac{v^2}{2 * d}} \tag{49}$$

Where:

$\boldsymbol{D_{Braking}}$: Braking distance,

$\boldsymbol{d}$: Deceleration of vehicle.

$$\boldsymbol{D_{Braking} = \frac{(33.33)^2}{2 * 6.86} = 80.96\ m}$$

The time needed to stop the vehicle is determined using Equation (50):

$$\boldsymbol{t = \frac{v}{d}} \tag{50}$$

Where:

$\boldsymbol{t}$: Time to stop the vehicle.

$$t = \frac{33.33}{6.86}$$

$$\underline{\boldsymbol{t = 4.8s}}$$

4.6.1. Convection

To calculate heat transfer coefficient h, the rotor is considered flat. Now that the rotor is subject to Newton's law of cooling, plus the fact that the rotor is dispersing heat on both sides, therefore, the Equation (51) is formed:

$$\boldsymbol{Q_{conv} = hl(T_\infty - T_s)2} \tag{51}$$

To calculate the film temperature, Equation (52) is implemented:

$$\boldsymbol{T_{Film} = \frac{T_s + T_\infty}{2}} \tag{52}$$

Where:

$\boldsymbol{T_{Film}}$: Film temperature

$$T_{Film} = \frac{945 + 20}{2}$$

For

$$\underline{\boldsymbol{T_{Film}} = \mathbf{482.5}\ ℃}$$

The following values were considered from the Table of air properties at 1 atm pressure.

Thermal Conductivity of air (K_f)

$$\mathbf{K_f = 0.05015\ \frac{w}{mk}.}$$

kinematic viscosity ($\boldsymbol{v}$)

$$\boldsymbol{\nu = 6.219\ * 10^{-5}\ \frac{m^2}{s}.}$$

Prandtl number ($\boldsymbol{P_r}$)

$$\boldsymbol{P_r = 0.6948.}$$

Front rotor calculation :

Reynolds number

$$\boldsymbol{Re = \frac{VL}{\nu}} \tag{53}$$

Where:

$\boldsymbol{Re}$: Reynold number,

$\boldsymbol{V}$**:** Velocity of air,

$\boldsymbol{L}$: Distance travelled by air,

$\boldsymbol{\nu}$: Kinematic viscosity.

$$Re = \frac{(33.33) * (0.0625)}{6.219\ * 10^{-5}}$$

$$\underline{\boldsymbol{Re = 33496.1 < 5 * 10^5}}$$

As $Re < 5\ * 10^5$, for a flow over a flat plate, the flow is laminar.

Average Nusselt number

$$\boldsymbol{n_{avg} = 0.664 * R_e^{\frac{1}{2}} * P_r^{\frac{1}{3}}} \tag{54}$$

Where:

$\boldsymbol{n_{avg}}$: Average Nusselt number.

$$n_{avg} = 0.664 * (33496.1)^{\frac{1}{2}} * (0.6948)^{\frac{1}{3}}$$

$$\underline{\boldsymbol{n_{avg} = 107.6}}$$

Since

$$\boldsymbol{n_{avg} = \frac{h * L}{k}} \quad (55)$$

Means that

$$\boldsymbol{h = \frac{n_{avg} * k}{L}} \quad (56)$$

$$h = \frac{107.635 * 0.05015}{0.0625}$$

$$\underline{\boldsymbol{h = 86.3 \frac{w}{m^2 k}}}$$

Rear rotor calculation:

Reynolds number

$$\boldsymbol{Re = \frac{VL}{\nu}}$$

$$\boldsymbol{Re = \frac{(33.33) * (0.06)}{6.219 * 10^{-5}}}$$

$$\underline{\boldsymbol{Re = 32156.3}}$$

As $Re < 5 * 10^5$, for a flow over a flat plate, the flow is laminar.

Average Nusselt number

$$\boldsymbol{n_{avg} = 0.664 * R_e^{\frac{1}{2}} * P_r^{\frac{1}{3}}}$$

$$\boldsymbol{n_{avg} = 0.664 * (32156.3)^{\frac{1}{2}} * (0.6948)^{\frac{1}{3}}}$$

$$\underline{\boldsymbol{n_{avg} = 105.46}}$$

Since

$$\boldsymbol{n_{avg} = \frac{h * L}{k}}$$

Means that

$$\boldsymbol{h = \frac{n_{avg} * k}{L}}$$

$$h = \frac{105.46 * 0.05015}{0.06}$$

$$\underline{\boldsymbol{h = 88.1 \frac{W}{m^2 k}}}$$

And the obtained value of convection is applied on the rotor, as shown in Figure (33).

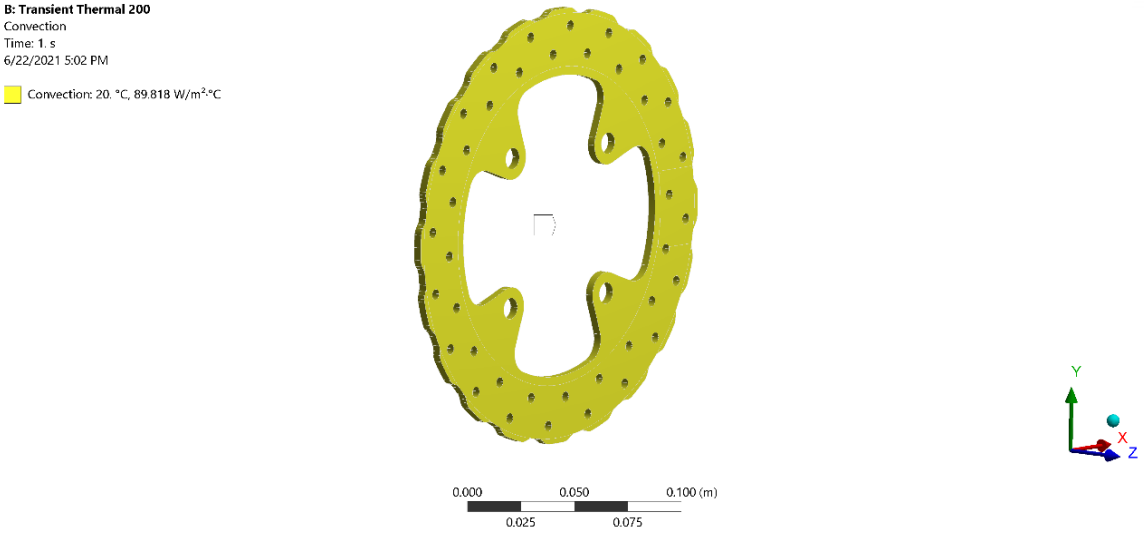

Figure 33 Convection applied on the rotor.

4.6.2. Heat flow

If the brakes are applied for 5 seconds, assuming all the kinetic energy is converted to thermal energy, the heat power may be computed from Equation (57).

$$\boldsymbol{Q_H = \frac{KE}{t}} \quad (57)$$

Where:

$\boldsymbol{Q_H}$: Heat flow,

$\boldsymbol{KE}$: kinetic energy,

$\boldsymbol{t}$: time.

$$Q_H = \frac{144416}{4.8}$$

$$\underline{\boldsymbol{Q_H = 30086.6\ W}}$$

Front

Since only about 55.9% of the vehicle's mass will move forward to the front, and since the power will be reduced.

$$Q_{Hf} = \frac{30086.6 * 0.559}{2} = 8409.2\ W$$

$$\underline{\boldsymbol{Q_{Hf} = 8.4\ kW}}$$

Rear

Since only about 55.9% of the vehicle's mass will move forward to the front, the power will be reduced.

$$Q_{Hr} = \frac{30086.6 * 0.440}{2} = 6619\ W$$

$$\underline{\boldsymbol{Q_{Hr} = 6.6\ kW}}$$

The obtained values are applied by selecting the two rotor faces that the brake pads make contact with, as shown in Figure (34).

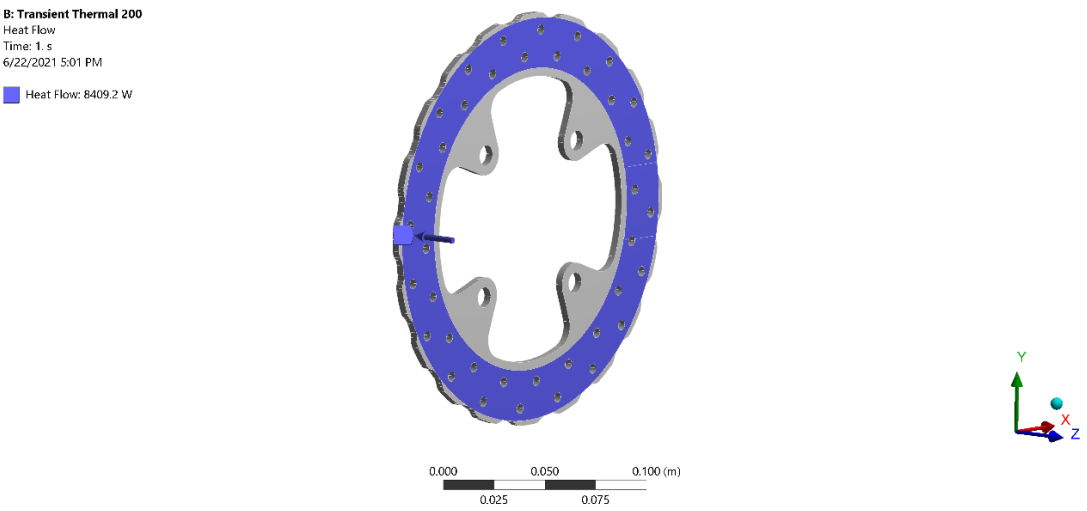

Figure 34 Heat flow applied on the rotor.

4.6.3. Define analysis setting

The temperature was obtained after Running the simulation for 5 seconds.

4.7. Structural analysis

The temperature distribution has been obtained once the car has come to a complete stop from a speed of 33.33 m/s. This temperature distribution will be included in our static analysis as a thermal loading condition. The material will be permitted to expand or contract in response to the temperature distribution.

Additionally, the loading condition is applied to mimic the load applied to the rotor by the brake pad. Ensure that the brake pad does not distort excessively during this extraordinary braking scenario.

4.7.1. Fixed support

The inner diameter of the rotor hub was selected to insert fixed support, as demonstrated in Figure (35).

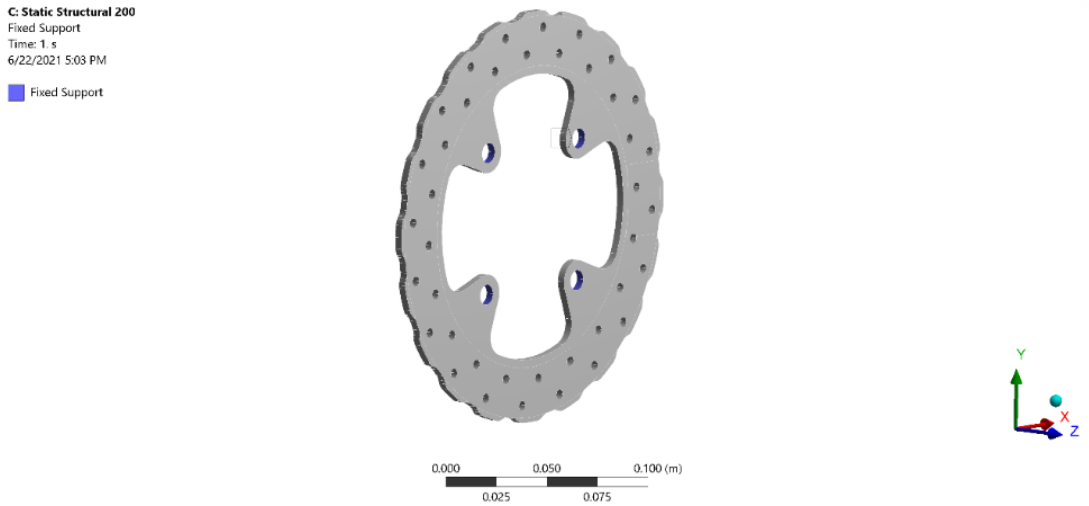

Figure 35 Fixed support applied on the rotor.

Then the temperatures from the thermal analysis must be included.

4.7.2. Pressure

Equation (58) will be used to determine the pressure generated by the calliper on the rotor:

$$\boldsymbol{P_{Rotor}} = \frac{\boldsymbol{F_{Calliper}}}{\boldsymbol{A_{pad}}} \tag{58}$$

Where:

$\boldsymbol{P_{Rotor}}$: Pressure on the rotor.

$$P_{Rotor} = \frac{2652.72}{970 * 10^{-6}}$$

$$\underline{\boldsymbol{P_{Rotor} = 2.73 * 10^{6} Pa}}$$

As seen in Figure (36), the acquired pressure value is applied to the rotor by choosing the split face where the brake pad will press on the rotor.

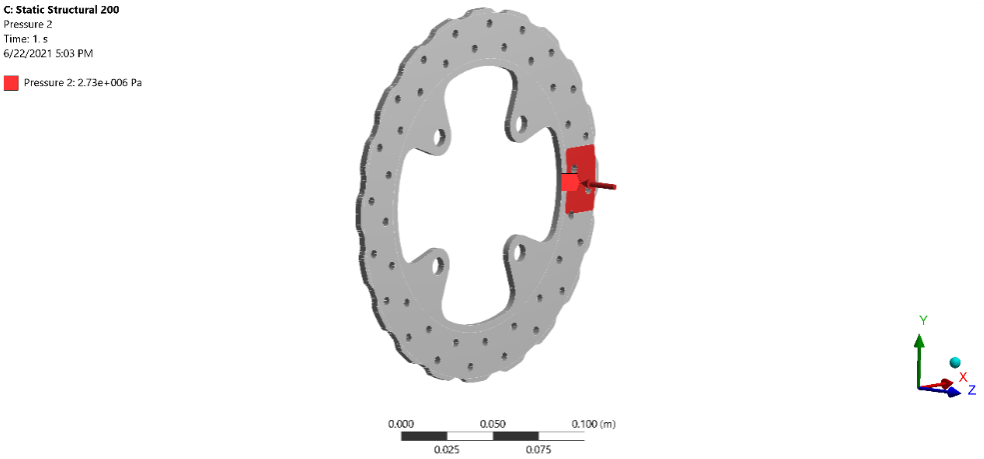

Figure 36 Pressure applied on the rotor.

4.7.3. Braking Force

Along with the load supplied to the rotor through the brake pad, the braking force has a frictional component in the circumferential direction. The frictional force may be estimated using the area of the pad application if the normal load applied to the Rotor is known **5305.45 *N*** and the friction coefficient between the rotor and pads ***0.39*** [41], and substituting in Equation (59).

$$\boldsymbol{F_{Friction} = \mu_{Pad} * F_{Callmping}} \quad (59)$$

Where:

$\boldsymbol{\mu_{Pad}}$: Pads coefficient of friction.

$$F_{Friction} = 0.39 * 5305.45$$

$$\boldsymbol{F_{Friction} = 2069.12\ N}$$

$$\boldsymbol{Each\ pad = 1034.5\ N}$$

After creating a cylindrical coordinate system, the two split faces on the rotor where the brake pads make contact were chosen, and a 1034 N value was input for the circumferential direction, as shown in Figure (37).

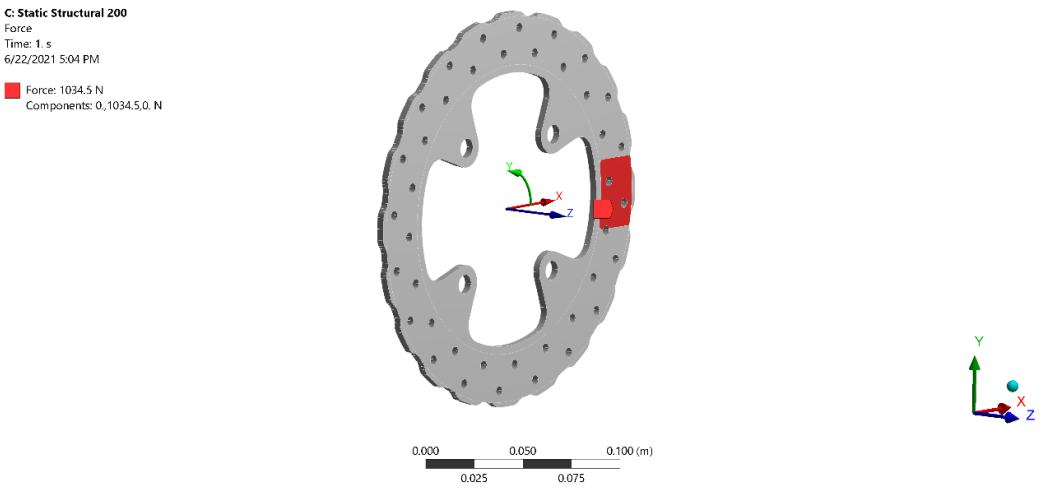

Figure 37 Friction force applied on the rotor.

5. Results and discussion

5.1. Introduction

This chapter will begin by representing the values obtained from the previous calculations. Then a complete assembly of the chosen and designed components of the braking system will be shown. Finally, the results of the finite element analysis results will be presented as figures and tables to compare the selected materials and select the one that best suits our application.

5.2. Assembly to the braking system

The selected components for the brake pedal are combined and demonstrated in two big principal assemblies. Design and assemblies were done using SOLIDWORKS software.

5.2.1. Pedal box assembly

The pedal box assembly consist of the following components and subassemblies shown in the exploded and collapsed views in Figure (38 and 39):

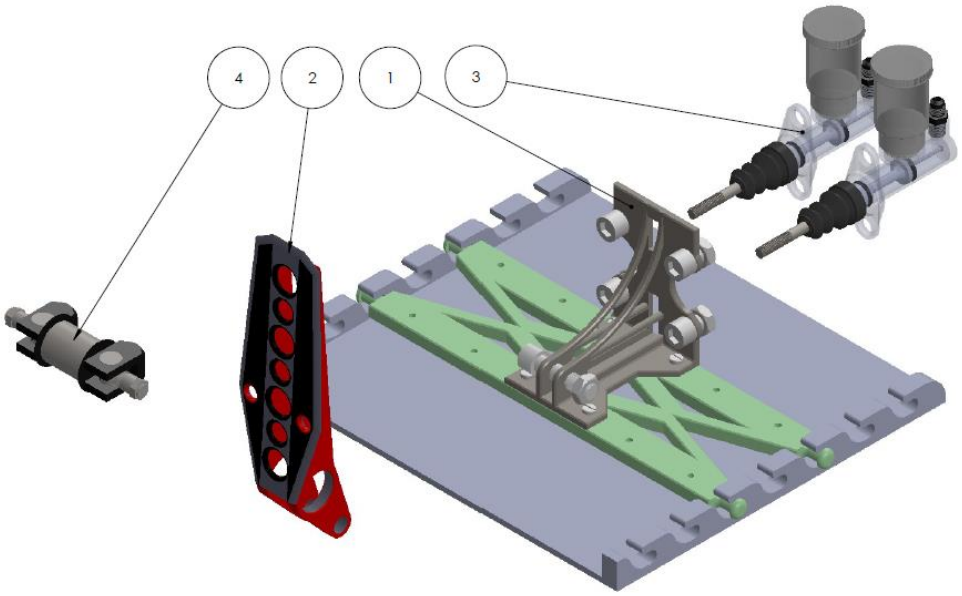

Figure 38 Pedal box assembly exploded view.

The components and subassemblies included is:

1. Brake pedal holder and base subassembly.
2. Pedal.
3. Master cylinder subassembly
4. Bias bar subassembly

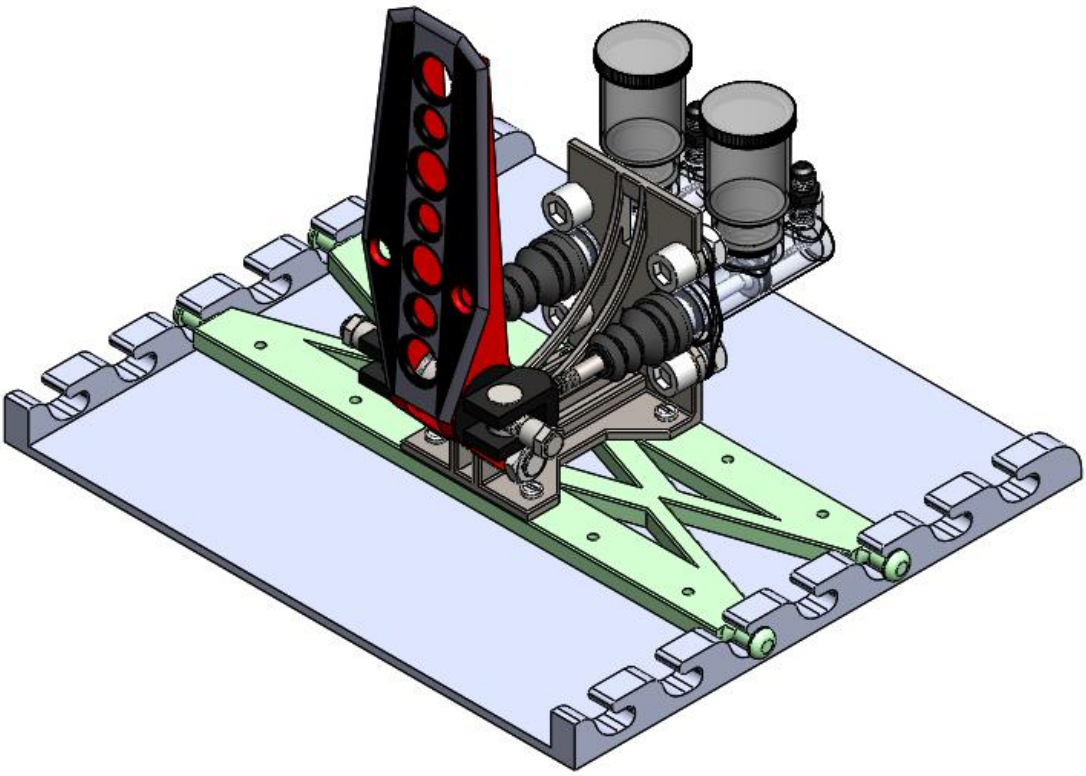

Figure 39 Pedal box assembly collapsed view.

5.2.2. Calliper and wheel hub assembly

The calliper and wheel hub assembly consist of the following components and subassemblies as shown in the exploded and collapsed views in figure (40 and 41):

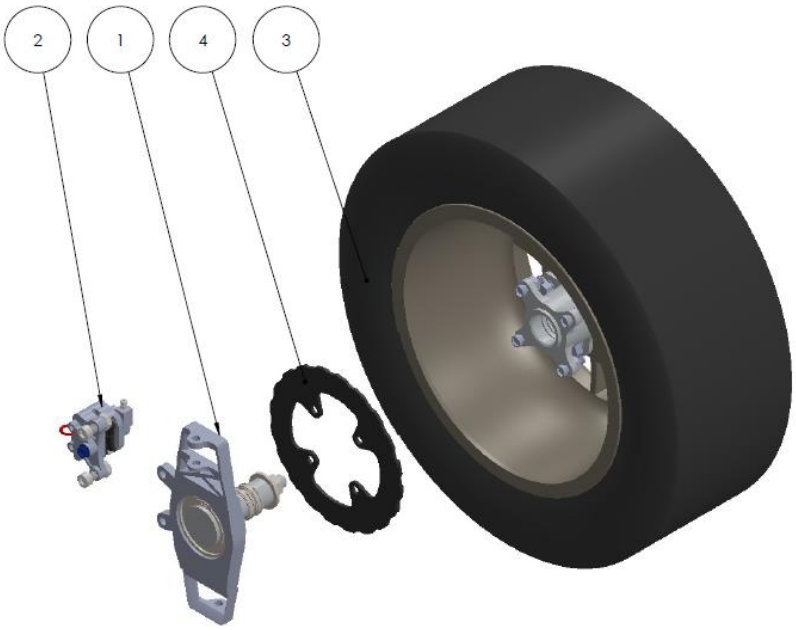

Figure 40 Calliper and wheel hub assembly exploded view.

The components and subassemblies included are:

1. Suspension connection hub
2. Calliper subassembly
3. Tire, Rim and Hub subassembly
4. Rotor

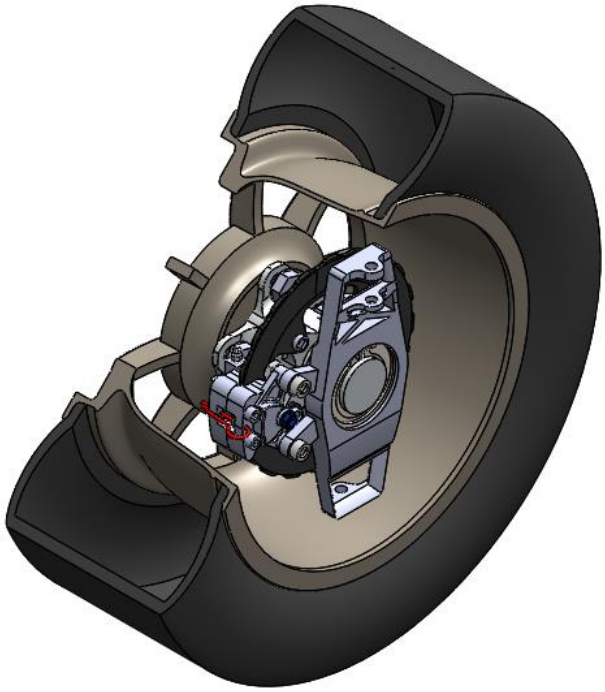

Figure 41 Calliper and wheel hub assembly collapsed view.

Table (9) represent the specifications of the main components of the braking system required by the formula student competition:

Table 9 brake system components specification

Brake System	Units	Front		Rear		
Rotors	4	(OD=205mm) (Effective Radius =83.1313mm) (Thickness=4mm)		(OD=180mm) (Effective Radius =75.6944mm) (Thickness=4mm)		
Master Cylinder	4	AP RACING CP2623 (Bore Size=19.1mm)		AP RACING CP2623 (Bore Size=19.1mm)		
Callipers	4	AP RACING CP4226 Piston Diameter=25.4 mm		AP RACING CP4226 Piston Diameter=25.4 mm		
Brake Pad/Lining Material	8	CP4226D27 APH420		CP4226D27 APH420		
Force and Pressures @ 1g Deceleration		Front Pres. (PA):	$2.73 * 10^6$	Rear Pres. (PA):	$2.73 * 10^6$	Pedal Force (N): 300

5.3. Calculation results and comparison

In the design of any braking system, the determination of the braking force is the most critical factor to consider. The braking force that is produced should always be higher than the braking force that is needed. From the result in Table (10), it can be concluded that the applied torque generated by the braking system is more than the necessary torque on both the front and rear axles, indicating that the vehicle will be able to pass the FSAE test by attaining a four-wheel lock.

Table 10 Required and applied torque comparison in between front and rear.

	Required Torque	**Applied Torque**
Front	$\mathbf{132.9\ Nm}$	$\mathbf{171.7\ Nm}$
Rear	$\mathbf{104.6\ Nm}$	$\mathbf{152.6\ Nm}$

5.4. Results of the simulation and discussion

5.4.1. Temperature

The following Figures (42, 43, 44 and 45) demonstrate the difference in global maximum temperatures for various materials (gray cast iron and aluminium alloy) and geometries (front and rear).

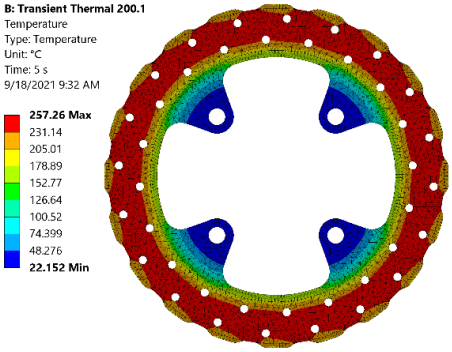

Figure 42 205 mm (Front) Gray Cast Iron Rotor Temperature.

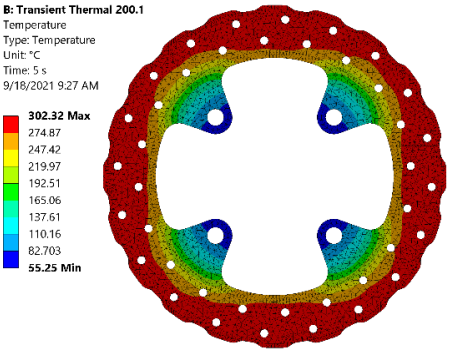

Figure 43 205 mm (Front) Aluminium Alloy Rotor Temperature.

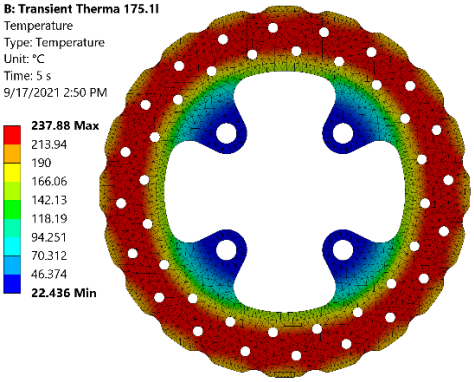

Figure 44 175 mm (Rear) Gray Cast Iron Rotor Temperature.

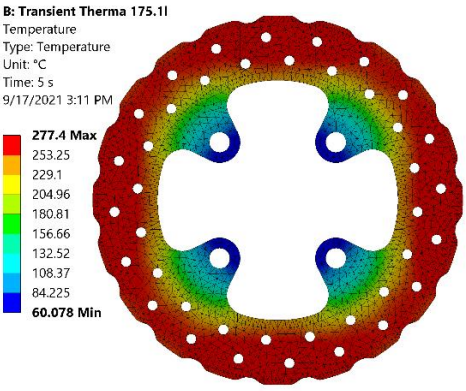

Figure 45 175 mm (Rear) Aluminium Alloy Rotor Temperature.

Due to the gray cast iron rotor's lower thermal conductivity, it reaches a lower temperature than the aluminium alloy rotor. Nonetheless, the rear rotor geometry attained a lower temperature, which is typical given that the front rotor absorbed more energy than the rear owing to the car's transmitted weight. Table (11) demonstrate the temperature results that were obtained by the transient thermal simulation.

The following results were obtained by applying the obtained temperature and the boundary condition to static structural analysis.

Table 11 Temperature results comparison for drilled rotors.

Temperature	[°C]	Gray Cast Iron	Al Alloy
Front (205 mm)	Max	257.26	302.32
	Min	22.15	55.25
Rear (175 mm)	Max	237.88	277.4
	Min	22.43	60.07

5.4.2. Displacement field

The highest displacement values are distributed around the outer edge of the rotor where the Pads applies the pressure, and the maximum values are especially concentrated about 45 radial degrees from the fixed support, as seen in Figures 46, 47, 48 and 49. And the minimum values were distributed more toward the inner edge of the rotor and the fixed support.

Although the Deformation values were relatively low in both front and rear rotor materials, grey cast iron has fewer displacement values than aluminium alloy as compared in Table (12). The rear rotor with the smallest geometry deformed the least. Additionally, there was no discernible deflection on the z-axis, even though a tolerance distance should always be included.

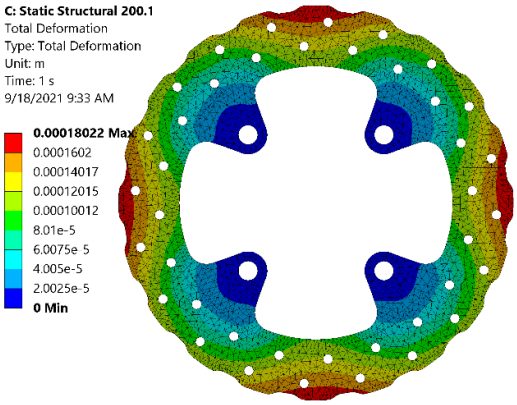

Figure 46 205 mm Gray Cast Iron Rotor Total displacement.

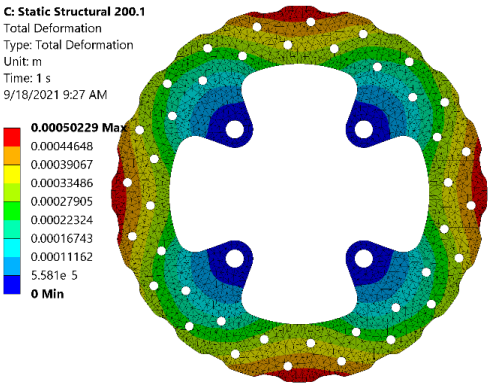

Figure 47 205 mm Aluminium Alloy Rotor Total displacement.

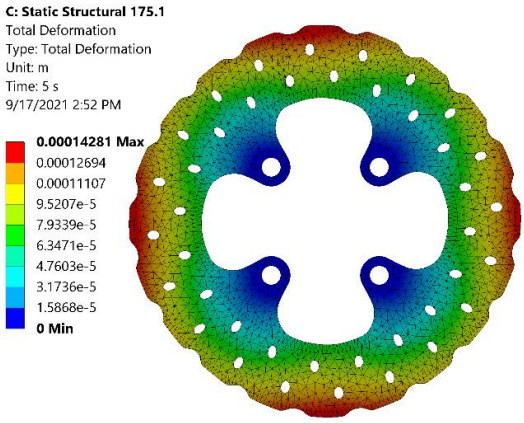

Figure 48 175 mm Gray Cast Iron Rotor Total displacement.

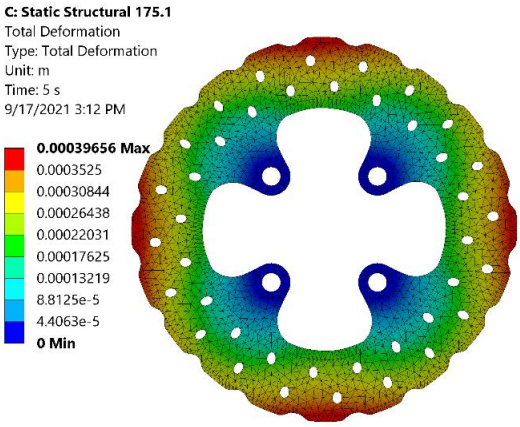

Figure 49 175 mm Aluminium Alloy Rotor Total displacement.

Table 12 Displacement results comparison for drilled rotors.

Displacement	[mm]	Gray Iron	Al Alloy
Front (205 mm)	Max	0,180	0,502
	Min	0	0
Rear (175 mm)	Max	0,142	0,396
	Min	0	0

5.4.3. Equivalent stress

Figures 50, 51, 52 and 53. represents arbitrary three-dimensional stress condition as a single positive stress value.

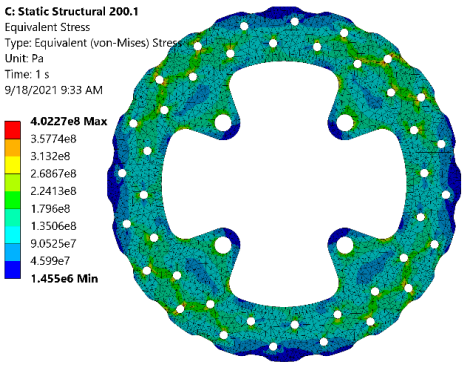

Figure 50 205 mm Gray Cast Iron Rotor Equivalent stress.

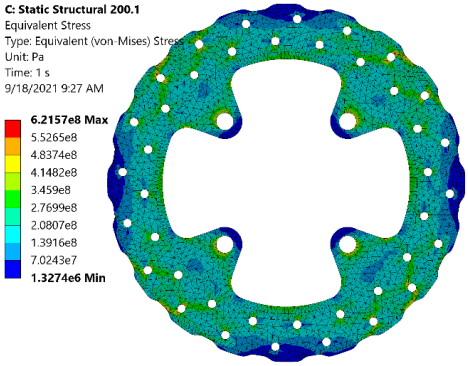

Figure 51 205 mm Aluminium Alloy Rotor Equivalent stress.

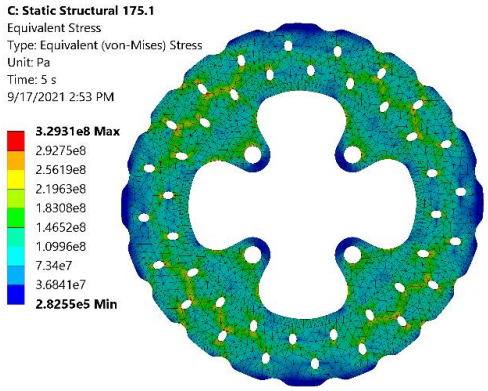

Figure 52 175 mm Gray Cast Iron Rotor Equivalent stress.

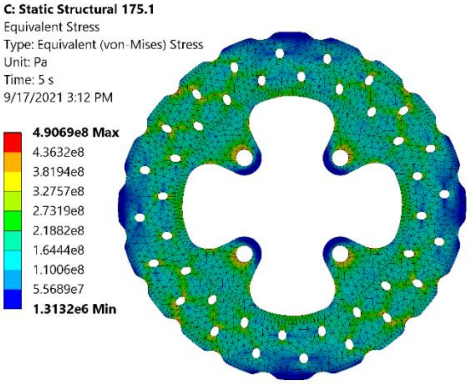

Figure 53 175 mm Aluminium Alloy Rotor Equivalent stress.

The most significant stress values are concentrated around the holes. in the front and rear rotors due to the irregularities in the geometry caused by the round holes, which interrupt the stress flow. Additionally, the stress values in Table (13) indicate that Gray cast iron endured a lower stress value than aluminium alloy concerning the front rotor and yet endured a lower stress value on the rear rotor.

Table 13 Equivalent stress results in comparison for drilled rotors.

Stress	[Pa]	Gray Iron	Al Alloy
Front (205 mm)	Max	4.0227×10^{8}	6.2157×10^{8}
	Min	1.455×10^{6}	1.3274×10^{6}
Rear (175 mm)	Max	3.2931×10^{8}	4.9069×10^{8}
	Min	2.8255×10^{5}	1.3132×10^{6}

5.4.4. Safety factor:

Since the safety factor is the ratio of material's limit strength to the maximum stress anticipated for the design, a factor of safety of one or higher is needed in practice to help prevent the possibility of failure.

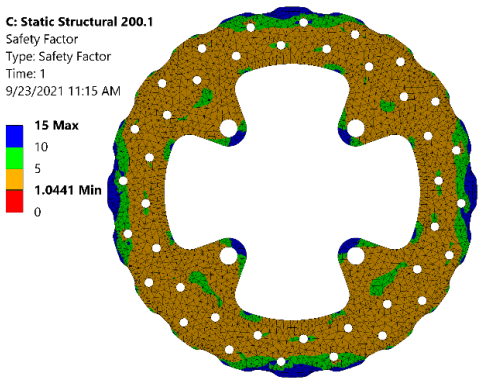

Figure 54 205 mm Gray Cast Iron Rotor Safety factor.

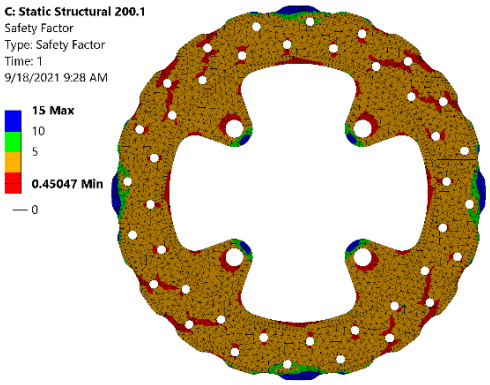

Figure 55 205 mm Aluminium Alloy Rotor Safety factor.

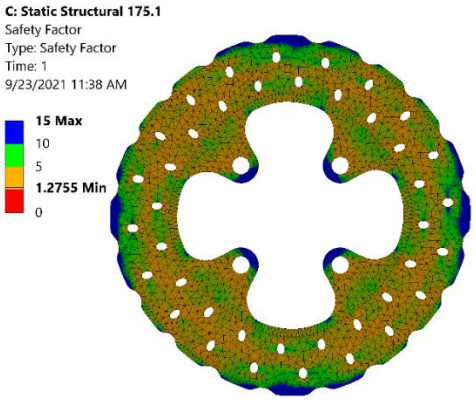

Figure 56 175 mm Gray Cast Iron Rotor safety factor.

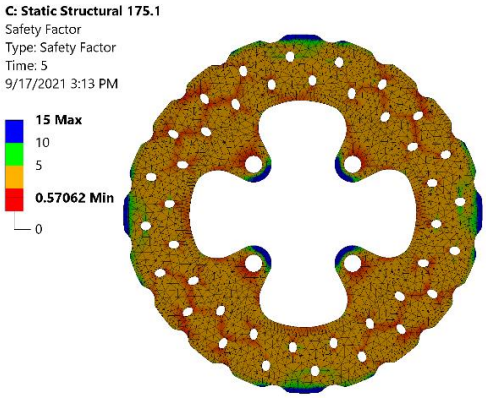

Figure 57 175 mm Aluminium Alloy Rotor Safety factor.

And as observed from Figures (54, 55, 56 and 57) and shown in Table (14), only Gray cast iron could achieve a safety factor score slightly above one for the front rotor and a higher score for the rear rotor, about 1.3, where the aluminium alloy could only score about 0.5 for front and rear which is an indicator for the design failure.

Table 14 Safety factor results in comparison for drilled rotors.

Safety Factor		Gray Iron	Al Alloy
Front (205 mm)	Max	15	15
	Min	1,0441	0,45047
Rear	Max	15	15

(175 mm)	Min	1,2755	0,57062

5.4.5. Undrilled rotor analysis

After observing the results from the previous simulation and deciding that Gray cast iron were the most suitable material for the application, it was noticed that the holes in the disc had a big influence on the stress distribution around it, which affected the value of the safety factor.

Another simulation was performed on the rear rotor selecting Gray cast iron using a geometry without holes, and the following results in Figure (58, 59, 60 and 61) were obtained.

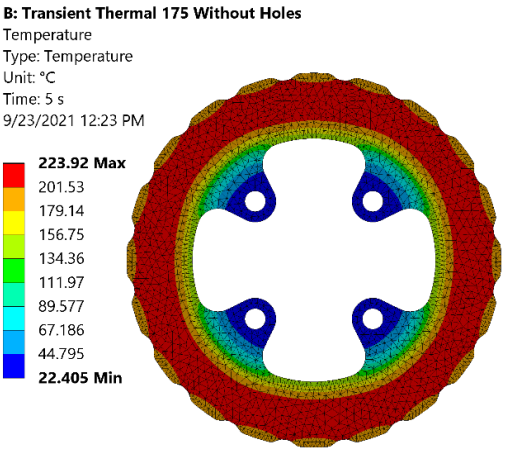

Figure 58 175 mm Gray Cast Iron Rotor Undrilled Temperature.

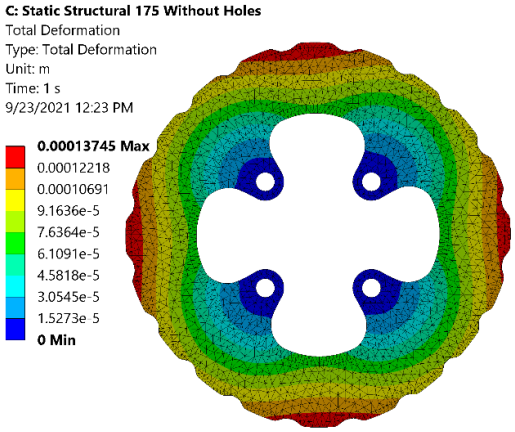

Figure 59 175 mm Gray Cast Iron Rotor Undrilled Total Displacement.

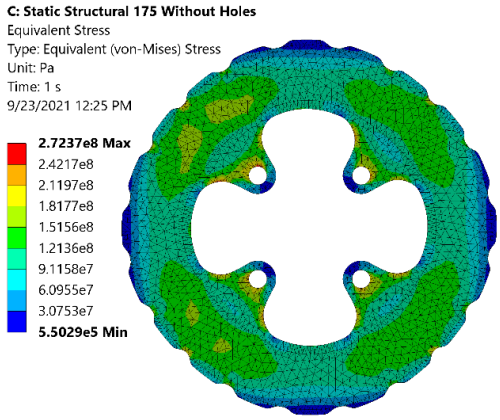

Figure 60 175 mm Gray Cast Iron Rotor Undrilled Equivalent stress.

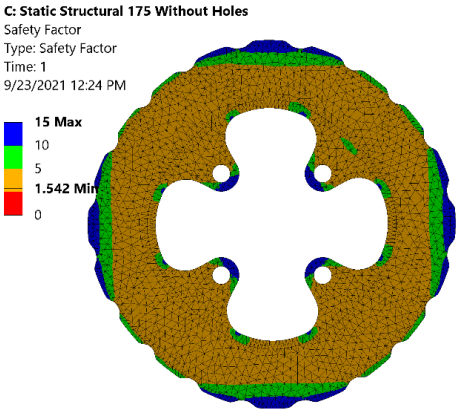

Figure 61 175 mm Gray Cast Iron Rotor Undrilled Safety Factor.

By eliminating the holes, more area was created for heat dissipation, resulting in a considerable temperature drop of roughly 14 degrees, as compared to the geometry with holes, as shown in Table (15). Additionally, the undisturbed stress flow inside the contact

region leads to a decrease in the stress concentration factor, resulting in a stress reduction of about 56.94 MPa. and a displacement reduction of approximately 0.005mm., this increased the safety factor by about 0.2.

Table 15 Results comparison of rear rotor gray cast iron drilled and undrilled

Rear Rotor Gray Cast Iron	**Unit**	**Drilled**	**Undrilled**
Temperature	[ºC]	237.88	223.92
Displacement	[mm]	0.14281	0.13745
Stress	[Pa]	3.2931×10^{8}	2.7237×10^{8}
Safety Factor		(Min=1.2755, Max=15)	(Min=1.5, Max=15)

6. Conclusions and future directions

6.1. Conclusions

The established work was dedicated to the research of braking systems and their effects on vehicle safety and behaviour. Its primary objective was to develop a brake system capable of being used in a formula student racing vehicle. Several methods based on automotive dynamics theory were used to do this, as well as a kinematic and dynamic analysis of the braking system, was carried out.

Due to the fact that the actual vehicle does not exist yet and the values were estimated by the IPB formula student team, the braking system is designed to provide adequate overall performance but not optimum performance, as many of its parameters have been chosen based on a set of values recommended by various automobile bibliographies.

Although the results of theoretical calculations using various methodologies and computer analyses were acceptable, nevertheless, as can be seen, it is necessary to continue improving the braking system and, therefore, the overall performance of the vehicle.

When the calculated required torque of the car is compared to the calculated generated torque from the braking system, it is found that the generated torque exceeds the required torque, which is satisfactory because it enables the driver to perform a four-wheel lock as required by the formula student's rules.

In the absence of a physical model to test, numerical simulation was applied to perform thermomechanical analyses, demonstrating its efficiency in simulating real-world conditions. The computed braking system values were utilised in conjunction with the applied boundary conditions to investigate the behaviour of front and rear rotors made of two different materials.

Gray cast iron performed better in temperature, total deformation, and stress, resulting in a higher overall safety factor number. Although aluminium alloy is a lightweight material compared to gray cast iron, its mechanical characteristics were insufficient. As a consequence of these findings, it was determined that the Gray cast iron rotor would be utilised in the IPB vehicle's braking system.

6.2. Future Directions

While the efficiency now attained is satisfactory and has been increased over time, it may be improved further, and hence particular emphasis will be paid to this attribute in future generations.

Since The brake pedal and its installation must be able to bear a force of 2000N without damaging the braking system or pedal box. It’s necessary to perform an analysis to check if the pedal box can withstand the force applied to the pedals.

Conducting a Cost & Manufacturing analysis of the braking system to be added to the total cost analysis of the vehicle, since it's going to be judged in the static event and attempting to discover a less expensive component with suitable performance.

Installing a brake pedal over-travel switch, as required by the rules. This switch must be configured in such a manner that it operates in all probable brake pedal and brake balance settings without causing harm to any vehicle component.

References

[1] A. Sharma and A. K. Marwah, “Braking Systems : Past , Present & Future,” vol. 2, no. 3, 2013.

[2] F. S. Uk, M. Engineers, and T. Imeche, “Concept Class UK 2020 Supplementary Rules Introduction,” 2020.

[3] M. Engineering, M. I. T. U. M. P, and M. P. Ujjain, “Braking Systems : Past , Present & Future * Akshat Sharma ** Amit Kumar Marwah Keywords : Braking systems , history of braking systems,” no. March, pp. 1991–1993, 2013.

[4] L. He, X. Wang, Y. Zhang, J. Wu, and L. Chen, “Modeling and Simulation Vehicle Air Brake System,” *Proc. from 8th Int. Model. Conf. Tech. Univeristy, Dresden, Ger.*, vol. 63, no. December 2014, pp. 430–435, 2011, doi: 10.3384/ecp11063430.

[5] L. Rudolf, *Brake Design and Safety*, 2nd ed. Society of Automotive Engineers, 1999.

[6] R. G. Rama, K. Reddy, V. Kumar, and S. Assistant, “Dynamic Analysis of Mechanical Braking System,” *Open J. Technol. Eng. Discip.*, vol. 2, no. 4, pp. 178–185, 2016, [Online]. Available: http://ojal.us/ojted/.

[7] J. F. Tarter, “Electric brake system modeling and simulation,” *SAE Tech. Pap.*, vol. 100, no. 1991, pp. 542–559, 1991, doi: 10.4271/911200.

[8] P. G. Anselma, S. P. Patil, and G. Belingardi, “Rapid optimal design of a light vehicle hydraulic brake system,” *SAE Tech. Pap.*, vol. 2019-April, no. April, pp. 1–10, 2019, doi: 10.4271/2019-01-0831.

[9] A. J. Day, H. P. Ho, K. Hussain, and A. Johnstone, “Brake system simulation to predict brake pedal feel in a passenger car,” *SAE Tech. Pap.*, vol. 4970, 2009, doi: 10.4271/2009-01-3043.

[10] “Tandem Master Cylinder.” https://www.itistudents.com/2021/06/tandem-master-cylinder.html (accessed Oct. 06, 2021).

[11] C. Wang and K. Shida, “A new method for on-line monitoring of brake fluid condition using an enclosed,” vol. 3625, doi: 10.1088/0957-0233/18/11/048.

[12] K. Lee, “Numerical Prediction of Brake Fluid Temperature,” no. 724, 2019.

[13] S. Ingale, S. Kothawade, A. Patankar, and R. Kulkarni, “Design and analysis of a brake caliper,” *Int. J. Mech. Eng. Technol.*, vol. 7, no. 4, pp. 227–233, 2016.

[14] “Advances in Manufacturing Systems: Select Proceedings of RAM 2020 - Google Books.” https://books.google.pt/books?hl=en&lr=&id=A0UgEAAAQBAJ&oi=fnd&pg=PA123&dq=brake+caliper+types&ots=FyV8dsikiU&sig=RDvNgJT3frVeLw9g1iX9khP4NRE&redir_esc=y (accessed Jun. 11, 2021).

[15] K. P. Rajurkar, *Advances in Manufacturing Systems*. USA: Springer, 2020.

[16] U. A. Curle, J. D. Wilkins, and G. Govender, “Industrial semi-solid rheocasting of aluminum A356 brake calipers,” *Adv. Mater. Sci. Eng.*, vol. 2011, 2011, doi: 10.1155/2011/195406.

[17] M. Kubota, T. Hamabe, Y. Nakazono, M. Fukuda, and K. Doi, “Development of a

lightweight brake disc rotor: a design approach for achieving an optimum thermal, vibration and weight balance," *JSAE Rev.*, vol. 21, no. 3, pp. 349–355, 2000, doi: 10.1016/S0389-4304(00)00050-3.

[18] W. Mark, "Brake Rotors," 2021. https://www.markwilliams.com/brake-rotor-material.html (accessed Oct. 06, 2021).

[19] M. A. Maleque, S. Dyuti, and M. M. Rahman, "Material selection method in design of automotive brake disc," *WCE 2010 - World Congr. Eng. 2010*, vol. 3, pp. 2322–2326, 2010.

[20] T. D. Gillespie, *Fundamentals of Vehicle Dynamics*. Warrendale: Society of Automotive Engineers, 1992.

[21] M. Kent, "Muscle spindle - Oxford Reference," *Oxford Dict. Sport. Sci. Med. (3 ed.)*, 2007, Accessed: Oct. 31, 2021. [Online]. Available: https://www-oxfordreference-com.proxy.lib.uwaterloo.ca/view/10.1093/acref/9780198568506.001.0001/acref-9780198568506-e-4535?rskey=lg06bM&result=2.

[22] Carol Hodanbosi, *Pascal's Principle and Hydraulics*. 1996.

[23] P. Kosky, R. Balmer, W. Keat, and G. Wise, *Exploring Engineering*, 3rd ed. .

[24] "Forced Convection Over a Flat Plate — Lesson 3 - ANSYS Innovation Courses." https://courses.ansys.com/index.php/courses/forced-convection-in-external-flows/lessons/forced-convection-over-a-flat-plate-lesson-3/ (accessed Jun. 23, 2021).

[25] M. Bahrami, "Forced Convection Heat Transfer." doi: ENSC 388 (F09).

[26] A. A. Regulations, "Formula Student Rules 2022," 2022.

[27] B. Zhuming, *Finite element analysis applications: a systematic and practical approach*, 1st ed. .

[28] P. de Buhan and S. Maghous, "A Numerical Method for Predicting t he Yield Strength of Structures," *Adv. Eng. Plast. its Appl.*, pp. 631–638, 1993, doi: 10.1016/B978-0-444-89991-0.50086-X.

[29] D. Gay and J. Gambelin, "Practical Aspects of Finite Element Modeling," *Model. Dimens. Struct.*, pp. 407–461, 2010, doi: 10.1002/9780470611289.ch8.

[30] P. Approach, *A Systematic and Practical Approach Finite Element Analysis Applications*. .

[31] "Practical Finite Element Analysis by Nitin S Gokhale, Sanjay S Deshpande, Sanjeev V Bedekar, Anand N Thite (z-lib.org).pdf." .

[32] T. D. Canonsburg, "ANSYS Workbench User ' s Guide," vol. 15317, no. November, pp. 724–746, 2010.

[33] Ansys, "Equivalent Stress Solid Mechanics I-Understanding the Physics," 2020.

[34] M. W. Al-Grafi, M. K. Mohamed, and F. A. Salem, "Analysis of Vehicle Friction Coefficient by Simulink/Matlab," *Int. J. Control. Autom. Syst.*, vol. 2, no. 2, 2013, Accessed: Oct. 18, 2021. [Online]. Available: http://www.researchpub.org/journal/jac/jac.html.

[35] "CP2623 Type AP Racing Master Cylinder." https://apracing.com/race-

car/master-cylinders/flange-mounted-types/vertical-flange-types/cp2623-type (accessed Oct. 18, 2021).

[36] “AP Racing brake fluid reservoir 75cc: screw-in to CP2623 cylinders.” https://www.burtonpower.com/ap-racing-brake-fluid-reservoir-75cc-screw-in-to-cp2623-cp4709-12.html (accessed Oct. 18, 2021).

[37] “CP4226-2S0 AP Racing Callipers.” https://apracing.com/special-vehicles/motorcycle/brake-calipers/cp4226-2s0?switch=1 (accessed Oct. 18, 2021).

[38] “CP4226D27 AP Racing Pads.” https://apracing.com/race-car/brake-pads/2-piston-caliper-pad-profiles/cp4226d27-motorcycle (accessed Oct. 18, 2021).

[39] OZ Group, “Formula Student OZ Wheels Program.” https://www.ozracing.com/images/content/OZ_Formula_Student_Wheels_Program-2016-eng.pdf (accessed Sep. 30, 2021).

[40] ANSYS, “SOLID187 3-D 10-Node Tetrahedral Structural Solid Geometry.” https://www.mm.bme.hu/~gyebro/files/ans_help_v182/ans_elem/Hlp_E_SOLID187.html (accessed Oct. 20, 2021).

[41] “AP Racing Brake Pads.” https://apracing.com/race-car/formula-student-sae/brake-pads (accessed Oct. 18, 2021).

Appendix A

Aluminium alloy film temperature

To calculate the film temperature, the rotor is considered as a flat plan and to find the forced convective heat transfer coefficient h.

Now that the rotor is subject to the Newton's law of cooling, plus the fact that the rotor is dispersing heat on both sides, therefore, the following equation is formed:

$$\boldsymbol{Q_{conv} = hA(T_{\infty} - T_s)2}$$

$$\boldsymbol{T_{Film} = \frac{T_s + T_{\infty}}{2}}$$

$$T_{Film} = \frac{470 + 20}{2} = 245\ ℃$$

For $\boldsymbol{T_{Film} = 245}$ ℃

Thermal Conductivity of air (K_f)

$\boldsymbol{K_f = 0.04104 \frac{w}{mk}.}$

kinematic viscosity (v)

$\boldsymbol{\nu = 4.091 * 10^{-5} \frac{m^2}{s}.}$

Prandtl number (P_r)

$\boldsymbol{P_r = 0.6946.}$

Front:

Reynolds number

$$\boldsymbol{Re = \frac{VL}{\nu}}$$

Where:

V = Velocity of air

L = Distance travelled by air = 2πr

r = radius of disc = 0.1m

$$\boldsymbol{Re} = \frac{(33.33) * (0.0625)}{4.091 * 10^{-5}} = \mathbf{50919.7 < 5 * 10^5}$$

As, $Re < 5 * 10^5$, for a flow over flat plate, the flow is laminar.

Average Nusselt number

$$\boldsymbol{n_{avg} = 0.664 * R_e^{\frac{1}{2}} * P_r^{\frac{1}{3}}}$$

$$n_{avg} = 0.664 * (50919.7)^{\frac{1}{2}} * (0.6946)^{\frac{1}{3}} = \mathbf{132.695}$$

Since

$$n_u = \frac{h * L}{k}$$

Means that

$$h = \frac{n_u * k}{L}$$

$$h = \frac{132.695 * 0.04104}{0.0625} = \mathbf{87.1328}\frac{\boldsymbol{w}}{\boldsymbol{m^2 k}}$$

Rear:

Reynolds number

$$\boldsymbol{Re = \frac{VL}{\nu}}$$

$$\boldsymbol{Re = \frac{(33.33) * (0.06)}{4.091 * 10^{-5}} = 48882.9 < 5 * 10^5}$$

As, $Re < 5 * 10^5$, for a flow over flat plate, the flow is laminar.

Average Nusselt number

$$\boldsymbol{n_{avg} = 0.664 * R_e^{\frac{1}{2}} * P_r^{\frac{1}{3}}}$$

$$\boldsymbol{n_{avg} = 0.664 * (48882.9)^{\frac{1}{2}} * (0.6946)^{\frac{1}{3}} = 130.014}$$

Since

$$n_u = \frac{h * L}{k}$$

Means that

$$h = \frac{n_u * k}{L}$$

$$h = \frac{130.014 * 0.04104}{0.06} = \boldsymbol{88.9296 \frac{w}{m^2 k}}$$

TABLE A–9

Properties of air at 1 atm pressure

Temp. T, °C	Density ρ, kg/m^3	Specific Heat c_p J/kg-K	Thermal Conductivity k, W/m-K	Thermal Diffusivity α, m^2/s	Dynamic Viscosity μ, kg/m-s	Kinematic Viscosity ν, m^2/s	Prandtl Number Pr
−150	2.866	983	0.01171	4.158×10^{-6}	8.636×10^{-6}	3.013×10^{-6}	0.7246
−100	2.038	966	0.01582	8.036×10^{-6}	1.189×10^{-6}	5.837×10^{-6}	0.7263
−50	1.582	999	0.01979	1.252×10^{-5}	1.474×10^{-5}	9.319×10^{-6}	0.7440
−40	1.514	1002	0.02057	1.356×10^{-5}	1.527×10^{-5}	1.008×10^{-5}	0.7436
−30	1.451	1004	0.02134	1.465×10^{-5}	1.579×10^{-5}	1.087×10^{-5}	0.7425
−20	1.394	1005	0.02211	1.578×10^{-5}	1.630×10^{-5}	1.169×10^{-5}	0.7408
−10	1.341	1006	0.02288	1.696×10^{-5}	1.680×10^{-5}	1.252×10^{-5}	0.7387
0	1.292	1006	0.02364	1.818×10^{-5}	1.729×10^{-5}	1.338×10^{-5}	0.7362
5	1.269	1006	0.02401	1.880×10^{-5}	1.754×10^{-5}	1.382×10^{-5}	0.7350
10	1.246	1006	0.02439	1.944×10^{-5}	1.778×10^{-5}	1.426×10^{-5}	0.7336
15	1.225	1007	0.02476	2.009×10^{-5}	1.802×10^{-5}	1.470×10^{-5}	0.7323
20	1.204	1007	0.02514	2.074×10^{-5}	1.825×10^{-5}	1.516×10^{-5}	0.7309
25	1.184	1007	0.02551	2.141×10^{-5}	1.849×10^{-5}	1.562×10^{-5}	0.7296
30	1.164	1007	0.02588	2.208×10^{-5}	1.872×10^{-5}	1.608×10^{-5}	0.7282
35	1.145	1007	0.02625	2.277×10^{-5}	1.895×10^{-5}	1.655×10^{-5}	0.7268
40	1.127	1007	0.02662	2.346×10^{-5}	1.918×10^{-5}	1.702×10^{-5}	0.7255
45	1.109	1007	0.02699	2.416×10^{-5}	1.941×10^{-5}	1.750×10^{-5}	0.7241
50	1.092	1007	0.02735	2.487×10^{-5}	1.963×10^{-5}	1.798×10^{-5}	0.7228
60	1.059	1007	0.02808	2.632×10^{-5}	2.008×10^{-5}	1.896×10^{-5}	0.7202
70	1.028	1007	0.02881	2.780×10^{-5}	2.052×10^{-5}	1.995×10^{-5}	0.7177
80	0.9994	1008	0.02953	2.931×10^{-5}	2.096×10^{-5}	2.097×10^{-5}	0.7154
90	0.9718	1008	0.03024	3.086×10^{-5}	2.139×10^{-5}	2.201×10^{-5}	0.7132
100	0.9458	1009	0.03095	3.243×10^{-5}	2.181×10^{-5}	2.306×10^{-5}	0.7111
120	0.8977	1011	0.03235	3.565×10^{-5}	2.264×10^{-5}	2.522×10^{-5}	0.7073
140	0.8542	1013	0.03374	3.898×10^{-5}	2.345×10^{-5}	2.745×10^{-5}	0.7041
160	0.8148	1016	0.03511	4.241×10^{-5}	2.420×10^{-5}	2.975×10^{-5}	0.7014
180	0.7788	1019	0.03646	4.593×10^{-5}	2.504×10^{-5}	3.212×10^{-5}	0.6992
200	0.7459	1023	0.03779	4.954×10^{-5}	2.577×10^{-5}	3.455×10^{-5}	0.6974
250	0.6746	1033	0.04104	5.890×10^{-5}	2.760×10^{-5}	4.091×10^{-5}	0.6946
300	0.6158	1044	0.04418	6.871×10^{-5}	2.934×10^{-5}	4.765×10^{-5}	0.6935
350	0.5664	1056	0.04721	7.892×10^{-5}	3.101×10^{-5}	5.475×10^{-5}	0.6937
400	0.5243	1069	0.05015	8.951×10^{-5}	3.261×10^{-5}	6.219×10^{-5}	0.6948
450	0.4880	1081	0.05298	1.004×10^{-4}	3.415×10^{-5}	6.997×10^{-5}	0.6965
500	0.4565	1093	0.05572	1.117×10^{-4}	3.563×10^{-5}	7.806×10^{-5}	0.6986
600	0.4042	1115	0.06093	1.352×10^{-4}	3.846×10^{-5}	9.515×10^{-5}	0.7037
700	0.3627	1135	0.06581	1.598×10^{-4}	4.111×10^{-5}	1.133×10^{-4}	0.7092
800	0.3289	1153	0.07037	1.855×10^{-4}	4.362×10^{-5}	1.326×10^{-4}	0.7149
900	0.3008	1169	0.07465	2.122×10^{-4}	4.600×10^{-5}	1.529×10^{-4}	0.7206
1000	0.2772	1184	0.07868	2.398×10^{-4}	4.826×10^{-5}	1.741×10^{-4}	0.7260
1500	0.1990	1234	0.09599	3.908×10^{-4}	5.817×10^{-5}	2.922×10^{-4}	0.7478
2000	0.1553	1264	0.11113	5.664×10^{-4}	6.630×10^{-5}	4.270×10^{-4}	0.7539

Note: For ideal gases, the properties c_p, k, μ, and Pr are independent of pressure. The properties ρ, ν, and α at a pressure P (in atm) other than 1 atm are determined by multiplying the values of ρ at the given temperature by P and by dividing ν and α by P.

Source: Data generated from the EES software developed by S. A. Klein and F. L. Alvarado. Original sources: Keenan, Chao, Keyes, Gas Tables, Wiley, 198; and Thermophysical Properties of Matter, Vol. 3: Thermal Conductivity, Y. S. Touloukian, P. E. Liley, S. C. Saxena, Vol. 11: Viscosity, Y. S. Touloukian, S. C. Saxena, and P. Hestermans, IFI/Plenum, NY, 1970, ISBN 0-306067020-8.

Appendix B

2D Braking system assembly drawings.

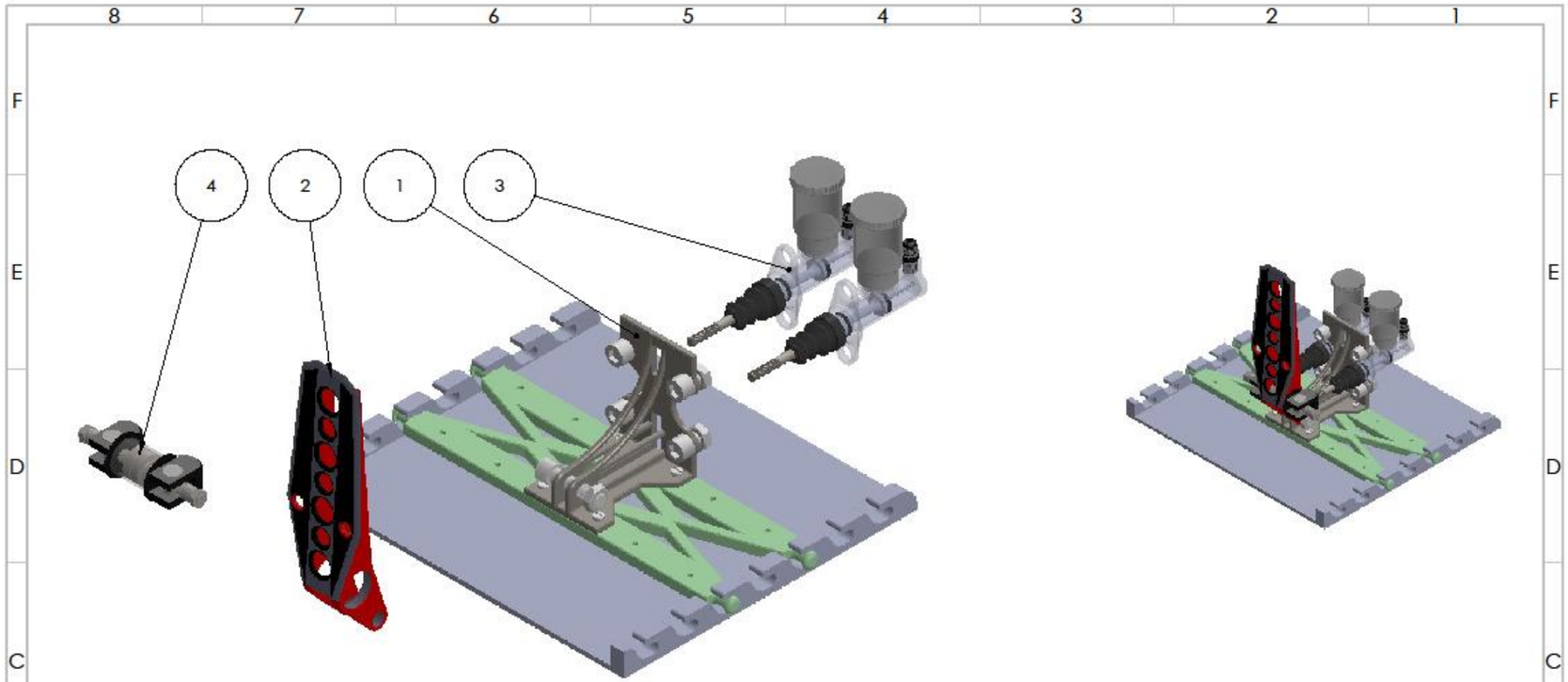

ITEM NO.	DESCRIPTION	QTY.
1	Base Assembly	1
2	BRAKE PEDAL	1
3	Master Cylinder Assembly	2
4	Balance Bar Assembly	1

	Date	Name
Draw.	25/October 2021	Emad Sweed
Verif.		João Eduardo Pinto Castro Ribeiro

Pedal Box Assembly

ESTIG-IPB

Scale 1:2

Exploded View

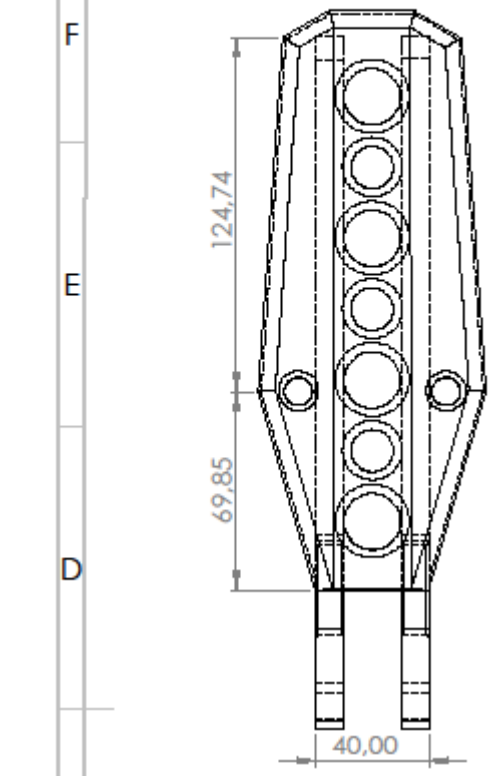

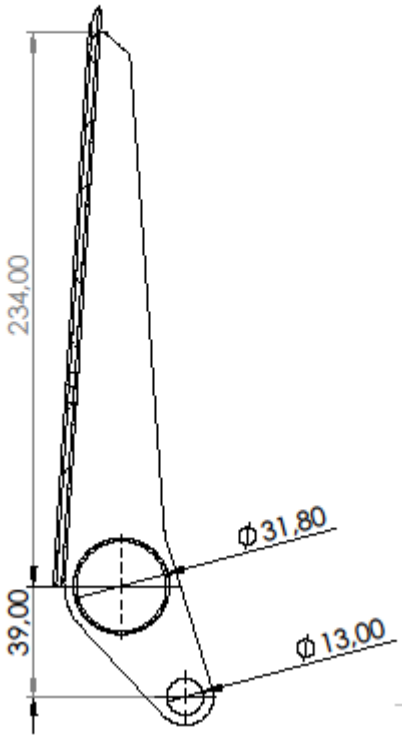

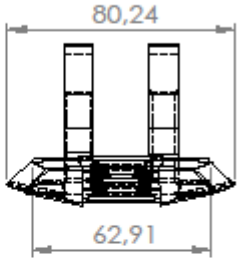

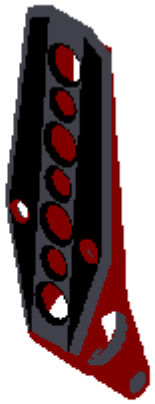

	Date	Name		
Draw.	15/10 /2021	Emad Sweed	BrakePedal	ESTIG-IPB
Verif.		João Eduardo Pinto Castro Ribeiro		
Scale 1:2			Pedal Box Assembly	Material:
				Number: 2

SOLIDWORKS Educational Product. For Instructional Use Only.

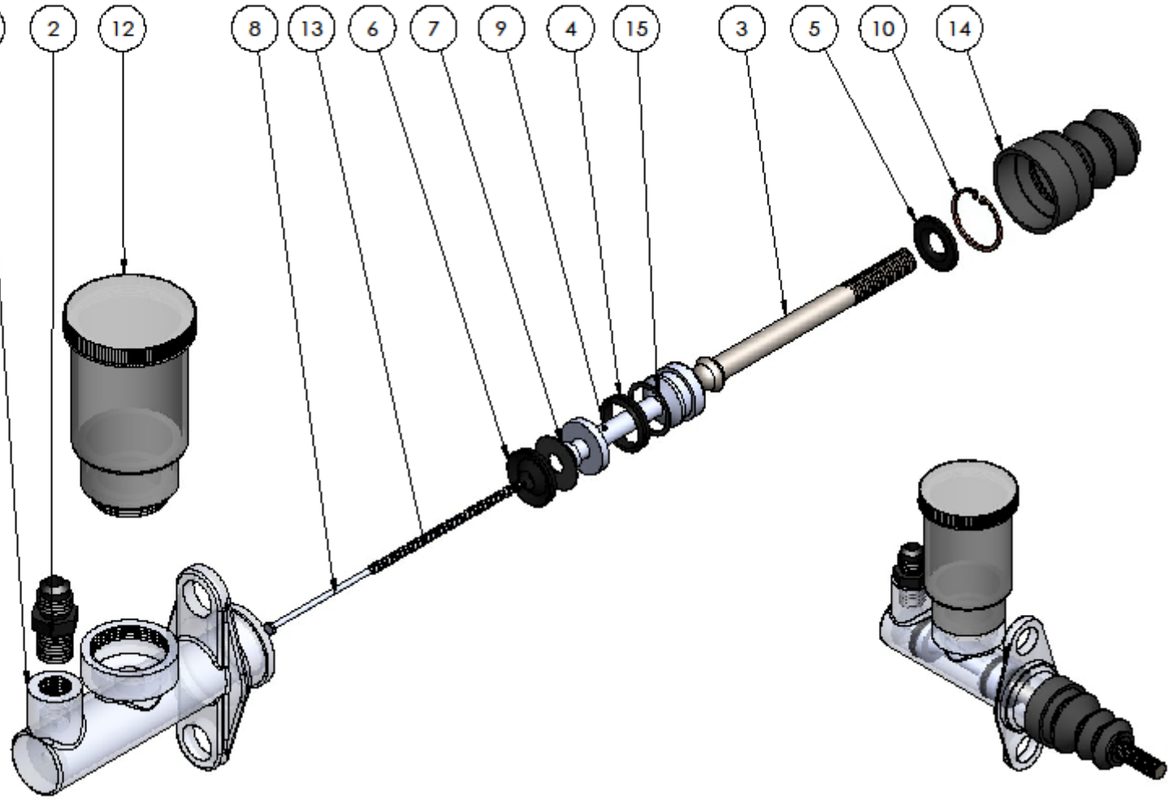

ITEM NO.	DESCRIPTION	QTY.
1	Master Cylinder Body	1
2	Master Cylinder Outlet M10-1.5	1
3	Master Cylinder Pushrod	1
4	Secondary Seal	1
5	Piston Stop Washer	1
6	Primary Seal	1
7	Primary Washer	1
8	Spring Guid Pin	1
9	Piston	1
10	Circlip	1
11	Reservoir	1
12	Reservoir Cover	1
13	Master Cylinder Return Spring	1
14	Master Cylinder Boot	1
15	Secondary Washer	1

	Date	Name		
Draw.	14/10/2021	Emad Sweed	CP2623 Master Cylinder Assembly	ESTIG-IPB
Verif.		João Eduardo Pinto Castro Ribeiro		
Scale 1:1			Exploded View	

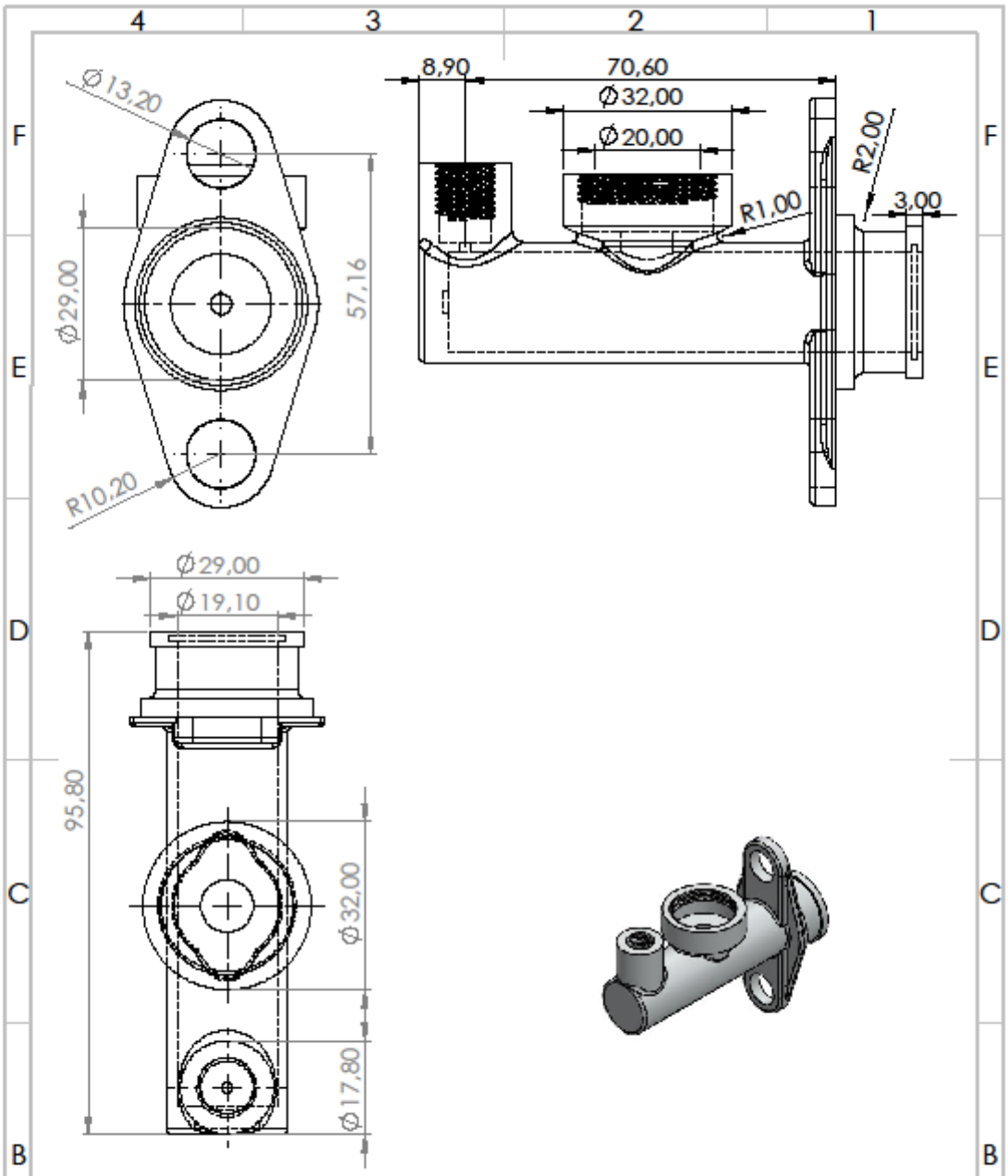

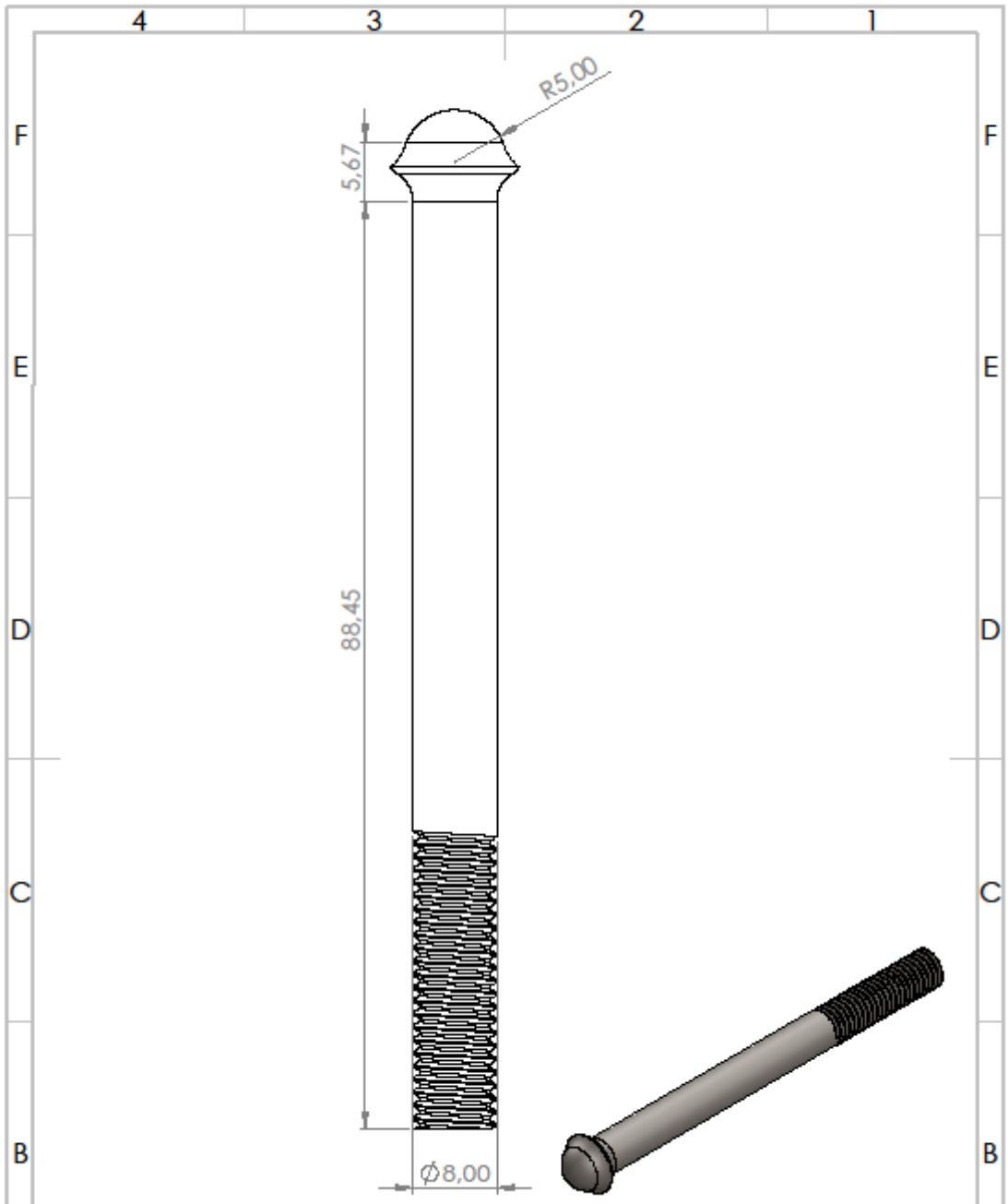

	Date	Name	CP2623 Master Cylinder Assembly	ESTIG-IPB
Draw.	15/10 /2021	Emad Sweed		
Verif.		João Eduardo Pinto Castro Ribeiro		
Scale 2:1		Pushrod	Material:	
			Number: 3	

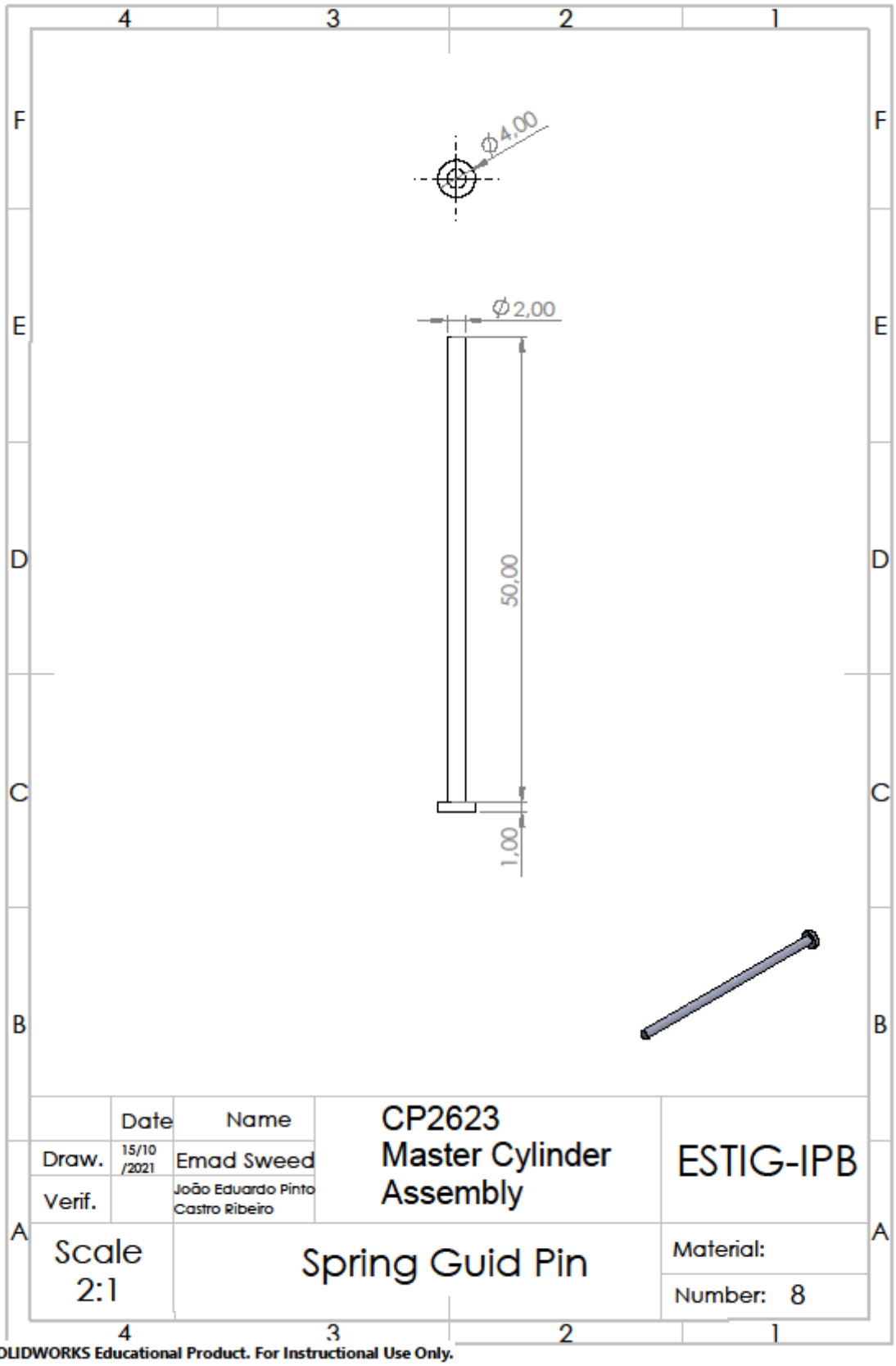
4
3
2
1
F
E
D
C
B
A
Ø4,00
Ø2,00
50,00
1,00
Date
Name
Draw.
15/10 /2021
Emad Sweed
Verif.
João Eduardo Pinto Castro Ribeiro
CP2623
Master Cylinder Assembly
ESTIG-IPB
Scale 2:1
Spring Guid Pin
Material:
Number: 8
SOLIDWORKS Educational Product. For Instructional Use Only.

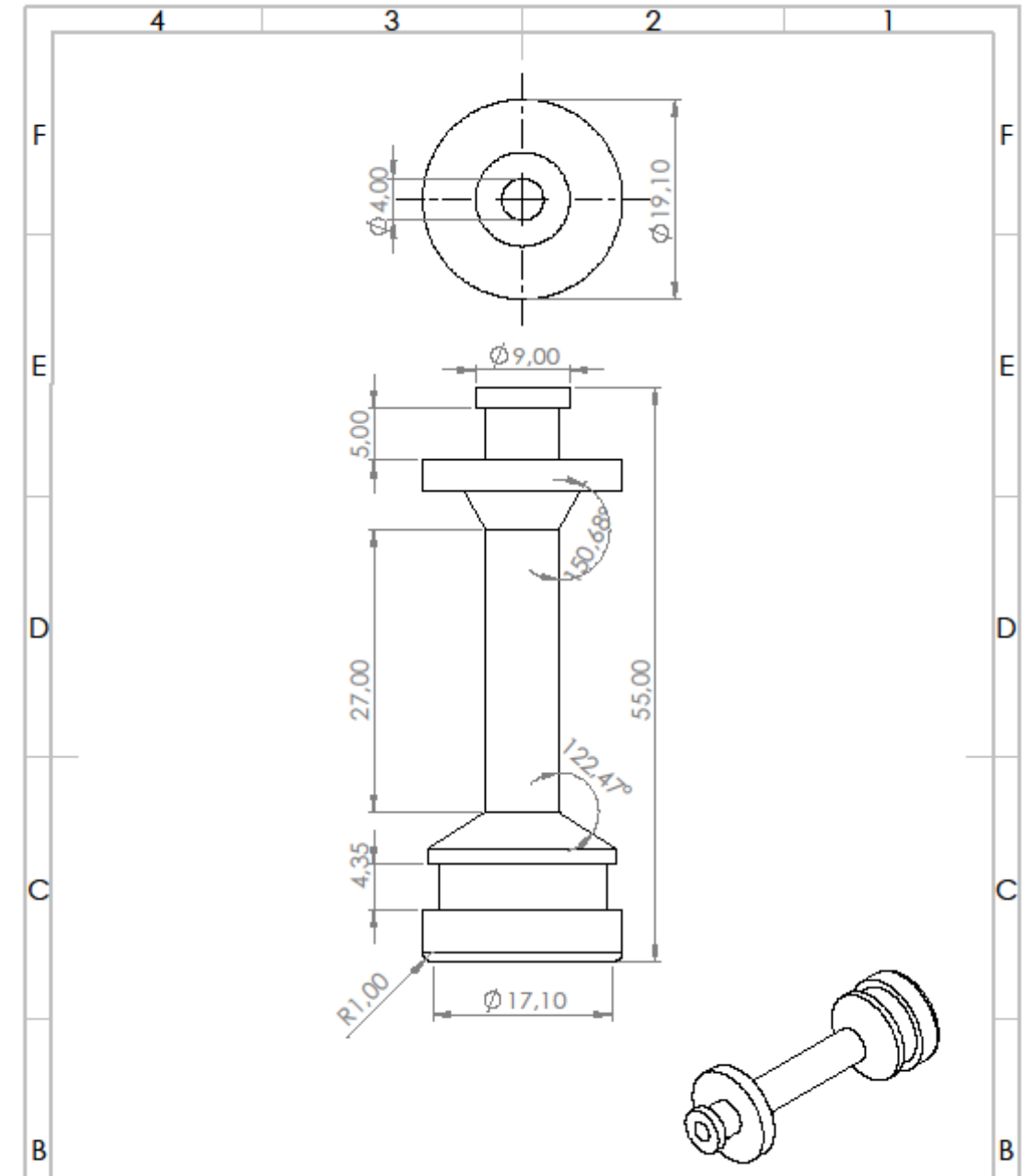

	Date	Name		
Draw.	15/10 /2021	Emad Sweed	CP2623 Master Cylinder Assembly	ESTIG-IPB
Verif.		João Eduardo Pinto Castro Ribeiro		
Scale 2:1			Piston	Material:
				Number: 9

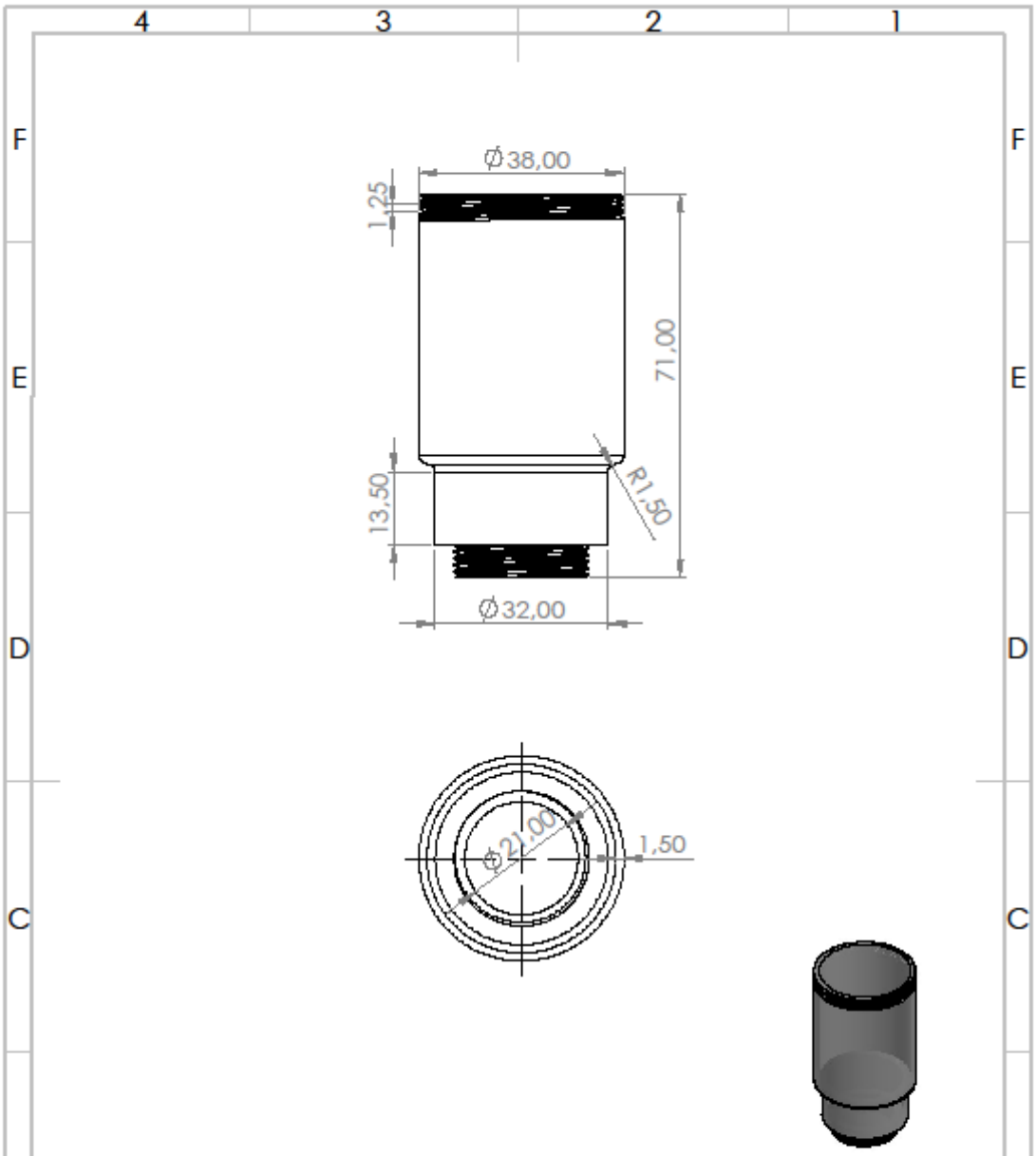

	Date	Name		
Draw.	15/10 /2021	Emad Sweed	CP2623 Master Cylinder Assembly	ESTIG-IPB
Verif.		João Eduardo Pinto Castro Ribeiro		
Scale 1:1			Reservoir	Material:
				Number: 11

SOLIDWORKS Educational Product. For Instructional Use Only.

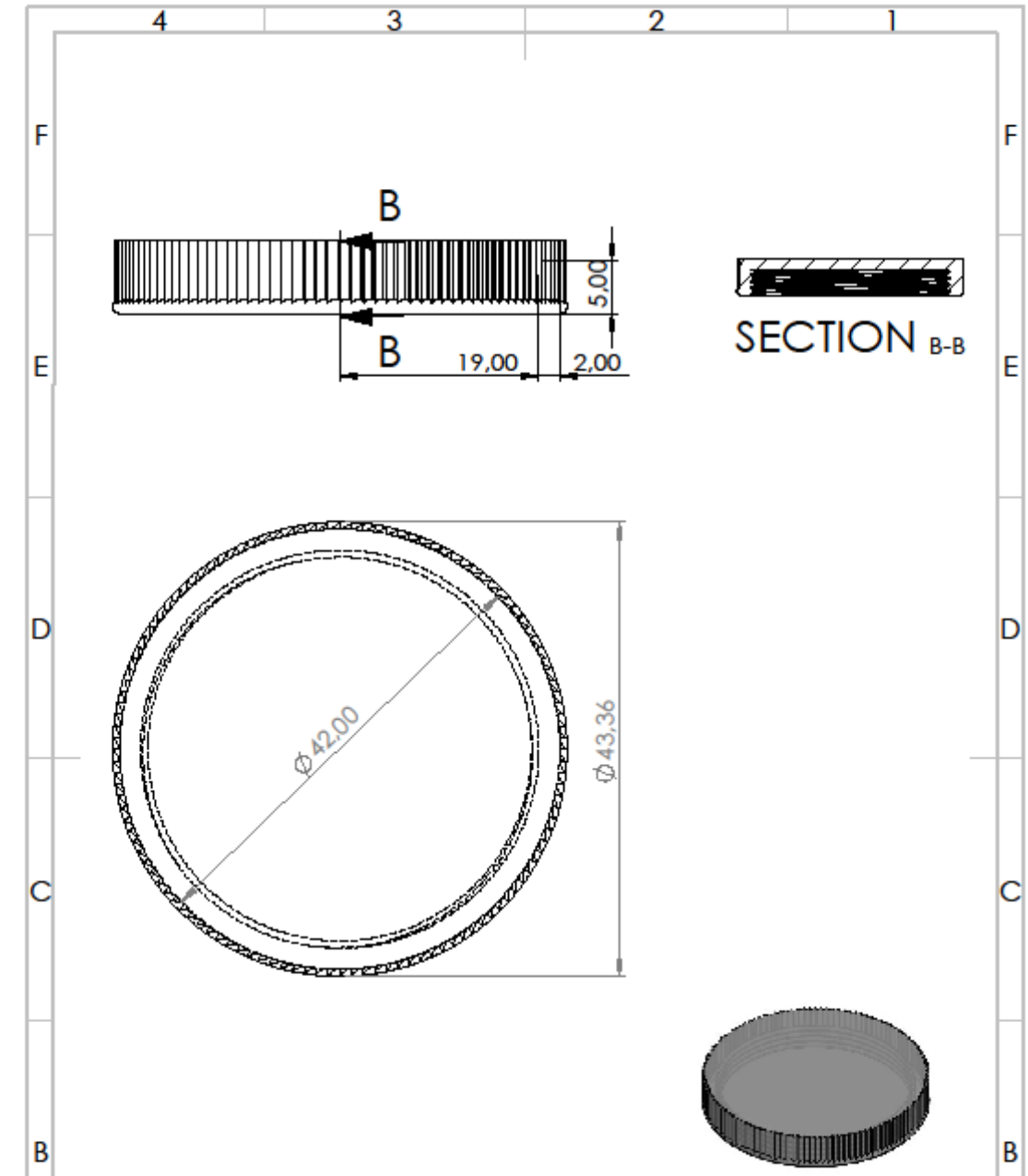
B
B
5,00
19,00
2,00
SECTION B-B
Ø42,00
Ø43,36
Date
Name
Draw.
15/10 /2021
Emad Sweed
Verif.
João Eduardo Pinto Castro Ribeiro
CP2623
Master Cylinder Assembly
ESTIG-IPB
Scale 2:1
Reservoir Cover
Material:
Number: 12
SOLIDWORKS Educational Product. For Instructional Use Only.

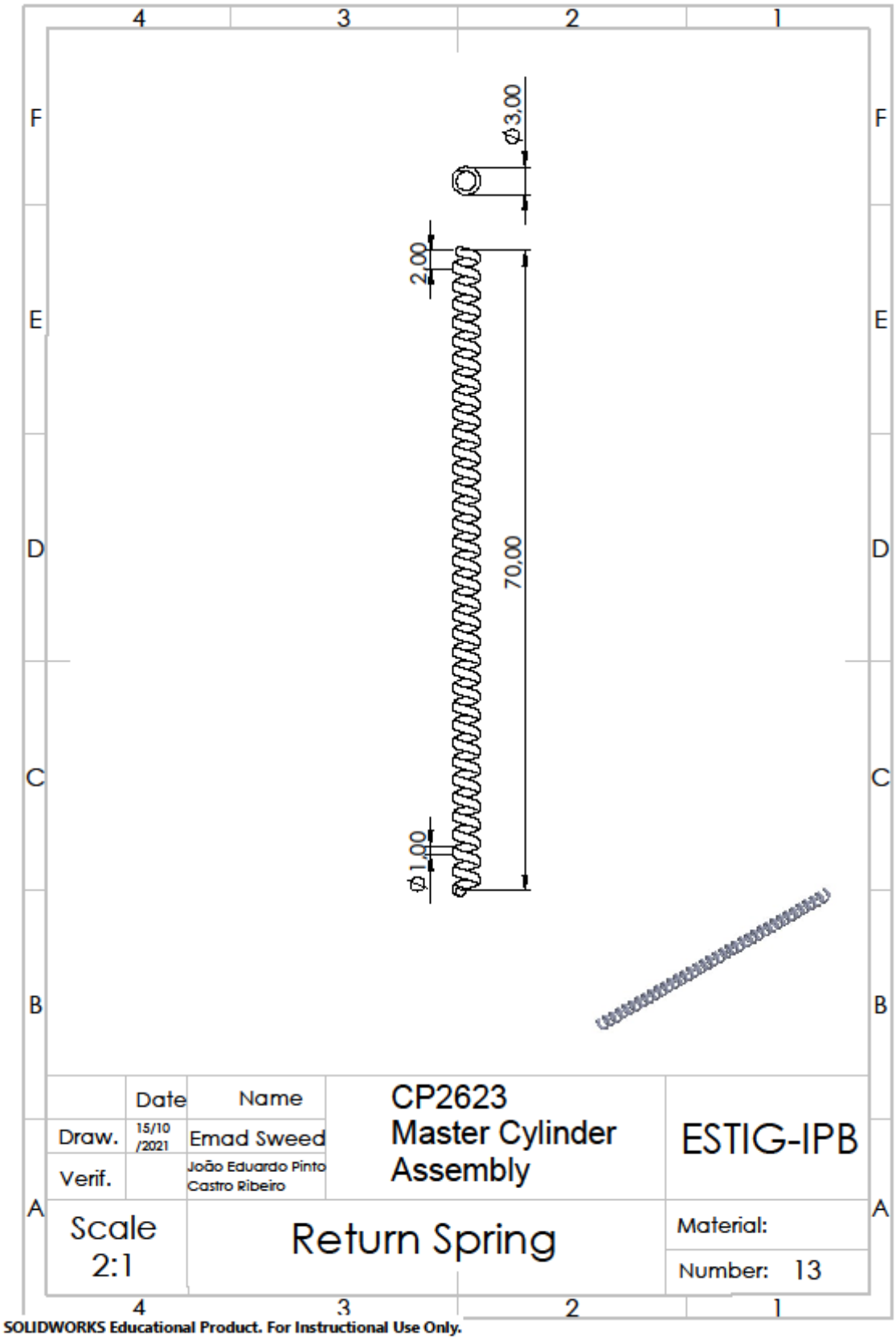
4
3
2
1
F
E
D
C
B
A
Ø3,00
2,00
70,00
Ø1,00
Date
Name
Draw.
15/10 /2021
Emad Sweed
Verif.
João Eduardo Pinto Castro Ribeiro
CP2623
Master Cylinder Assembly
ESTIG-IPB
Scale 2:1
Return Spring
Material:
Number: 13
SOLIDWORKS Educational Product. For Instructional Use Only.

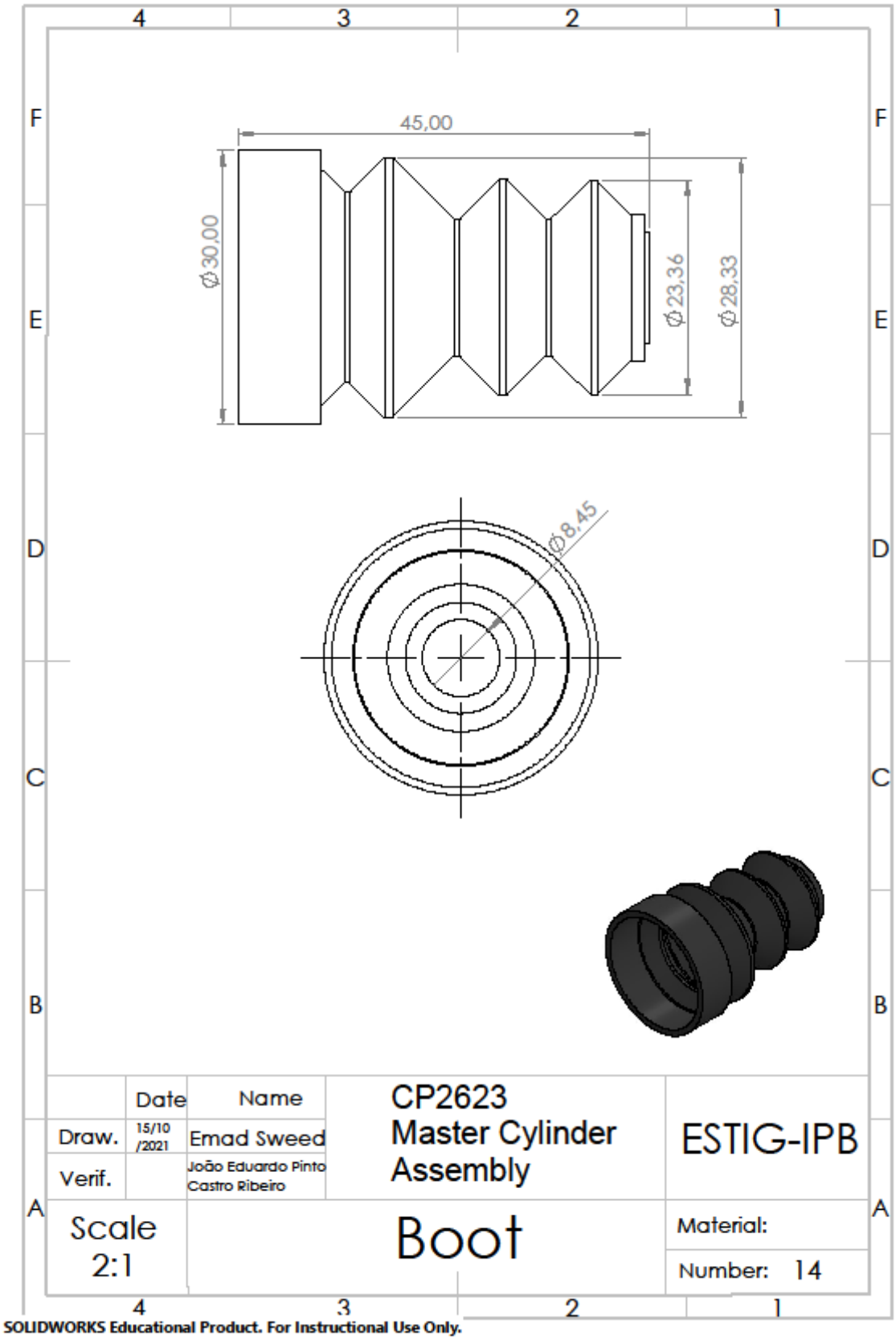

	Date	Name		
Draw.	15/10 /2021	Emad Sweed	CP2623 Master Cylinder Assembly	ESTIG-IPB
Verif.		João Eduardo Pinto Castro Ribeiro		
Scale 2:1			Boot	Material:
				Number: 14

SOLIDWORKS Educational Product. For Instructional Use Only.

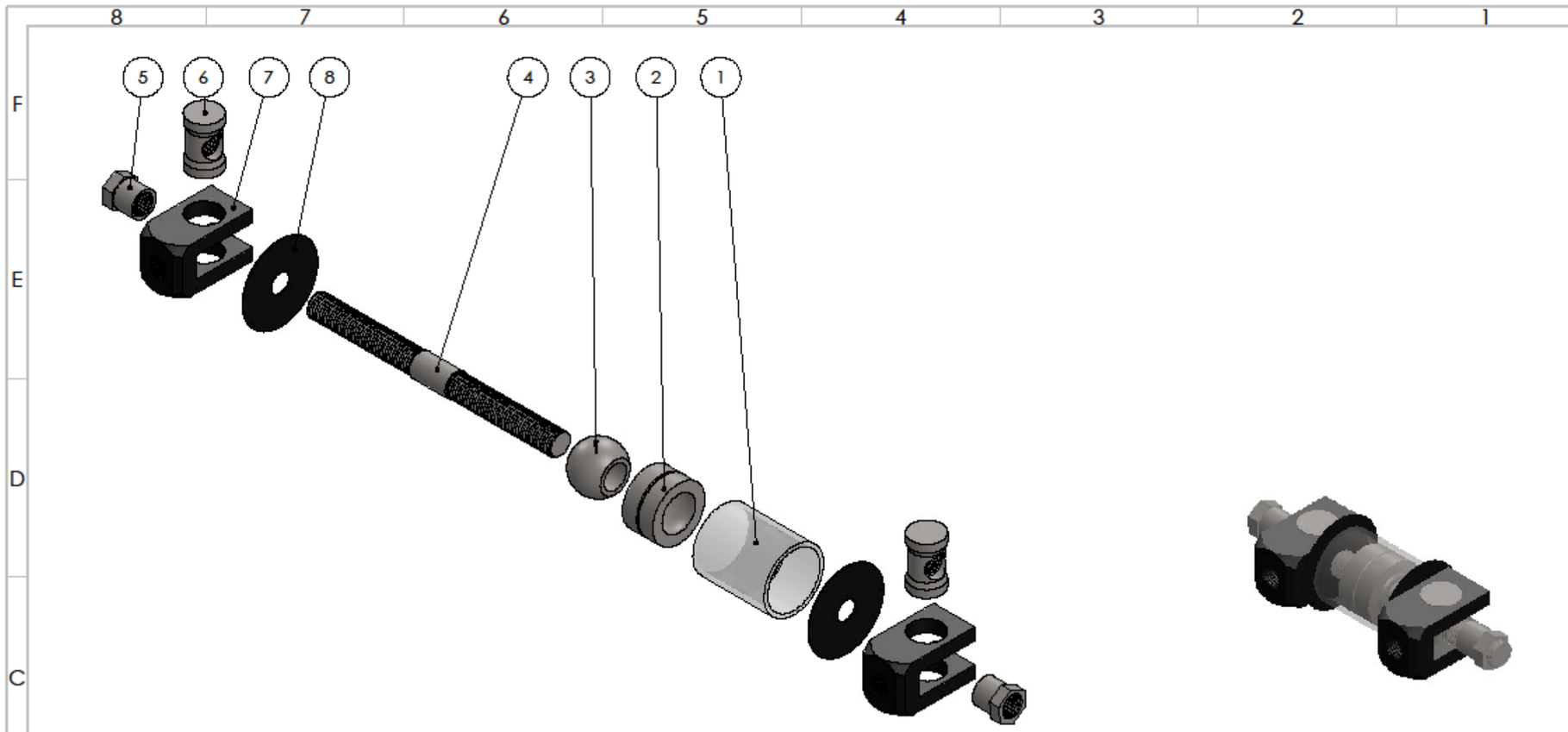

ITEM NO.	DESCRIPTION	QTY.
1	Pivot Sleeve BALANCE BAR	1
2	Spherical Bearing BALANCE BAR	1
3	Adjusting Shaft Holder	1
4	Adjusting Shaft Balance Bar	1
5	Jam Nut BALANCE BAR	2
6	Barrel Nut BALANCE BAR	2
7	Clevis BALANCE BAR	2
8	Shim Washer BALANCE BAR	2

	Date	Name
Draw.	18/10/2021	Emad Sweed
Verif.		João Eduardo Pinto Castro Ribeiro

Balance Bar Assembly

ESTIG-IPB

Scale 1:2

Exploded View

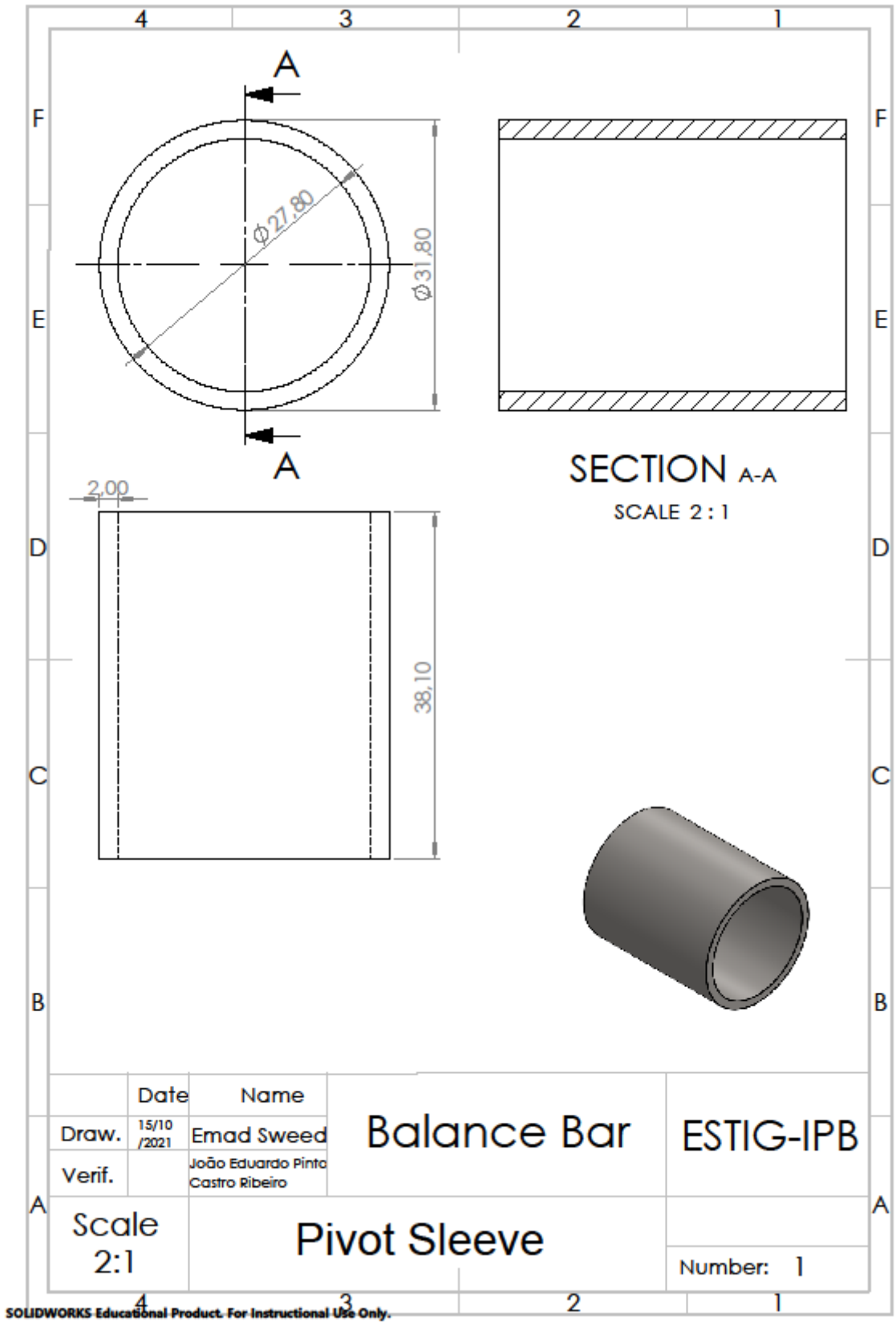
A
A
Ø27,80
Ø31,80
SECTION A-A
SCALE 2 : 1
2,00
38,10
Date
Name
Draw.
15/10 /2021
Emad Sweed
Verif.
João Eduardo Pinto Castro Ribeiro
Balance Bar
ESTIG-IPB
Scale 2:1
Pivot Sleeve
Number: 1
SOLIDWORKS Educational Product. For Instructional Use Only.

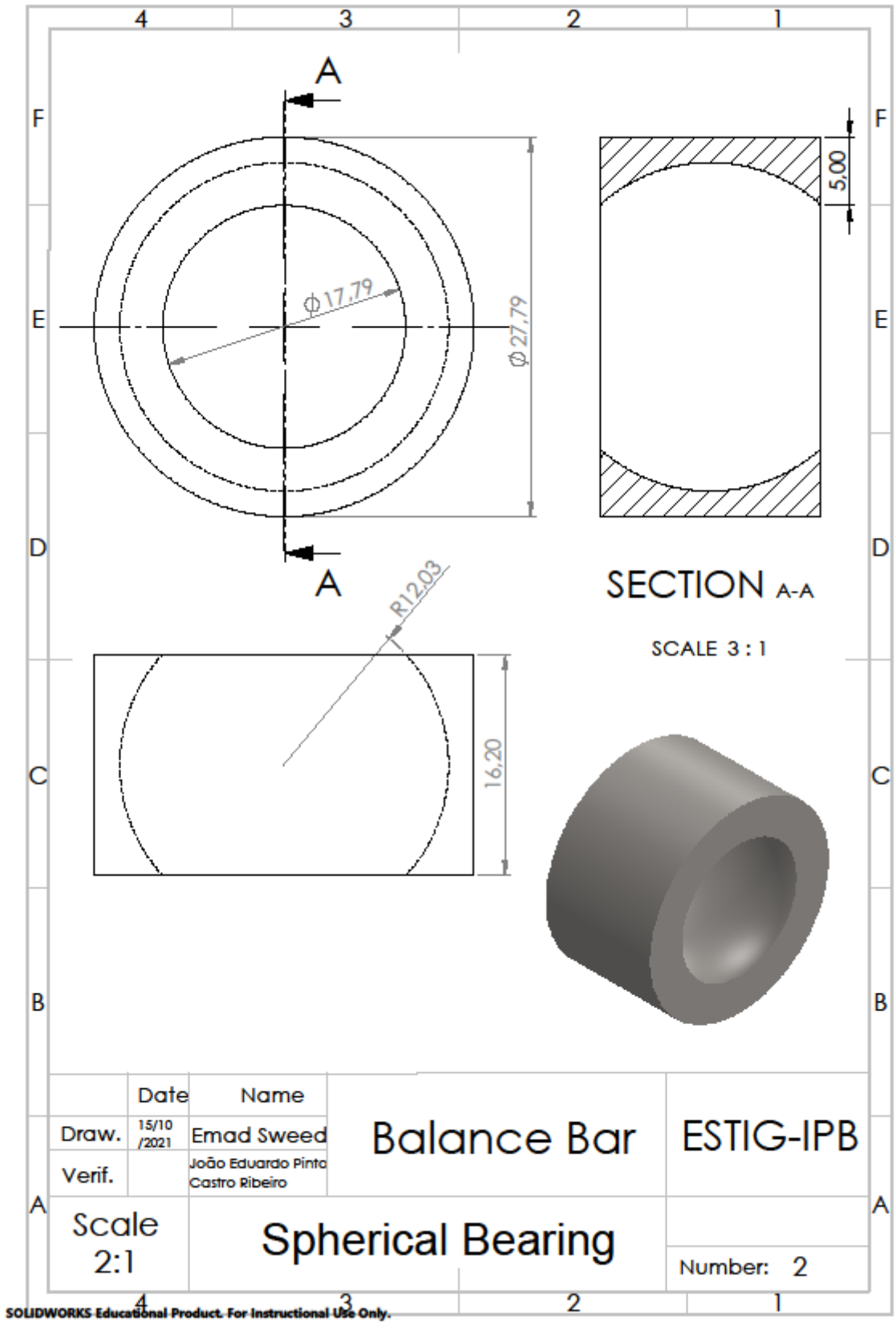
A
A
Ø17,79
Ø27,79
5,00
SECTION A-A
SCALE 3 : 1
R12,03
16,20
Date
Name
Draw.
15/10 /2021
Emad Sweed
Verif.
João Eduardo Pinto Castro Ribeiro
Balance Bar
ESTIG-IPB
Scale 2:1
Spherical Bearing
Number: 2
SOLIDWORKS Educational Product. For Instructional Use Only.

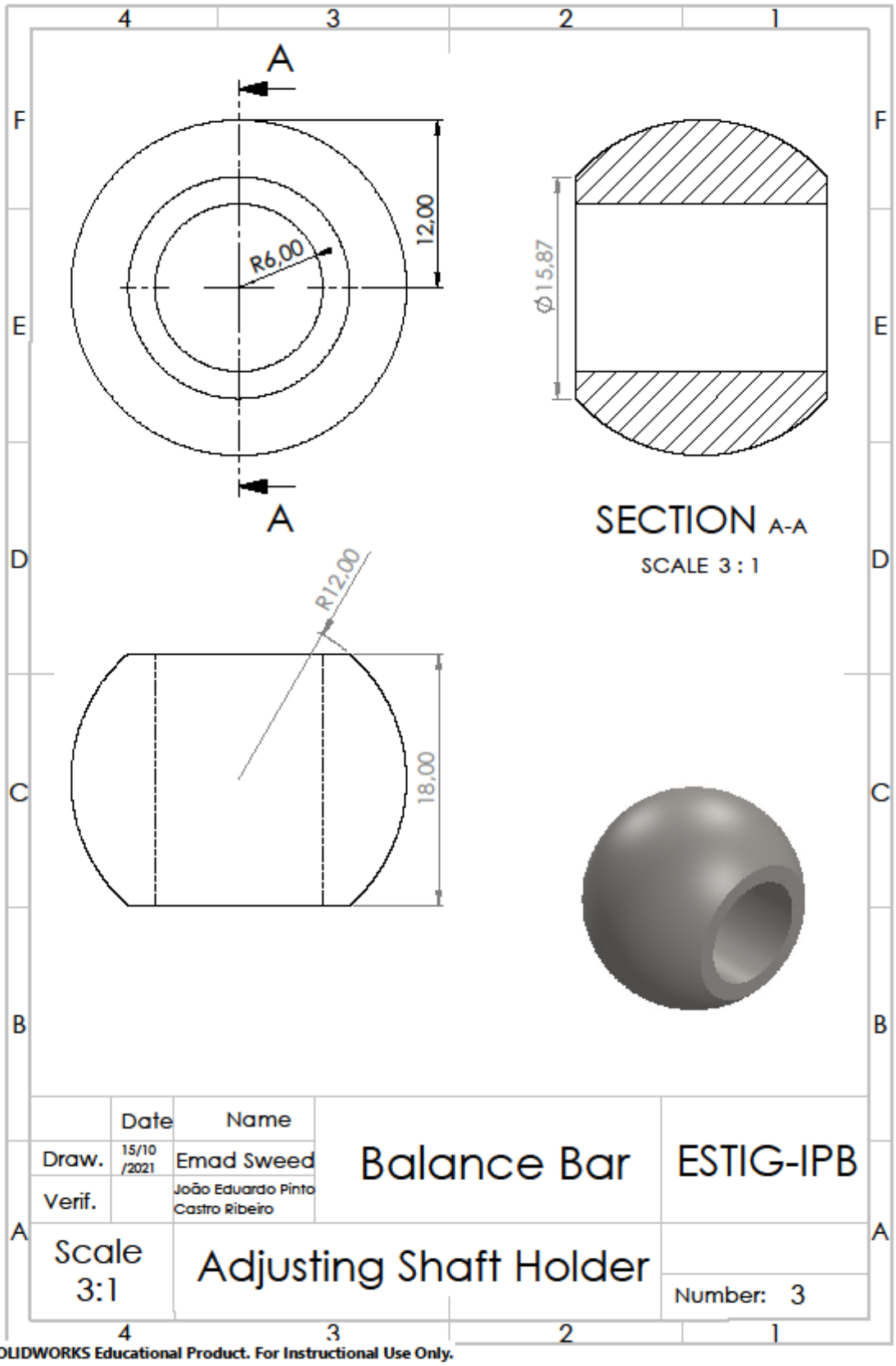
A
R6,00
12,00
A
Ø15,87
SECTION A-A
SCALE 3 : 1
R12,00
18,00
Date
Name
Draw.
15/10 /2021
Emad Sweed
Verif.
João Eduardo Pinto Castro Ribeiro
Balance Bar
ESTIG-IPB
Scale 3:1
Adjusting Shaft Holder
Number: 3
SOLIDWORKS Educational Product. For Instructional Use Only.

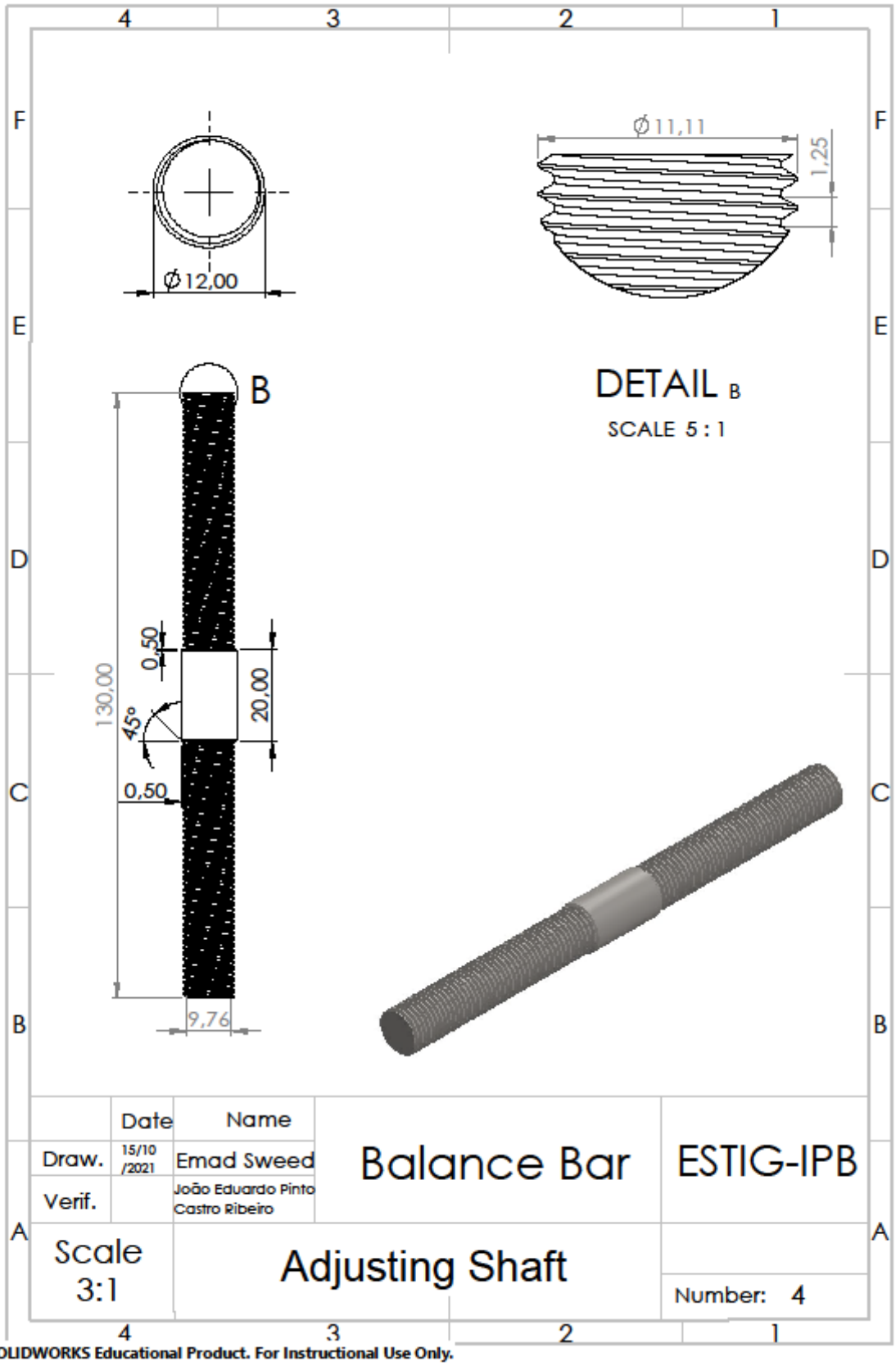
Ø12,00
Ø11,11
1,25
B
DETAIL B
SCALE 5 : 1
130,00
0,50
20,00
45°
0,50
9,76
Date
Name
Draw.
15/10 /2021
Emad Sweed
Verif.
João Eduardo Pinto Castro Ribeiro
Balance Bar
ESTIG-IPB
Scale 3:1
Adjusting Shaft
Number: 4
SOLIDWORKS Educational Product. For Instructional Use Only.

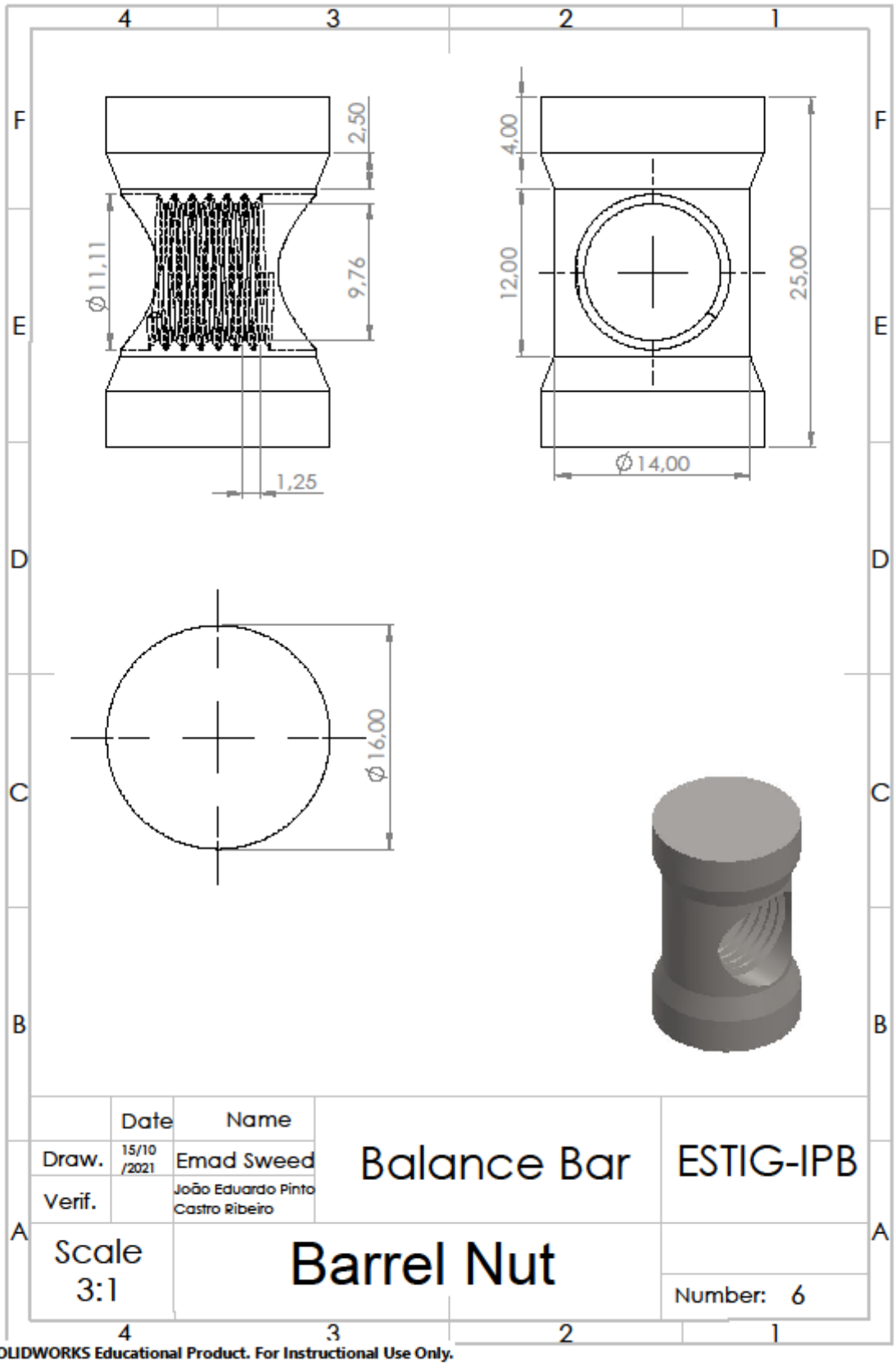
4
3
2
1
F
E
D
C
B
A
2,50
Ø11,11
9,76
1,25
4,00
12,00
25,00
Ø14,00
Ø16,00
Date
Name
Draw.
15/10
/2021
Emad Sweed
Verif.
João Eduardo Pinto
Castro Ribeiro
Balance Bar
ESTIG-IPB
Scale
3:1
Barrel Nut
Number: 6
SOLIDWORKS Educational Product. For Instructional Use Only.

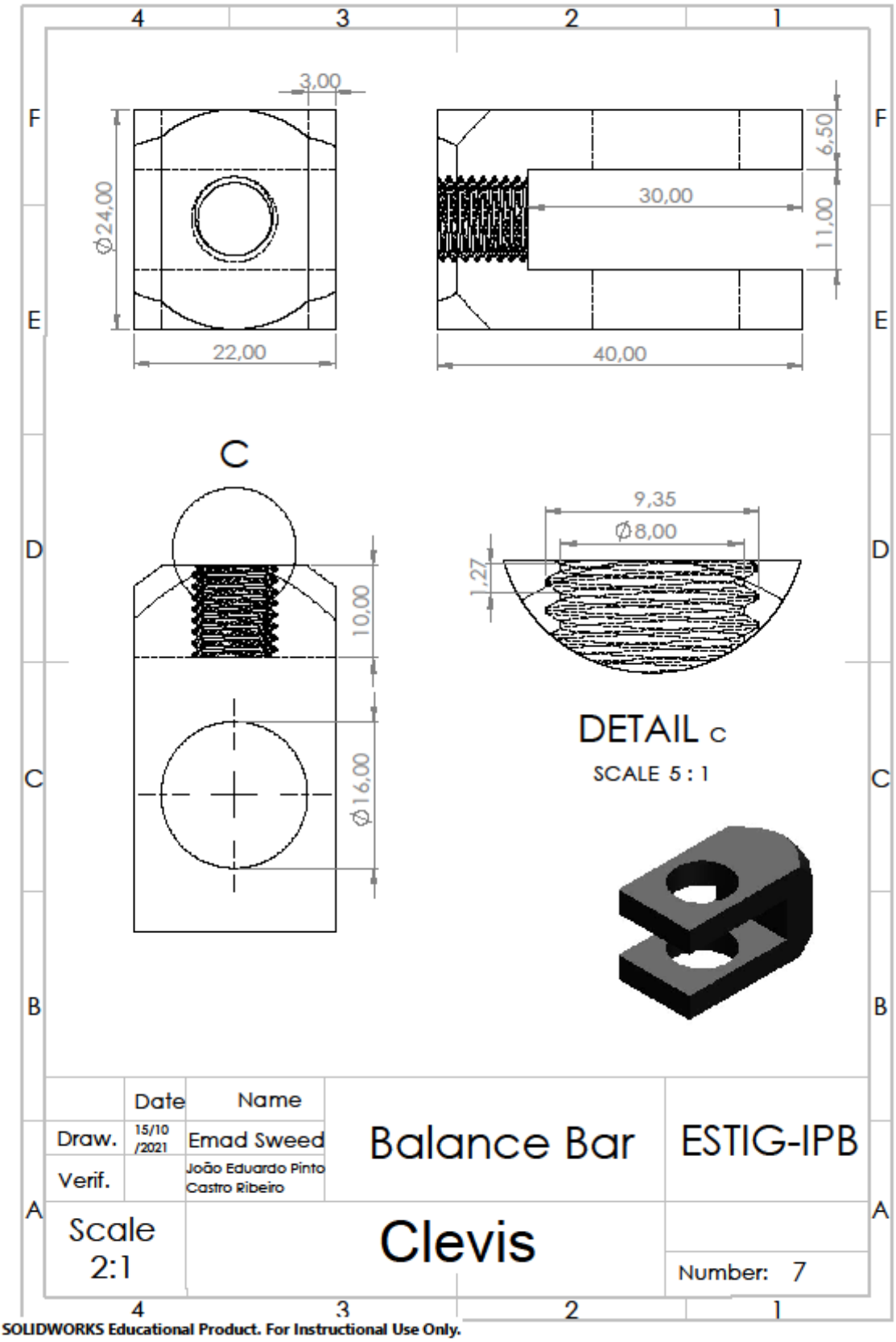
3,00
Ø24,00
22,00
6,50
30,00
11,00
40,00
C
10,00
Ø16,00
9,35
Ø8,00
1,27
DETAIL C
SCALE 5 : 1
Date
Name
Draw.
15/10 /2021
Emad Sweed
Verif.
João Eduardo Pinto Castro Ribeiro
Balance Bar
ESTIG-IPB
Scale 2:1
Clevis
Number: 7
SOLIDWORKS Educational Product. For Instructional Use Only.

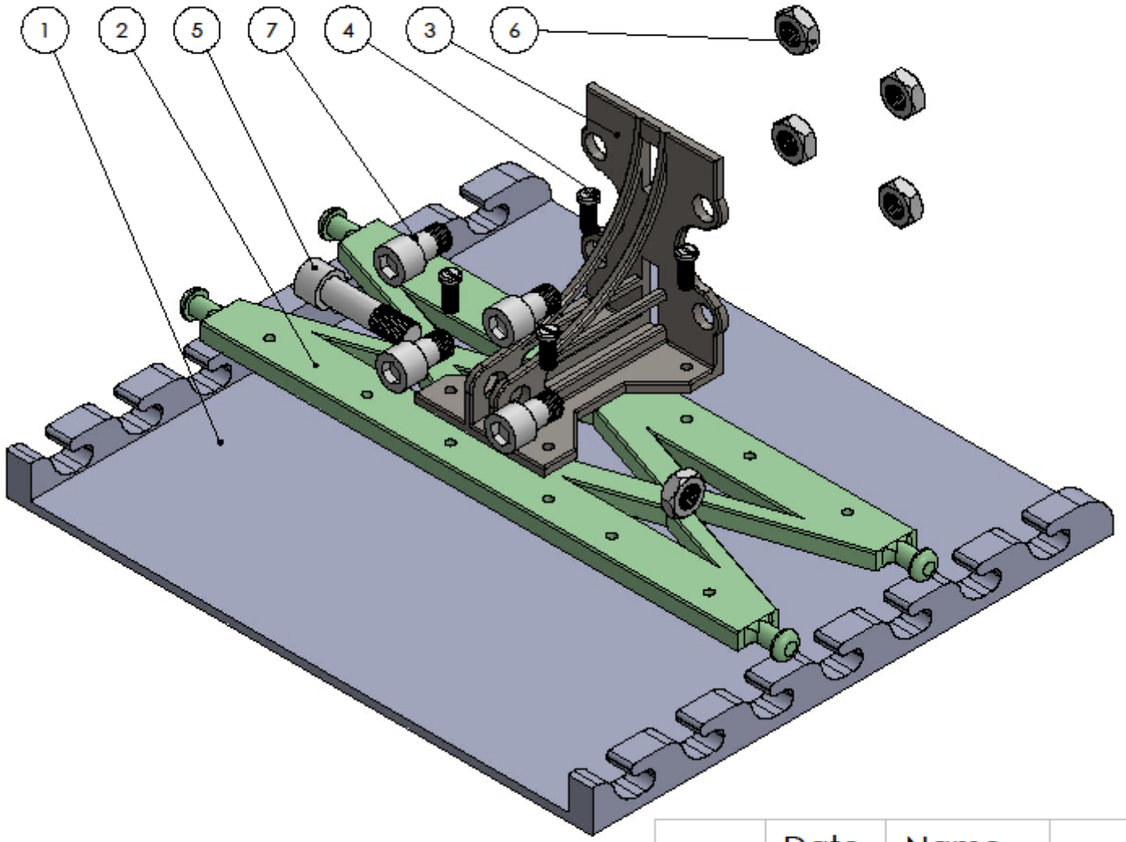

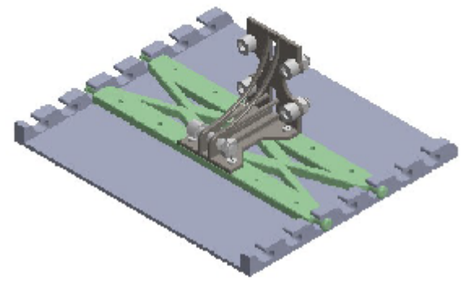

ITEM NO.	DESCRIPTION	QTY.
1	Pedal Box Support	1
2	PEDAL BOX BASE	1
3	Pedal And Master Cylinder Holder	1
4	Screw 6mm	4
5	Hex Socket Head Screw 13-50	1
6	Nut 13	5
7	Hex Socket Head Screw 13-20	4

	Date	Name		
Draw.	17/10/2021	Emad Sweed	Base Assembly	ESTIG-IPB
Verif.		João Eduardo Pinto Castro Ribeiro		
Scale 1:2			Exploded View	

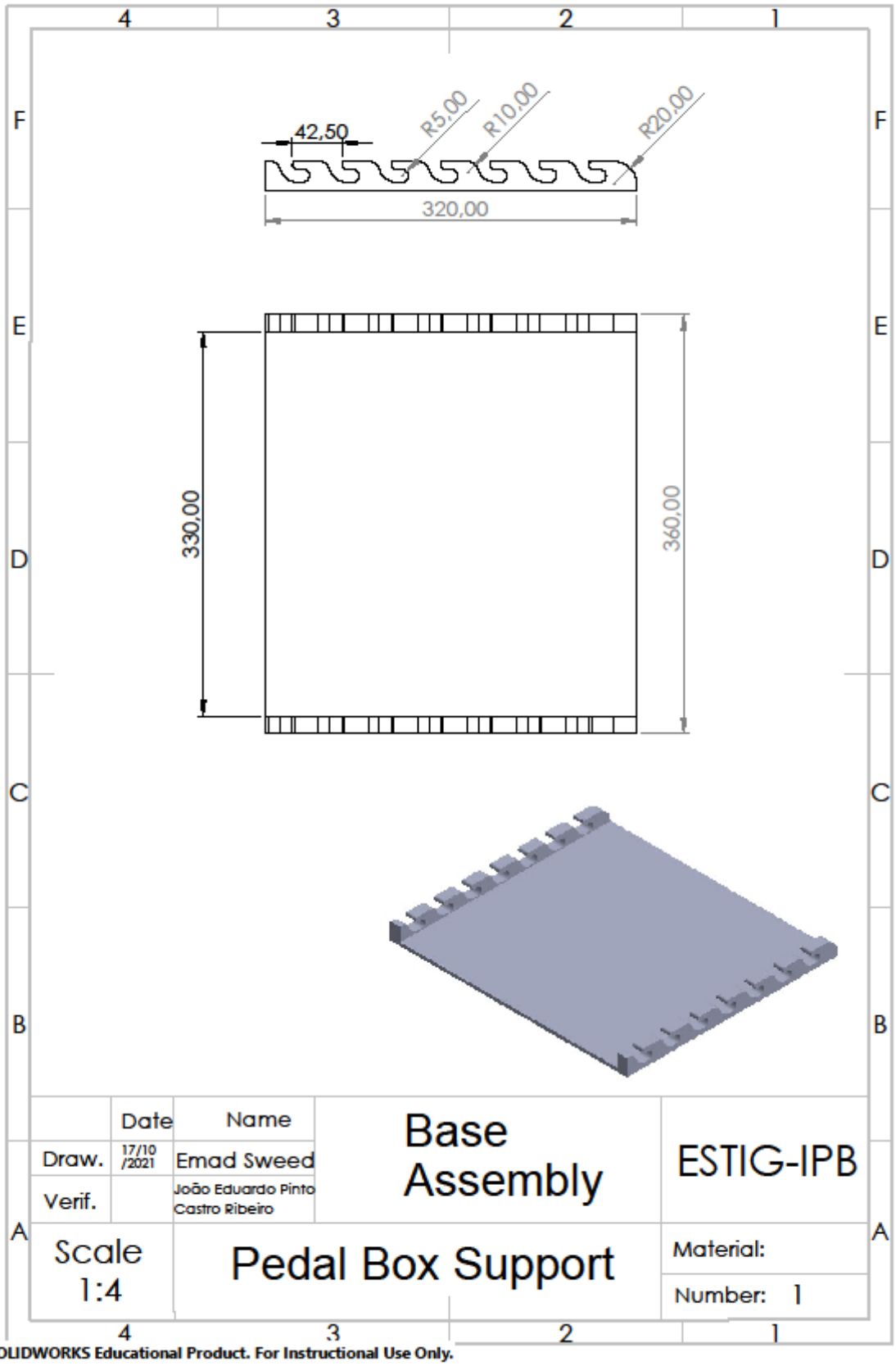
4
3
2
1
F
E
D
C
B
A
42,50
R5,00
R10,00
R20,00
320,00
330,00
360,00
Date
Name
Draw.
17/10
/2021
Emad Sweed
Verif.
João Eduardo Pinto
Castro Ribeiro
Base
Assembly
ESTIG-IPB
Scale
1:4
Pedal Box Support
Material:
Number: 1
SOLIDWORKS Educational Product. For Instructional Use Only.

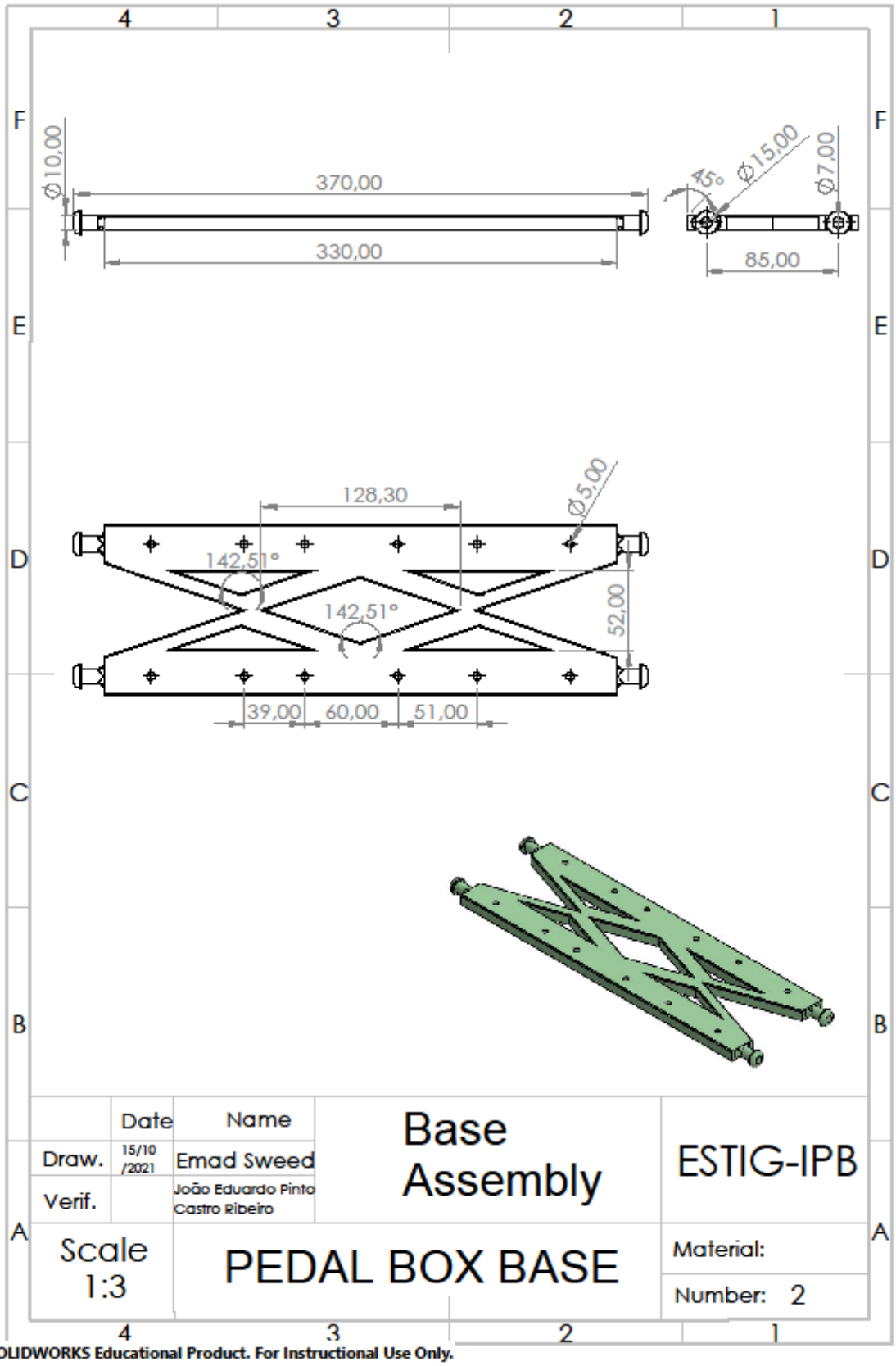
4
3
2
1
F
E
D
C
B
A
Ø10,00
370,00
330,00
45°
Ø15,00
Ø7,00
85,00
128,30
Ø5,00
142,51°
142,51°
52,00
39,00
60,00
51,00
Date
Name
Draw.
15/10 /2021
Emad Sweed
Verif.
João Eduardo Pinto Castro Ribeiro
Base Assembly
ESTIG-IPB
Scale 1:3
PEDAL BOX BASE
Material:
Number: 2
SOLIDWORKS Educational Product. For Instructional Use Only.

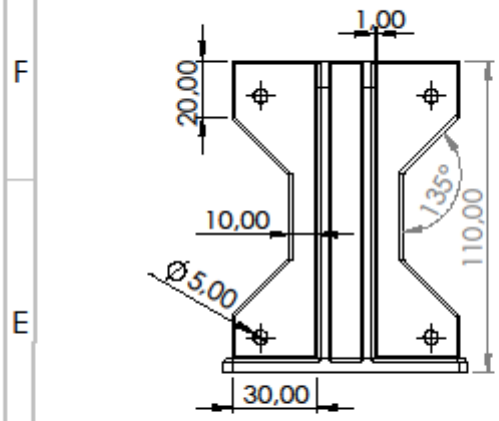

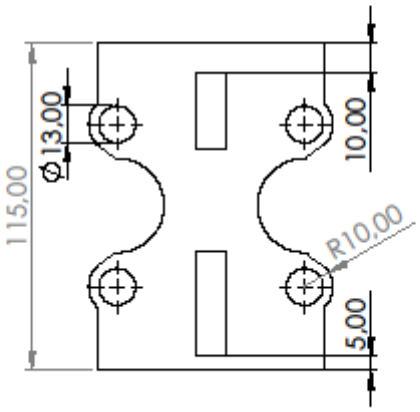

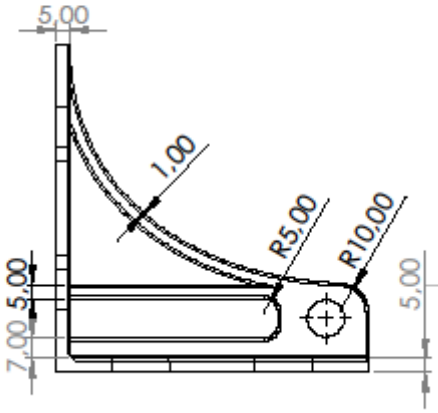

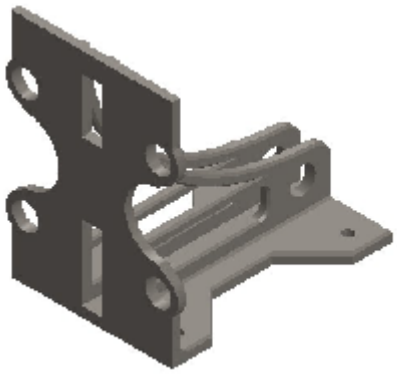

	Date	Name		
Draw.	15/10 /2021	Emad Sweed	Base Assembly	ESTIG-IPB
Verif.		João Eduardo Pinto Castro Ribeiro		
Scale 1:2		Pedal And Master Cylinder Holder	Material:	
			Number: 3	

SOLIDWORKS Educational Product. For Instructional Use Only.

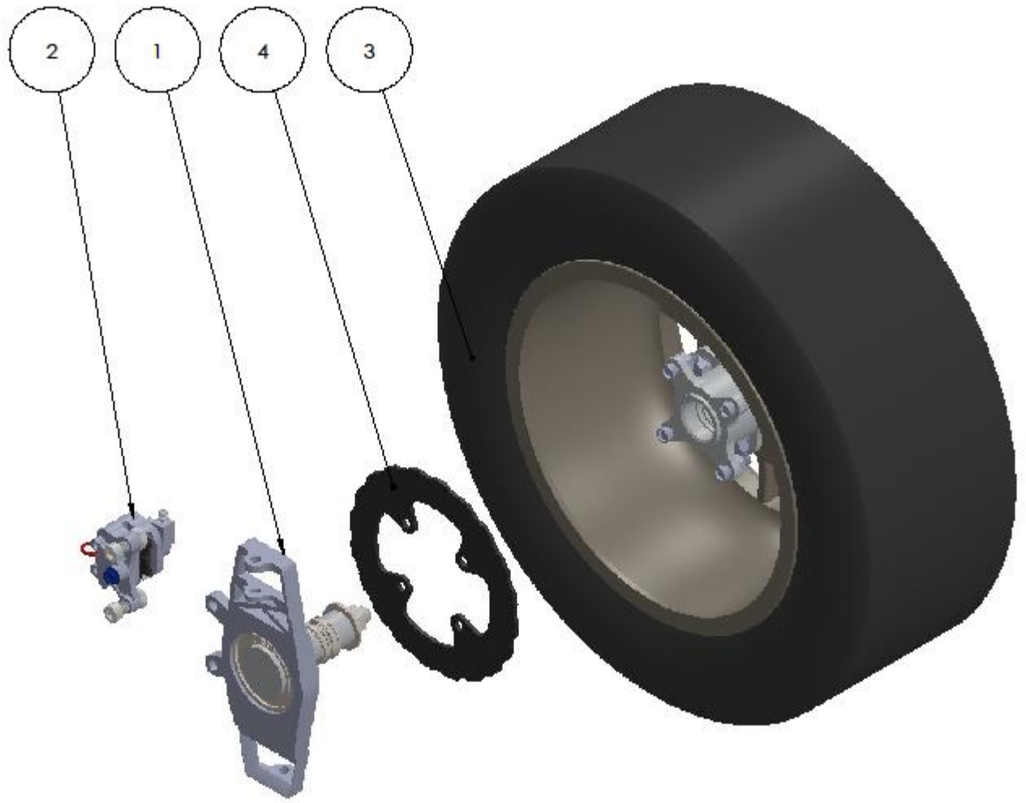

ITEM NO.	DESCRIPTION	QTY.
1	Front Suspension Assembly	1
2	CP4226-2S0 Caliper Assembly	1
3	wheel assembly	1
4	200 mm Front Disc Without Holes	1

	Date	Name
Draw.		Emad Sweed
Verif.		João Eduardo Pinto Castro Ribeiro

CP2623
Master Cylinder Assembly

ESTIG-IPB

Scale 1:1

Exploded View

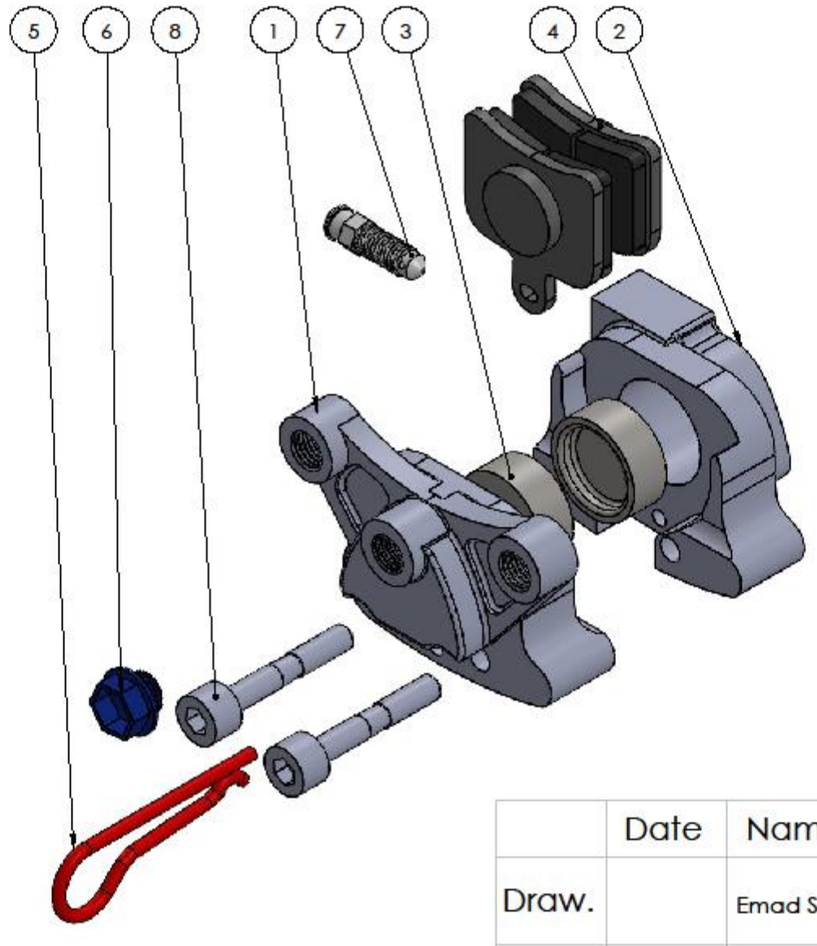

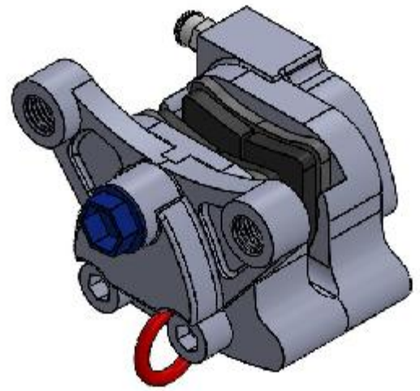

ITEM NO.	DESCRIPTION	QTY.
1	4226 Body Part1	1
2	4226 Body Part2	1
3	Caliper Piston	2
4	4226 Pad	2
5	Pad Retainer	1
6	Hydraulic Threads Cover	1
7	Bleed Screw M7 x 1.0	1
8	M7 Nail	2

	Date	Name		
Draw.		Emad Sweed	CP4226-2S0 Caliper	ESTIG-IPB
Verif.		João Eduardo Pinto Castro Ribeiro		
Scale 1:1			Exploded View	

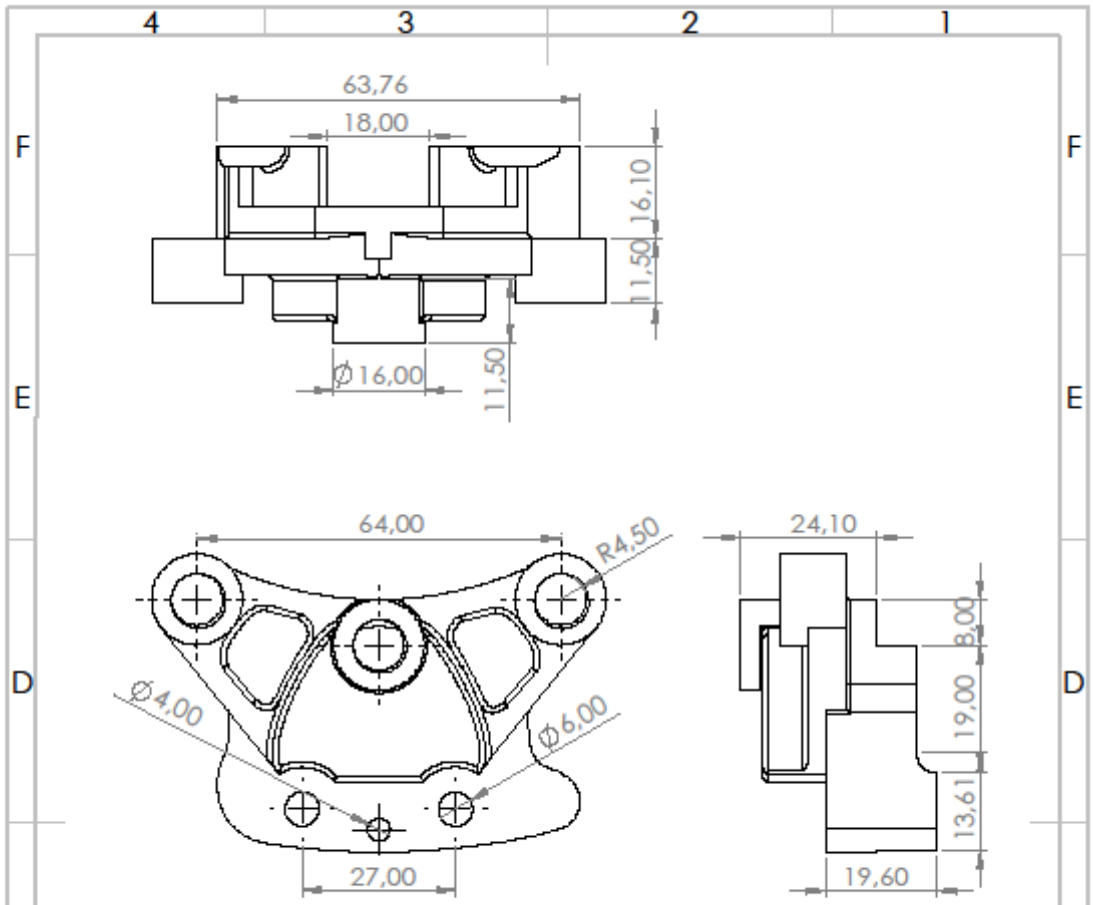

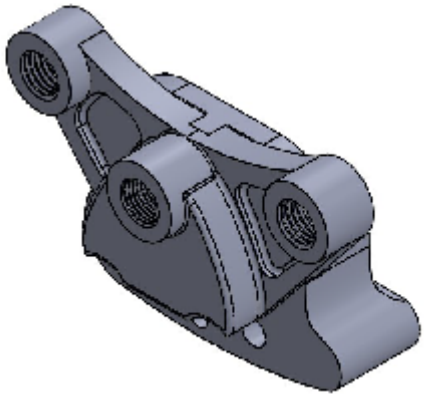

	Date	Name		
Draw.	15/10 /2021	Emad Sweed	CP4226-2S0 Caliper	ESTIG-IPB
Verif.		João Eduardo Pinto Castro Ribeiro		
Scale 1:1			4226 Body Part1	Number: 1

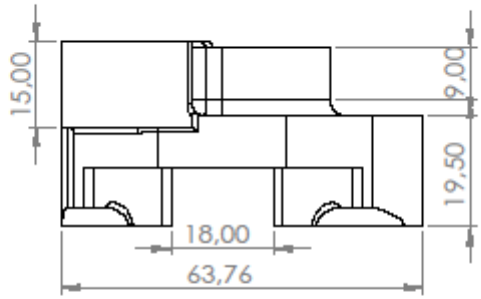

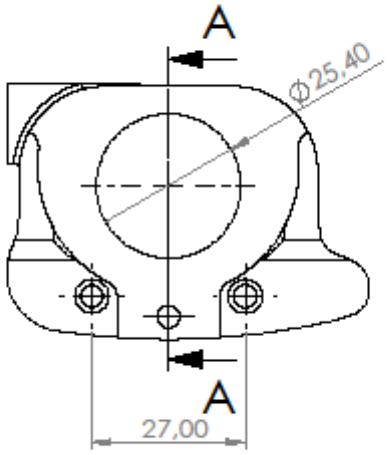

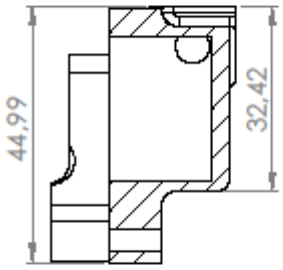

SECTION A-A

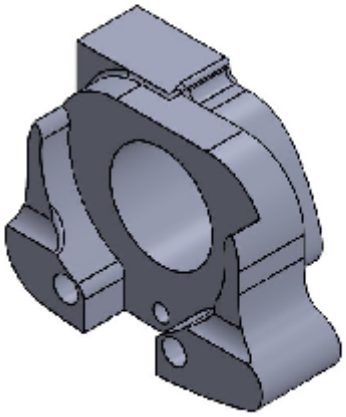

	Date	Name		
Draw.	15/10 /2021	Emad Sweed	CP4226-2S0 Caliper	ESTIG-IPB
Verif.		João Eduardo Pinto Castro Ribeiro		
Scale 1:1		4226 Body Part2		Number: 2

SOLIDWORKS Educational Product. For Instructional Use Only.

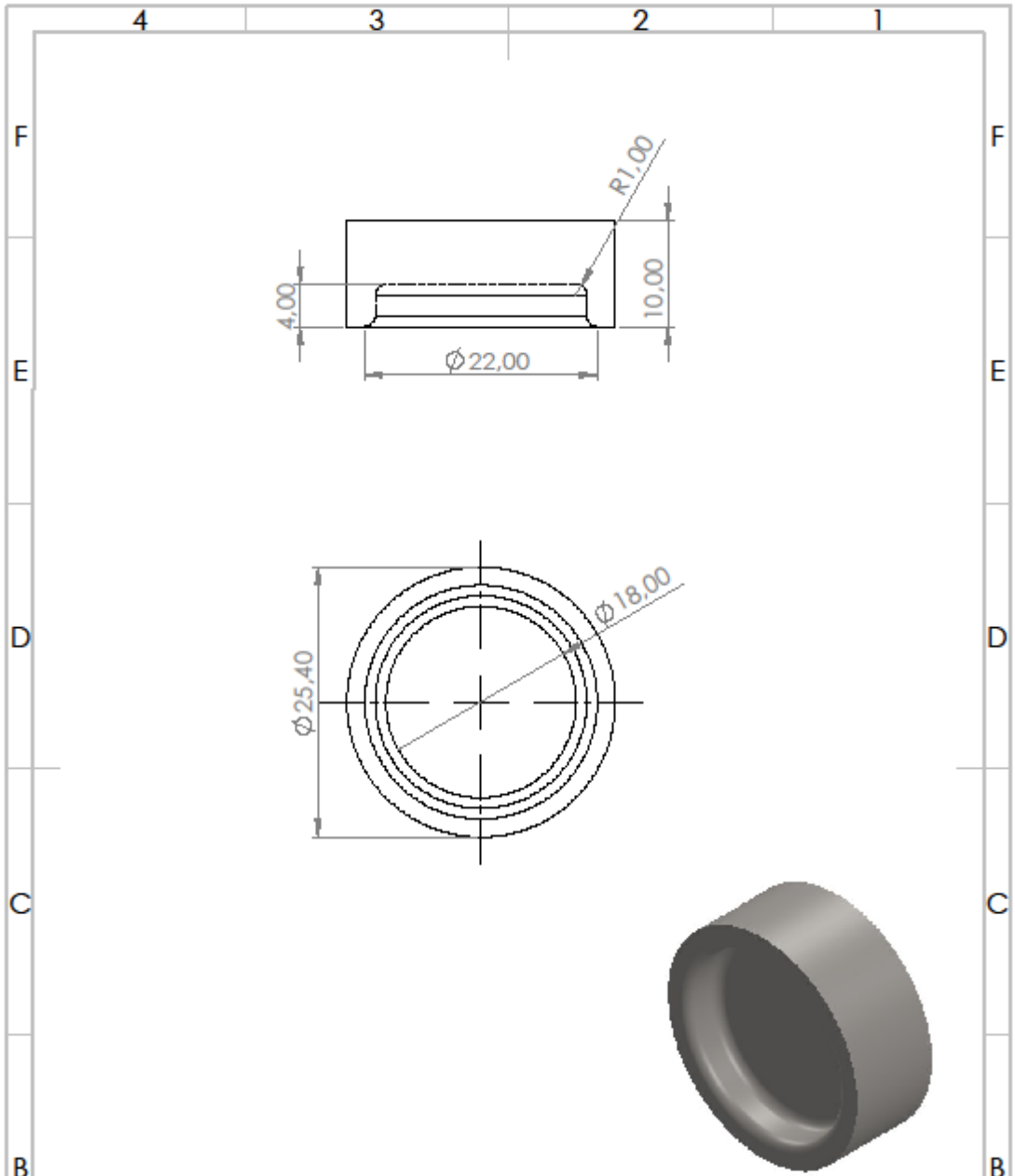

	Date	Name		
Draw.	15/10 /2021	Emad Sweed	CP4226-2S0 Caliper	ESTIG-IPB
Verif.		João Eduardo Pinto Castro Ribeiro		
Scale 2:1			Caliper Piston	Number: 3

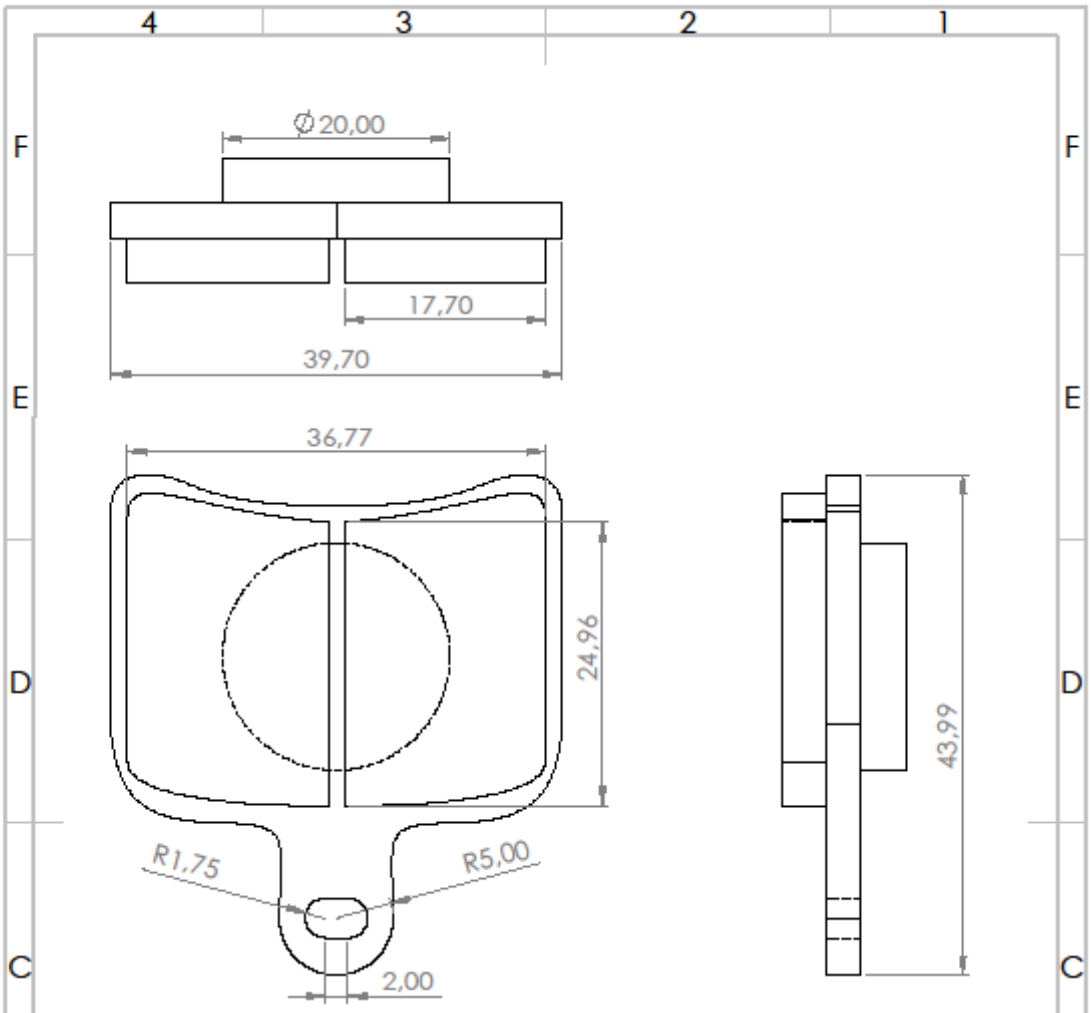

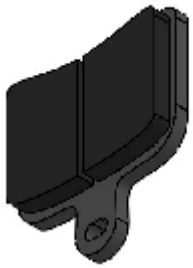

	Date	Name		
Draw.	15/10 /2021	Emad Sweed	CP4226-2S0 Caliper	ESTIG-IPB
Verif.		João Eduardo Pinto Castro Ribeiro		
Scale 2:1			4226 Pad	Number: 4

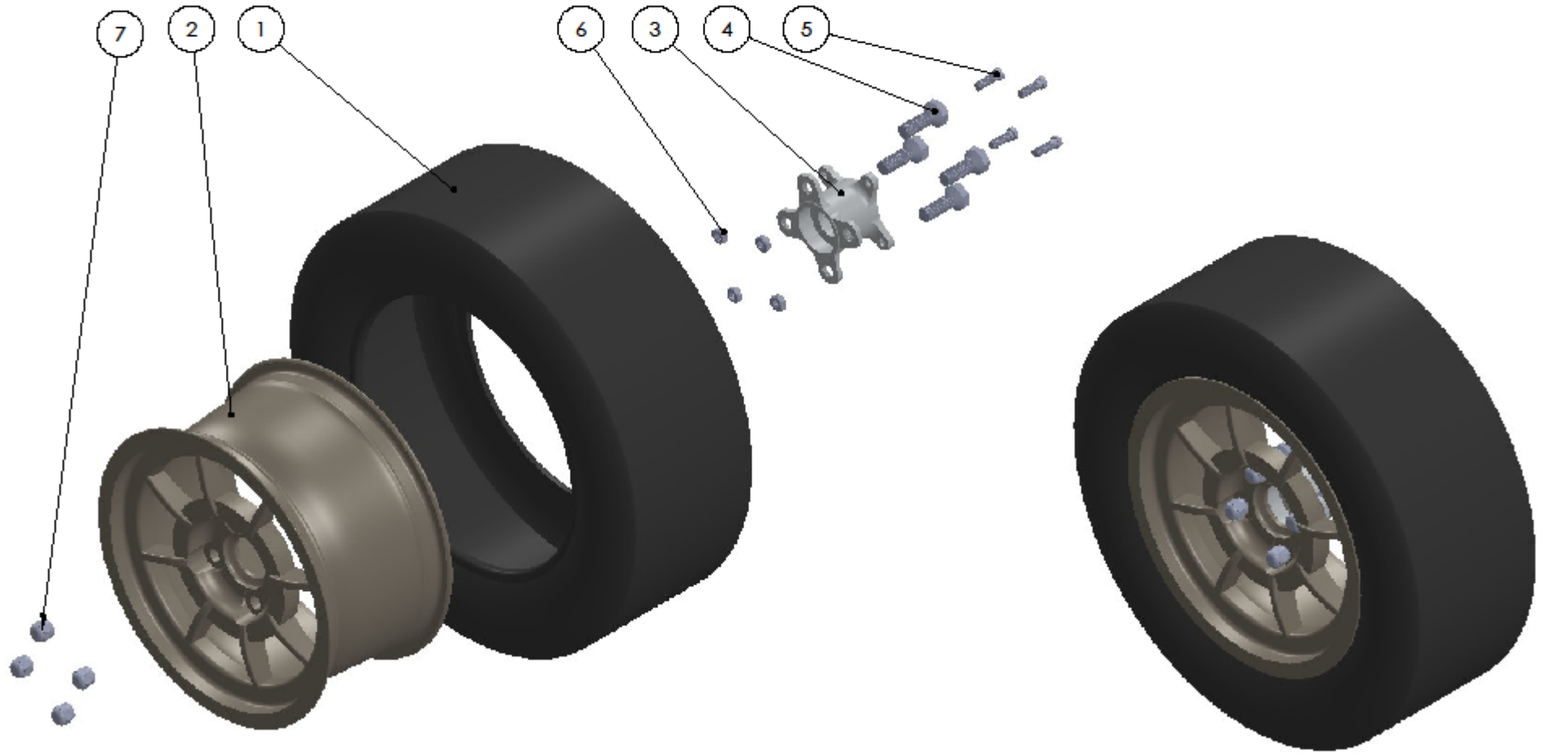

ITEM NO.	DESCRIPTION	QTY.
1	17854 R13 Tire	1
2	OZ Mg Cast 713 Rim	1
3	Hub	1
4	M16 Rim lug	4
5	M10 -1-30 mm	4
6	M10 -1 Nut	4
7	Rim Lug Nut	4

	Date	Name		
Draw.	20/October 2021	Emad Sweed	WHeel Hub Assembly	ESTIG-IPB
Verif.		João Eduardo Pinto Castro Ribeiro		
Scale 1:5			Exploded View	

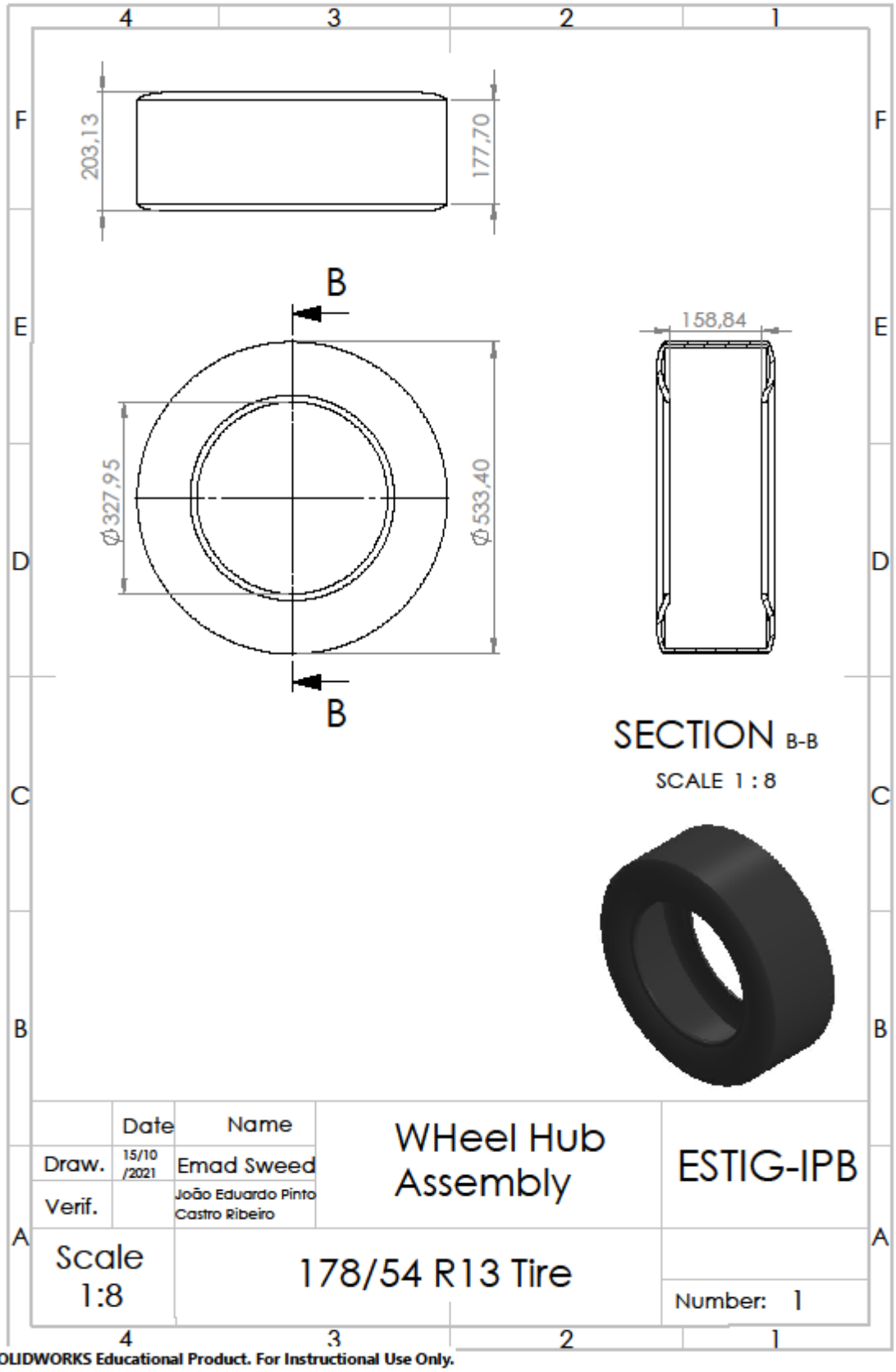
4
3
2
1
F
E
D
C
B
A
203,13
177,70
B
Ø327,95
Ø533,40
158,84
B
SECTION B-B
SCALE 1 : 8
Date
Name
Draw.
15/10 /2021
Emad Sweed
Verif.
João Eduardo Pinto Castro Ribeiro
WHeel Hub Assembly
ESTIG-IPB
Scale 1:8
178/54 R13 Tire
Number: 1
SOLIDWORKS Educational Product. For Instructional Use Only.

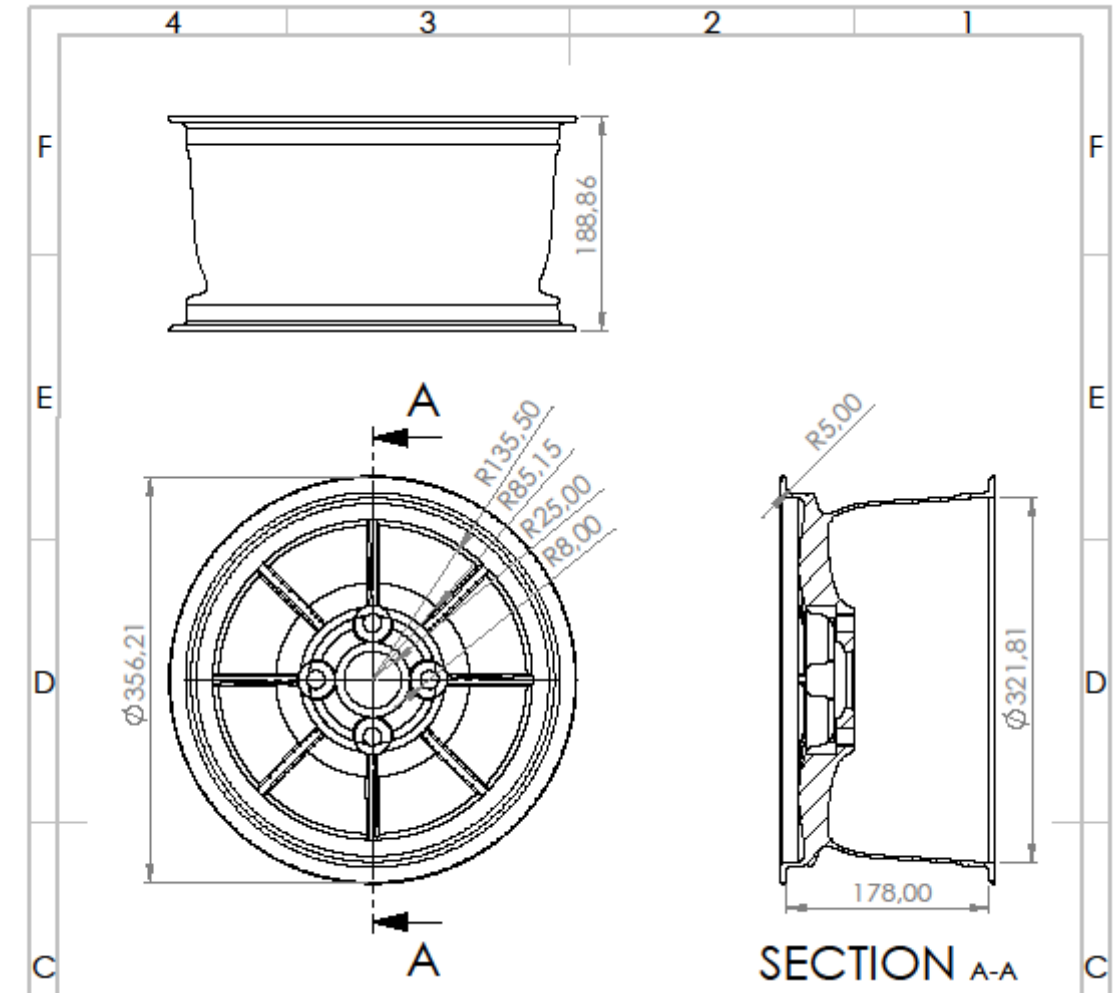

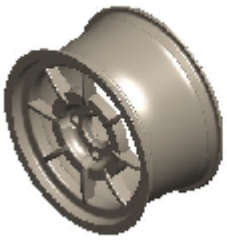

	Date	Name		
Draw.	15/10 /2021	Emad Sweed	Wheel Hub Assembly	ESTIG-IPB
Verif.		João Eduardo Pinto Castro Ribeiro		
Scale 1:5		OZ Mg Cast 7*13 Rim		Number: 2

SOLIDWORKS Educational Product. For Instructional Use Only.

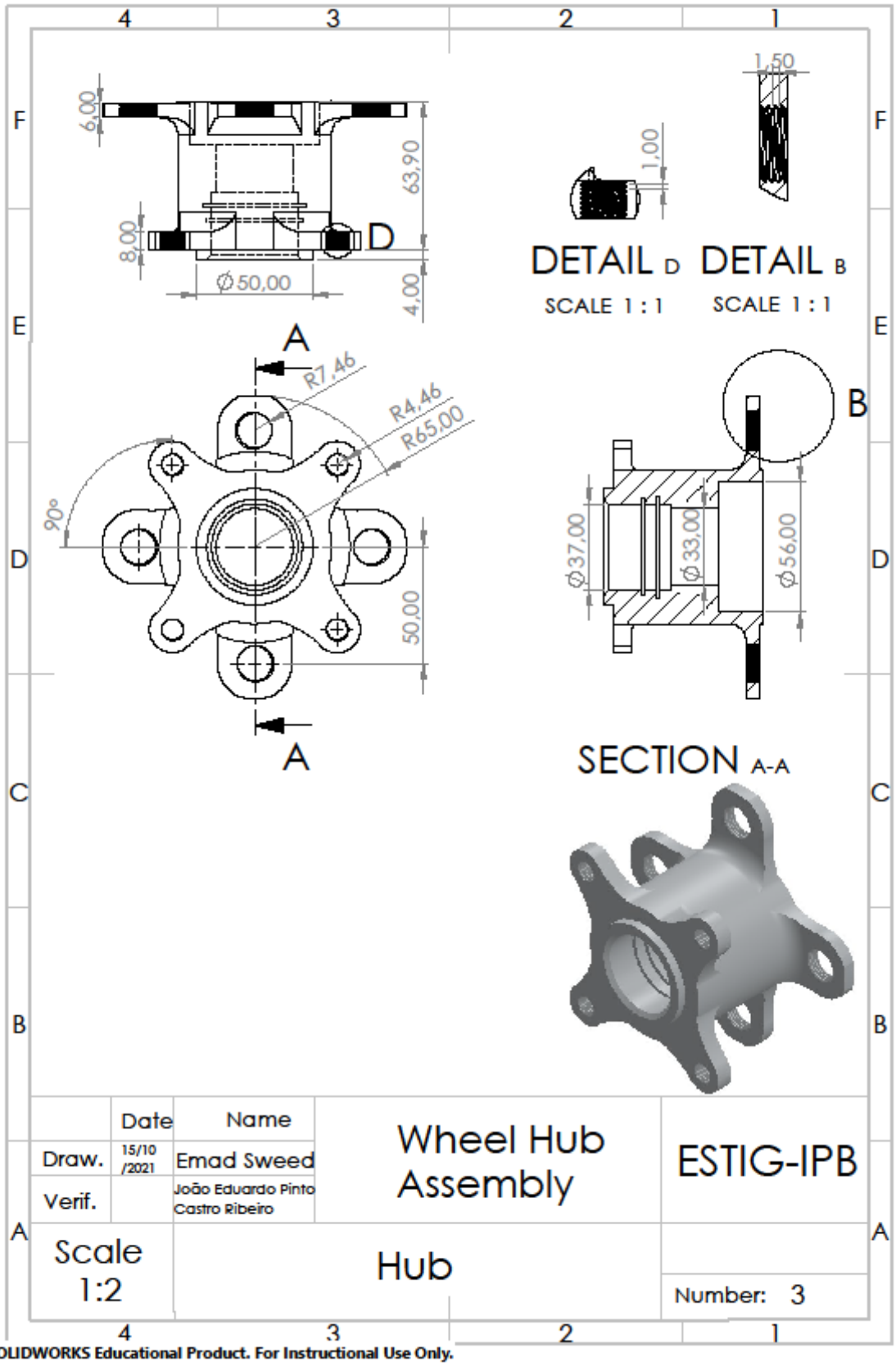
6,00
63,90
8,00
D
Ø50,00
4,00
1,00
1,50
DETAIL D
SCALE 1 : 1
DETAIL B
SCALE 1 : 1
A
R7,46
R4,46
R65,00
90°
50,00
A
B
Ø37,00
Ø33,00
Ø56,00
SECTION A-A
Date
Name
Draw.
15/10 /2021
Emad Sweed
Verif.
João Eduardo Pinto Castro Ribeiro
Wheel Hub Assembly
ESTIG-IPB
Scale 1:2
Hub
Number: 3
SOLIDWORKS Educational Product. For Instructional Use Only.

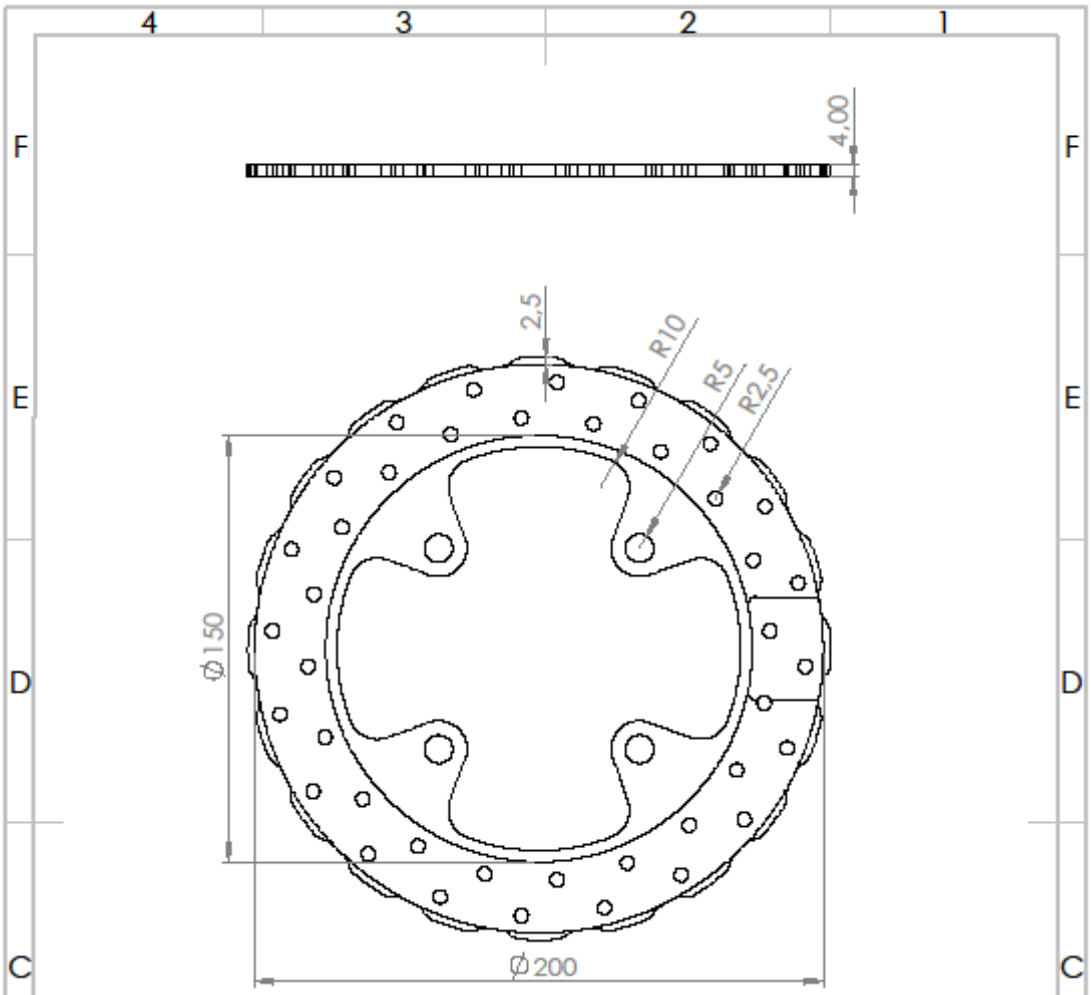

	Date	Name		
Draw.	15/10 /2021	Emad Sweed	Caliper and Rotor Assembly	ESTIG-IPB
Verif.		João Eduardo Pinto Castro Ribeiro		
Scale 1:2			Front Drilled Rotor	Material: Gray Cast Iron
				Number: N/A

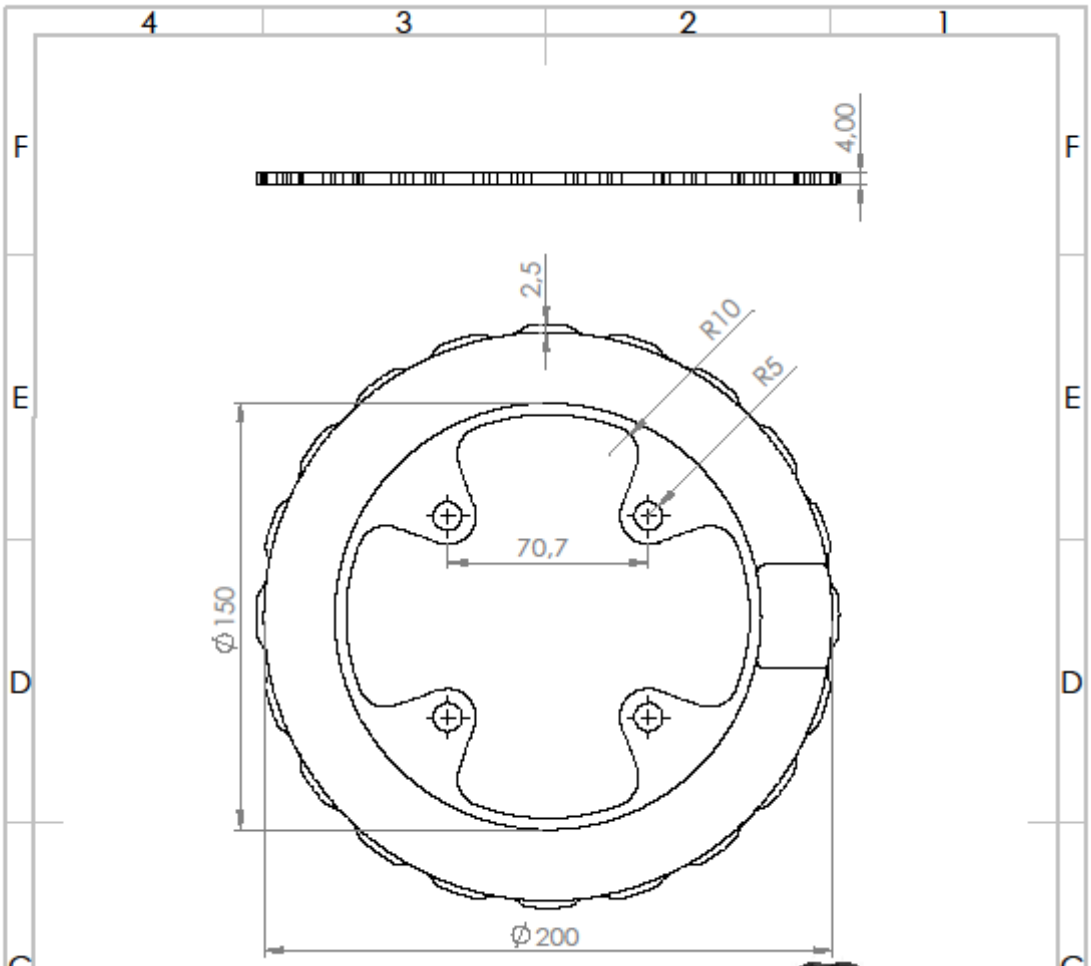

	Date	Name		
Draw.	15/10 /2021	Emad Sweed	Caliper and Rotor Assembly	ESTIG-IPB
Verif.		João Eduardo Pinto Castro Ribeiro		
Scale 1:2			Front Undrilled Rotor	Material: Gray Cast Iron
				Number: N/A

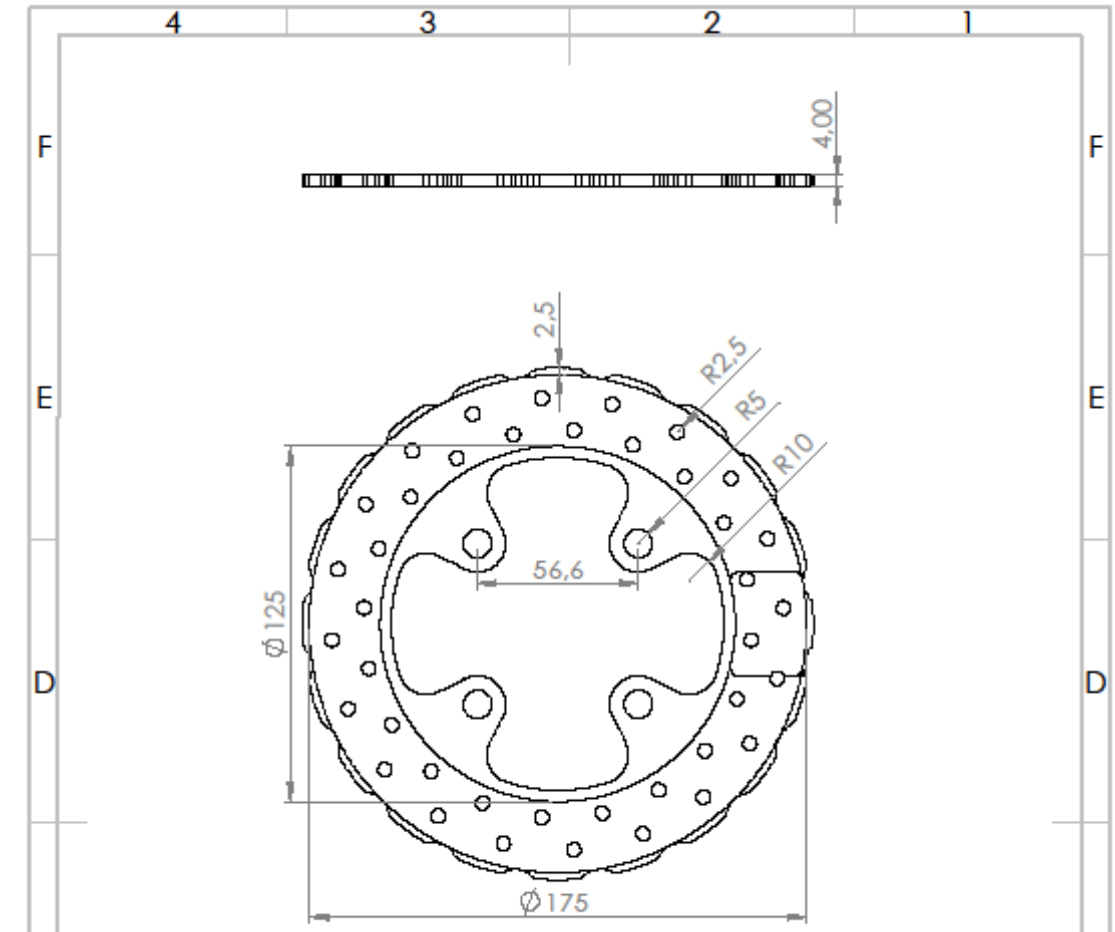

	Date	Name		
Draw.	15/10 /2021	Emad Sweed	Caliper and Rotor Assembly	ESTIG-IPB
Verif.		João Eduardo Pinto Castro Ribeiro		
Scale 1:2			Rear Drilled Rotor	Material: Gray Cast Iron Number: N/A

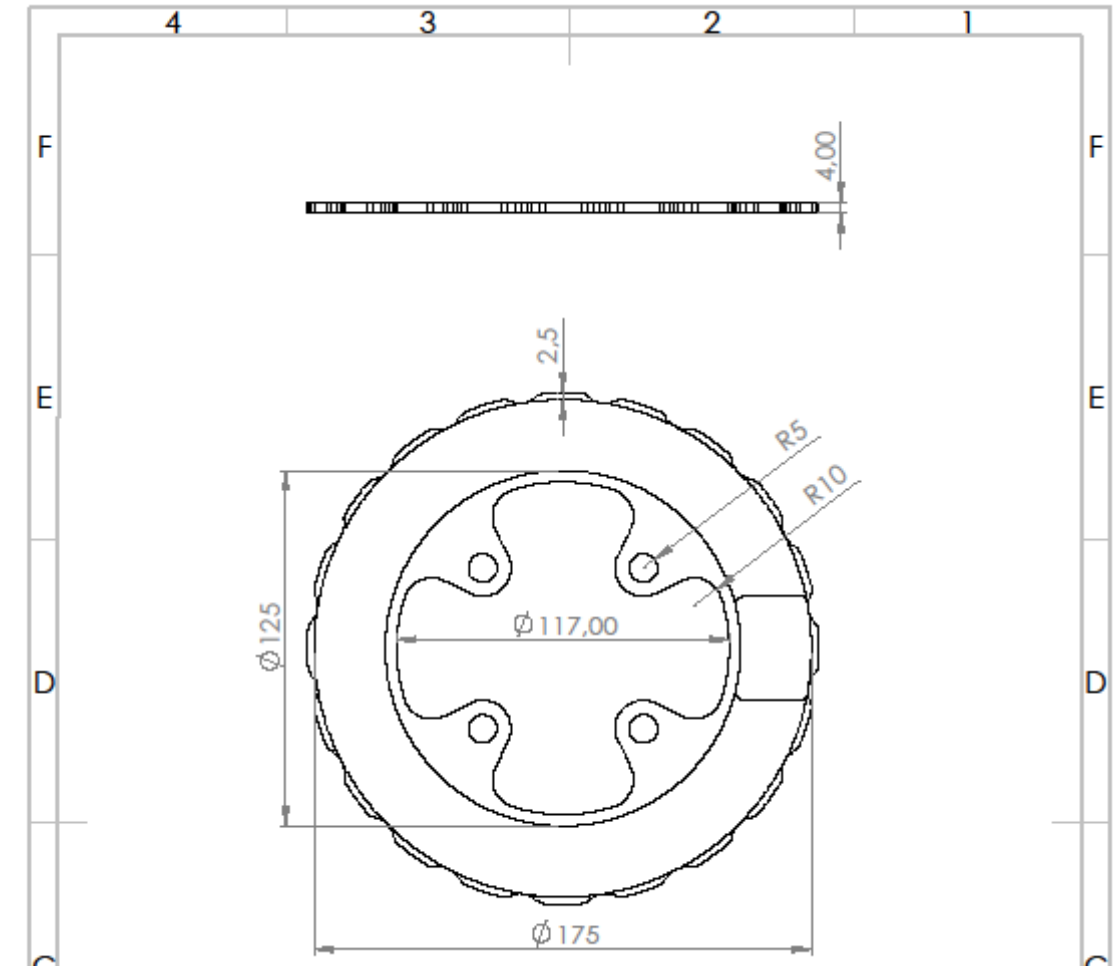

	Date	Name		
Draw.	15/10 /2021	Emad Sweed	Caliper and Rotor Assembly	ESTIG-IPB
Verif.		João Eduardo Pinto Castro Ribeiro		
Scale 1:2			Rear undrilled Rotor	Material: Gray Cast Iron
				Number: N/A